REACTOR MATERIALS

A Quarterly Technical Progress Review

Prepared for DIVISION OF TECHNICAL INFORMATION, U. S. ATOMIC ENERGY COMMISSION,
by BATTELLE MEMORIAL INSTITUTE

Fall 1967

● VOLUME 10

● NUMBER 3

TECHNICAL PROGRESS REVIEWS

The United States Atomic Energy Commission publishes the Technical Progress Reviews to meet the needs of industry and government for concise summaries of current nuclear developments. Each journal digests and evaluates the latest findings in a specific area of nuclear technology and science. *Nuclear Safety* is a bimonthly journal; the other three are quarterly journals.

Isotopes and Radiation Technology
P. S. Baker, A. F. Rupp, and Associates
Isotopes Information Center, Oak Ridge National Laboratory

Nuclear Safety
Wm. B. Cottrell, W. H. Jordan, J. P. Blakely, and Associates
Nuclear Safety Information Center, Oak Ridge National Laboratory

Reactor and Fuel-Processing Technology
Argonne National Laboratory

Reactor Materials
E. M. Simons and Associates
Battelle Memorial Institute

All are available from the U. S. Government Printing Office. See the back cover for ordering instructions.

The views expressed in this publication do not necessarily represent those of the United States Atomic Energy Commission, its divisions or offices, or of any Commission advisory committee or contractor.

Availability of Reports Cited in This Review

United States Atomic Energy Commission (USAEC) reports are available at USAEC depository libraries and are sold by the Clearinghouse for Federal Scientific and Technical Information (CFSTI), National Bureau of Standards, U. S. Department of Commerce, 5285 Port Royal Road, Springfield, Va. 22151. All reports sold by CFSTI are $3.00 for printed copy and $0.65 for microfiche. Each separately bound part of a report is priced as a separate report. Some reports may not be available because of their preliminary nature; however, the information contained in them will generally be found in later progress or topical reports on the subject.

Other U. S. Government agency reports identified in this journal generally are available from CFSTI.

Private-organization reports should be requested from the originator.

United Kingdom Atomic Energy Authority (UKAEA) and Atomic Energy of Canada Limited (AECL) reports are available at USAEC depository libraries. UKAEA reports are sold by Her Majesty's Stationery Office, London; AECL reports are sold by the Technical Information Officer, Atomic Energy of Canada Limited, Chalk River, Ontario, Canada. UKAEA and AECL reports issued after March 1, 1967, are sold by CFSTI to purchasers in the United States and its territories.

Contents

Reactor Materials
Vol. 10, No. 3

Fuel and Fertile Materials (Section I)
Uranium and Uranium Alloys 135
Plutonium 138
Thorium 141
Metal–Ceramic Fuels 141
Coated-Particle Fuels 142
Uranium and Thorium Oxide Fuels . . . 143
Uranium Carbides, Nitrides, Phosphides, and Sulfides 144
Fuel–Water Reactions 147
Basic Studies of Irradiation Effects in Fuel Materials 147
References 149

Moderator Materials (Section II)
Graphite 152
Beryllium and Beryllium Alloys . . . 154
Beryllium Oxide 156
Solid Hydrides 156
References 157

Cladding and Structural Materials (Section III)
Corrosion by Aqueous and Gaseous Media 158
Corrosion by Nonaqueous Liquids . . . 162
Metal–Water Reactions 166
Irradiation Effects in Nonfuel Materials . . 167
Selected Metallurgical Aspects of Cladding and Structural Materials . . 175
Diffusion Studies 179
Selected Mechanical Properties of Cladding and Structural Materials . . 180
Nonfueled Refractories 185
Ceramic Technology 189
References 189

Special Fabrication Techniques (Section IV)
Melting and Fabrication of Cast Materials 194
Powder-Metallurgy Materials 196
Pressure Bonding 197
Plating 198
Welding and Brazing 199
Nondestructive Testing 200
References 201

Reactor Materials

is one of a series of technical progress reviews broadly covering the field of nuclear science and technology. Under the auspices of the USAEC Division of Technical Information, *Reactor Materials* is prepared by Battelle personnel from worldwide literature. It covers properties, behavior, and fabrication processes of materials applicable to nuclear reactor components and associated equipment.

The reader will recognize that the scope of this Review is too broad to permit detailed coverage of every topic. Rather, the authors and editors attempt to combine the highlights of significant new developments into an information summary of current research for both management and the technical specialist. As a rule, enough of the results are presented to define the research and summarize the findings. For readers desiring more information on any particular topic, a complete set of references is provided at the end of each section.

Each quarter a number of bibliographies, monographs, and books appear on subjects within the scope of *Reactor Materials*. Although the main purpose of this Review is to call attention to findings that are new and significant, such publications are noted in the text because they often represent excellent compilations of available information on important materials topics.

E. M. SIMONS
S. W. POREMBKA, JR.
D. L. KELLER

Battelle Memorial Institute

Issued quarterly by the U. S. Atomic Energy Commission. Use of funds for printing this publication approved by the Director of the Bureau of the Budget on July 8, 1966.

Section I

Reactor Materials

Fuel and Fertile Materials

Uranium and Uranium Alloys

Unalloyed Uranium

The heat capacity of high-purity alpha uranium from 1.7 to 25°K has been determined by investigators at Argonne National Laboratory.[1] The values obtained were significantly lower than those reported by other investigators. The coefficient of the electronic contribution to heat capacity, γ, was determined to be 9.88 ± 0.05 mj/(gram atom)(°K^2) and Debye Θ at 0°K was assessed to be 222 ± 2°K. The $C_p - C_v$ correction was evaluated between 15 and 80°K to show the effect of the anomalous expansive and compressive behavior of uranium between 20 and 45°K on the lattice heat capacity.

Russian investigators[2,3] determined the electrical resistivity of alpha-uranium pseudomonocrystals and the effect of irradiation on resistivity after an exposure of 7×10^{18} neutrons/cm^2. The results are presented in the subsection, Basic Studies of Irradiation Effects in Fuel Materials (pages 147-149).

At Argonne[4] the rate of penetration of Armco iron by molten uranium, U–34 at.% Fe eutectic, and U–77 at.% Fe eutectic was investigated in the range 740 to 1300°C. The phenomenon of particular interest was a penetration-rate reversal, i.e., the rate decreased with increasing temperature, between 1150 and 1244°C. Penetration rates at 1150°C were found to be 760 μm/sec in uranium, 690 μm/sec in the U–34 at.% Fe eutectic, and 5.5 μm/sec in the U–77 at.% Fe eutectic. At 1244°C the corresponding rates changed to 150, 130, and 5.7 μm/sec, respectively. The study showed that the penetration rate is related to the rate and mode of formation of UFe_2. The rate changes correlate well with the phases of the U–Fe equilibrium diagram.

The purification of uranium by zone-refining techniques was studied at Union Carbide Corporation.[5] After the best cleaning procedure, molten-zone width, direction and rate of travel of the molten zone, length of the zone-refined area, and degree of vacuum were established, purified uranium was prepared with total impurities of less than 30 ppm.

A method is described in a British[6] patent for the production of uranium metal suitable for extrusion into rodlike fuel elements by the reduction in a reaction vessel of UF_4 using a metallic reducing agent such as calcium or magnesium. A quantity of a reducible compound of iron and aluminum or of the pure metals is included with the reactants in the reaction vessel. The quantity included is that which is needed to provide the refined grain structure and other satisfactory metallurgical properties. The preferred reducible compounds of iron and aluminum are the hydrated trifluorides of each of the metals.

Other papers containing information on unalloyed uranium include: "The Wiedeman–Franz Ratio of Metallic Uranium at Elevated Temperatures,"[7] "Diffusion of Uranium in Molybdenum, Niobium, Zirconium, and Titanium,"[8] "Strain-Anneal Method of Growing Crystals of Alpha Uranium,"[9] "An X-Ray Study of the $\alpha \rightleftharpoons \beta$ Transformation in Uranium,"[10] "Compressive Behavior of Natural Uranium with the Aid of Upsetting Tests,"[11] and "Evidence for a Helical Crystallographic Texture in Uranium Bars of Magnox-Clad Fuel Elements."[12]

Alpha-Phase Uranium Alloys

Work by the Yugoslavians[13] on U–Mo alloys containing 0.4 to 0.6 wt.% molybdenum and 500 to 1500 ppm aluminum has been reported. The experiments showed that aluminum, which is almost insoluble in uranium, forms numerous nucleation centers, thereby preventing extensive grain growth and reducing the anisotropy, which in alloys with low molybdenum content leads to buckling of the fuel elements. An alloy containing 0.6 wt.% molybdenum and 500 ppm aluminum had the smallest and most uniform grain size that ranged from 0.04 to 0.06 mm.

British investigators[14] have determined the atomic positions of the metastable α_b'' phase occurring in U–Mo alloys from a specimen containing 10 at.% molybdenum. It was shown that, for specimens containing 9.2, 10, and 10.8 at.% molybdenum, this structure is a result of a transformation from a tetragonal phase which is based on the body-centered cubic structure of gamma uranium. It was suggested that this transformation probably occurred by a shear process. The relation between the atomic positions in the monoclinic cell and in the parent gamma phase and equilibrium alpha phase of uranium was discussed.

The $U-UO_2$ system was studied by the French.[15] The experiments were concerned primarily with determining the limits of the liquid $U-UO_2$ field as indicated in the diagram presented in Fig. I-1.

Battelle–Northwest[16] has reported on the irradiation resistance of high-purity uranium and dilute uranium alloys. The irradiation was performed at 700°C (in the beta phase) to burnups of 0.1 and 0.2 at.%. The specimen histories and results are presented in Table I-1. It was considered significant that: (1) volume change per at.% burnup was relatively small ($R \approx 15$), (2) swelling was relatively independent of irradiation temperature (from 610 to 700°C), (3) swelling was independent of composition or metallurgical history, and (4) swelling exhibited a linear variation with burnup. The volume changes observed are plotted in Fig. I-2, which also shows data obtained previously at 0.5 at.% burnup. The obvious conclusion upon examining this figure is that burnup is the primary variable of importance in determining swelling for the irradiation conditions investigated. A compilation of previous swelling data was also presented for uranium and dilute-uranium-alloy irradiations at various temperatures to burnups of 0.2 at.% or less (see Fig. I-3). This figure shows that, below about 640°C, the swelling of uranium varies greatly, depending on alloy content. This effect is consistent with the concept that, below 600°C, swelling in uranium occurs by mechanical processes and benefits derived from the alloying additions are due to their influence on these mechanical processes. Since swelling by these mechanisms decreases rapidly above 600°C, it is logical that the alloying additions have little or no effect. Thus the insensitivity of swelling to any of the variables except burnup, shown in Fig. I-2, is reasonable when the convergent nature of the curve in Fig. I-3 and the broad mini-

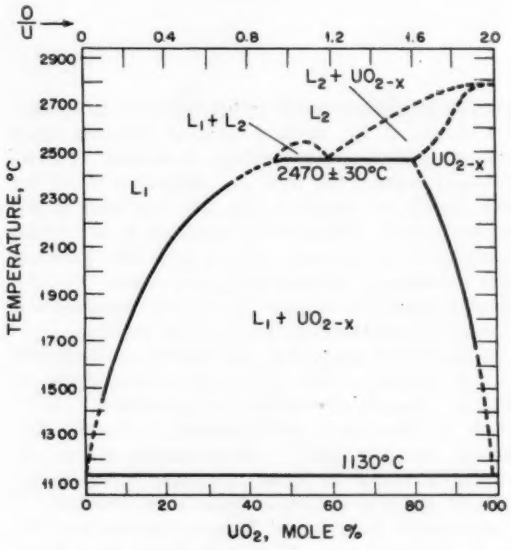

Fig. I-1 The $U-UO_2$ system.[15]

Table I-1 IRRADIATION HISTORY AND VOLUME CHANGE OF SPECIMENS* OF URANIUM AND URANIUM ALLOYS[16]

Type of material†	Heat-treatment	Irradiation temp., °C: Reactor up	Irradiation temp., °C: Reactor down	As-irradiated density (ρ_f), g/cm³	Swelling $\left(\frac{\Delta\rho}{\rho_f} \times 100\right)$, %	R, % swelling/at.% burnup
		Irradiated to 0.1 at.% Burnup				
U(PT 3-NA)	As extruded	660	460	18.71	1.5	15
U(T-3)	640°C, 4 days, furnace cool	660	460	18.22	4.4	44
U + Fe–Al–Si	As extruded	700	500	18.66	1.3	13
U + Fe–Al–Si	900°C, 1 hr, oil quench	700	500	18.58	1.6	16
U(PT 3-NA)	As extruded	680	505	18.84	0.7	7
U(PT 3-NA)	730°C, 15 min, oil quench	680	505	18.78	1.1	11
U(PT 3-NA)	As extruded	~640	~500	18.75	1.2	12
U(PT 3-NA)	730°C, 15 min, oil quench	~640	~500	18.65	1.7	17
U + Fe–Si	As extruded	620	450	18.91	0.3	3
U + Fe–Si	900°C, 1 hr, oil quench	620	450	18.66	1.8	18
		Irradiated to 0.2 at.% Burnup				
U(PT 3-NA)	As extruded	610	435	18.52	2.6	13
U(T-3)	640°C, 4 days, furnace cool	610	435	18.46	3.3	17
U + Fe–Al–Si	As extruded	700	500	18.30	3.1	16
U + Fe–Al–Si	900°C, 1 hr, oil quench	700	500	18.41	2.4	12
U(PT 3-NA)	As extruded	~690	~500	18.36	3.4	17
U(T-3)	730°C, 15 min, oil quench	~690	~500	18.37	3.7	18
U(PT 3-NA)	As extruded	675	490	18.48	2.7	14
U(PT 3-NA)	730°C, 15 min, oil quench	675	490	18.46	2.9	15
U + Fe–Si	As extruded	630	460	18.41	3.1	15
U + Fe–Si	900°C, 1 hr, oil quench	630	460	18.54	2.5	12

*Specimens were half-tubular in geometry, ½ in. in outside diameter by ⅝ in. long, and 0.030 in. in wall thickness.
†Compositions (in ppm) are

U(T-3): high-purity uranium containing 64 Fe, 5 Al, 25 Si, 6 C, 8 N
U(PT 3-NA): high-carbon, high-purity uranium containing 54 Fe, 10 Al, 34 Si, 480 C, 24 N
U + Fe–Al–Si: uranium containing 400 Fe, 645 Al, 85 Si, 500 C, 23 N
U + Fe–Si: uranium containing 140 Fe, 25 Al, 95 Si, 400 C, 14 N

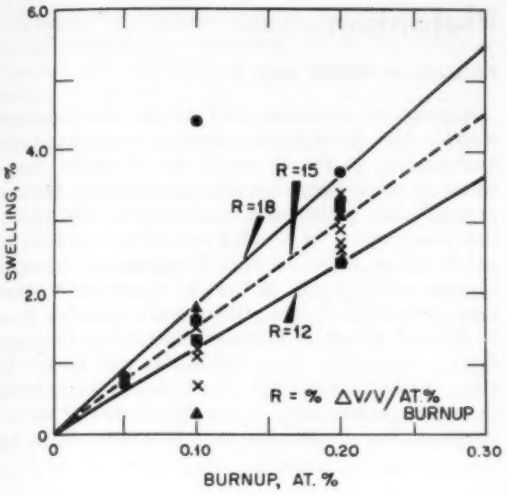

Fig. I-2 Burnup dependence of swelling for uranium specimens[16] irradiated in capsules controlled at 700°C. ●, high-purity, low-carbon uranium containing 64 ppm Fe, 5 ppm Al, 25 ppm Si, 6 ppm C, and 8 ppm N; ×, high-purity, high-carbon uranium containing 54 ppm Fe, 10 ppm Al, 34 ppm Si, 480 ppm C, and 24 ppm N; ▲, U + Fe–Si (uranium containing 140 ppm Fe, 25 ppm Al, 95 ppm Si, 400 ppm C, and 14 ppm N); ■, U + Fe–Al–Si (uranium containing 407 ppm Fe, 645 ppm Al, 85 ppm Si, 500 ppm C, and 23 ppm N).

mum in the high-purity-uranium curve in the 600 to 700°C range are considered.

It should be emphasized that these data pertain to relatively low burnup, <0.02 at.%. As the burnup is increased for irradiation temperatures above 600°C, fission-gas swelling will become more severe, and it is possible that alloying additions may also inhibit this type of swelling.

Gamma-Phase Uranium Alloys

Frankford Arsenal[17] has investigated the mechanical properties of a U–2 wt.% Mo–2 wt.% Zr–2 wt.% Nb–0.5 wt.% Ti alloy. Their data are compared with those previously obtained in Table I-2. In general, good agreement was observed except for the yield-strength values.

General

The Japanese[18] have studied Al–U alloy production by the direct reduction of UF_4 with aluminum. The main reaction is $UF_4(solid) + xAl(liquid) = UAl_{x-4/3}(liquid) + \frac{4}{3}AlF_3(solid)$. This reaction readily

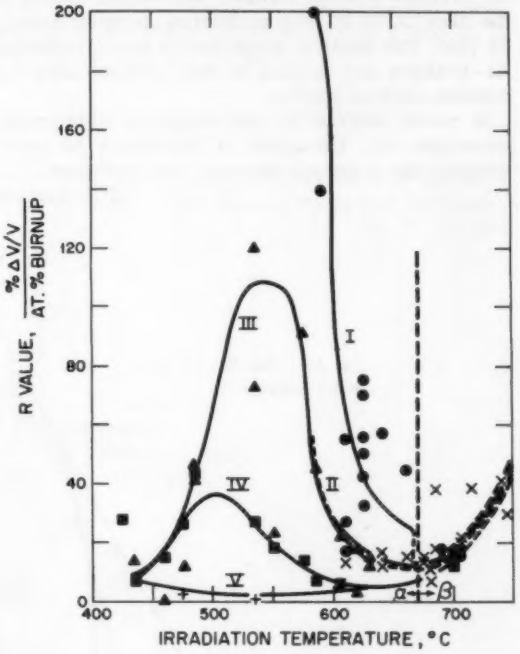

Fig. I-3 Temperature dependence of swelling for high-purity uranium and dilutely alloyed uranium for burnups of 0.2 at.% or less.[16] ●, curve I, high-purity, low-carbon uranium containing 64 ppm Fe, 5 ppm Al, 25 ppm Si, 6 ppm C, and 8 ppm N; ×, curve II, high-purity, high-carbon uranium containing 54 ppm Fe, 10 ppm Al, 34 ppm Si, 480 ppm C, and 24 ppm N; ▲, curve III, U + Fe–Si (uranium containing 140 ppm Fe, 25 ppm Al, 95 ppm Si, 400 ppm C, and 14 ppm N); ■, curve IV, U + Fe–Al–Si–standard (uranium containing 407 ppm Fe, 645 ppm Al, 85 ppm Si, 500 ppm C, and 23 ppm N); +, curve V, U + Fe–Al–Si–stabilized.

Table I-2 TENSILE PROPERTIES[17] OF WROUGHT U–2 WT.% Mo–2 WT.% Zr–2 WT.% Nb–0.5 WT.% Ti

	Frankford results,* specimens solution treated 16 hr at 1700°F				Army Materiel Research Agency results†			
					Extruded specimens	Specimens solution treated 4 to 8 hr, water quenched		
Specimen diameter, in.	0.252	0.252	0.252	0.505	0.252	0.252	0.252	0.252
Aging temperature, °F	500	600	600	600		400	500	600
Aging time, hr	4	5	6	6		4–8	4–8	4–8
Strength, 1000 psi								
Ultimate tensile	190	227	228	226	239	175	189	232
Yield (0.1% offset)	ND‡	224	224	ND	188	140	174	194
Elongation in 1-in. gauge length (except where noted), %	6.5	3.0	3.5	1.0§	3.9	6	4	3
Hardness, R_C	43	46–47	46–47	46–48	45	39	43	46

*Average of two tests. †Average of four tests. ‡Not determined. §2-in. gauge length.

goes to the right at 900 to 1200°C, and UF_4 is reduced to form Al–U alloy. The AlF_3 formed becomes AlF by the reaction, $AlF_3(solid) + 2Al(liquid) = AlF(gas)$; the equilibrium constant for this reaction is $\log K_2 = -22.157 - 33.810/T$. Thus, by the direct reduction under atmospheric pressure, followed by the redis-solution at a reduced pressure of 900 to 1200°C, fluorine is evaporated as AlF. The overall yield for the direct reduction is 90%, compared with 85% for the uranium-addition method. The carbon content in the alloy is 30 to 70 ppm; fluorine is approximately 30 ppm. The physical properties of direct-reduction Al–U alloys are as good as those obtained using the uranium-addition method.

A recent addition to the continuing bibliography concerned with the effect of irradiation on solid-uranium-based nuclear fuels has been published.[19]

(M. S. Farkas)

Plutonium

Plutonium Metal and Alloys

Argonne is continuing work on the development of metallic fuel alloys for fast-breeder applications with emphasis on U–Pu–Ti and U–Pu–Zr alloys. Properties of these alloys are summarized in an Argonne report.[20] The preliminary results of the postirradiation examination of U–18.5 wt.% Pu–14.1 wt.% Zr and U–15 wt.% Pu–10 wt.% Ti alloys irradiated to burnups of 12.5 and 10.7 at.%, respectively, have been reported.[21,22] The alloys were jacketed in a V–20 wt.% Ti alloy. Maximum jacket temperatures during irradiation were 655°C for the U–Pu–Zr alloy and 630°C for the U–Pu–Ti alloy. On the basis of neutron radiography during the course of the irradiation, the U–Pu–Zr alloy elongated 3% at 4.2

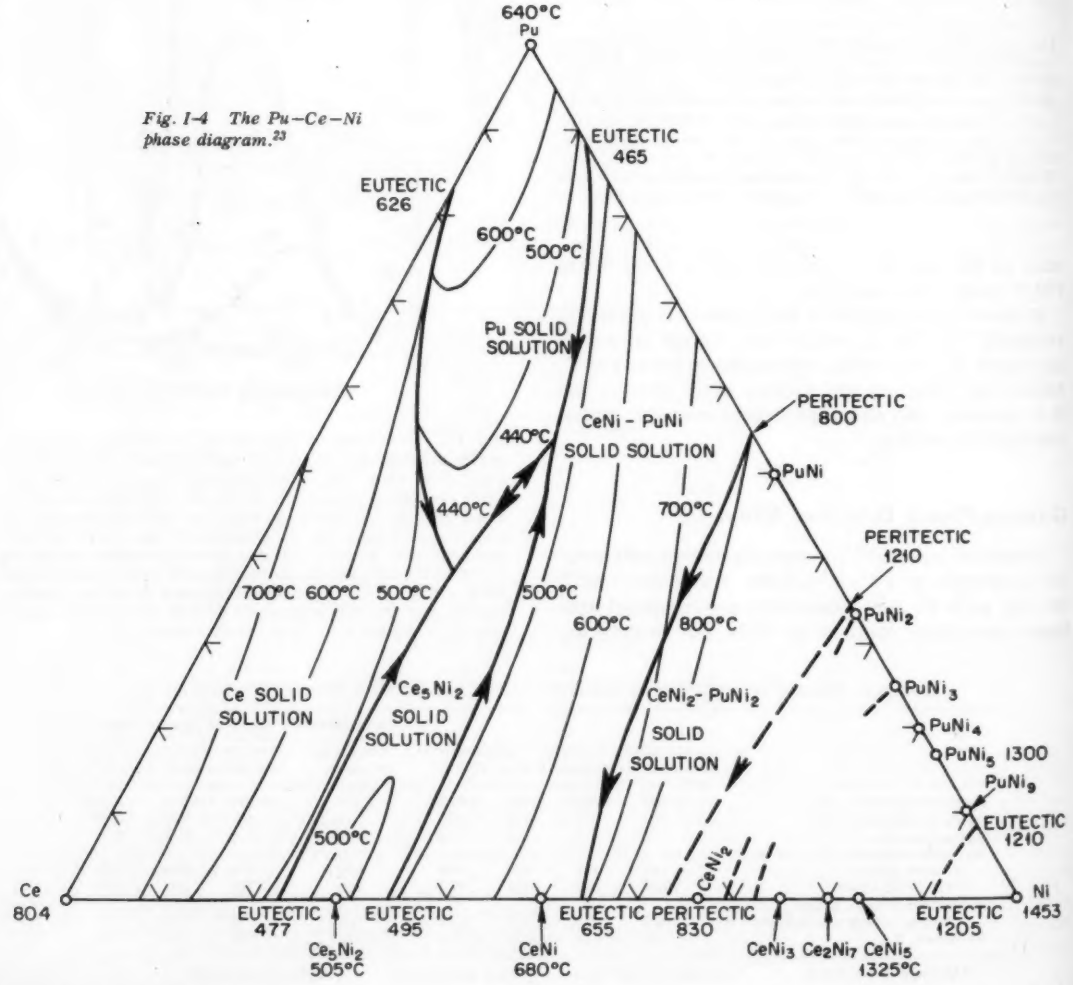

Fig. I-4 The Pu–Ce–Ni phase diagram.[23]

at.% burnup and did not change in length throughout the remainder of the irradiation. The U–Pu–Ti alloy elongated 14% at 4.6 at.% burnup and did not elongate further as burnup progressed. Jacket-diameter changes at the end of irradiation were very small. Metallographic examination showed that fission-gas bubbles in the U–Pu–Zr alloy were interconnected and that the fuel was cracked radially. Porosity in the U–Pu–Ti alloy was found to be finer, and no cracks were observed.

Mound has completed studies of phase equilibria in the Pu–Ce–Ni and Pu–Ce–Fe systems.[23] The phase diagrams for the systems, as determined by metallography, differential thermal analysis, electron-microprobe X-ray analysis, and X-ray diffraction, are shown in Figs. I-4 and I-5. Initial studies of the Pu–Y–Gd and Pu–Y–Nd systems indicate that the maximum solid solubility of plutonium is between 20 and 30 at.% in each system. A small endothermic reaction found in high-purity plutonium at 110°C has been attributed to relief of stresses in the metal and is probably accompanied by the formation of a small number of microcracks. The heat capacities of delta, delta-prime, and epsilon plutonium have been determined to be 8.76, 8.50, and 8.06 cal/(gram atom)(°C), respectively.

Los Alamos investigators[24] have measured the solubility of thulium in liquid plutonium in the temperature range 700 to 1000°C. Solubility increased from 1.67 wt.% thulium at 700°C to 6.15 wt.% thulium at 1000°C. The data fit the equation

$$\log N_{Tm} = 0.736 - 2.28 \times 10^3 \, T^{-1}$$

where N_{Tm} is the solubility expressed as the mole fraction, and T is the temperature in degrees Kelvin.

(V. W. Storhok)

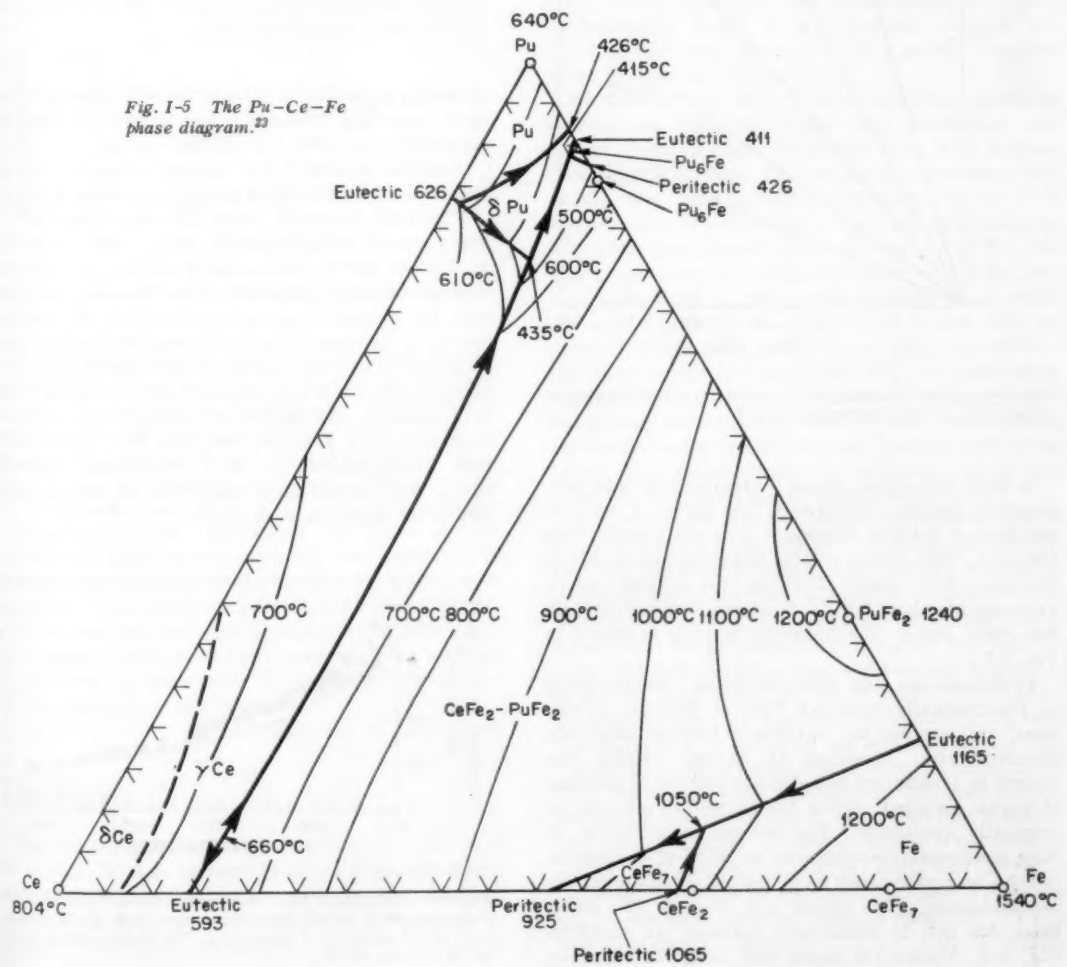

Fig. I-5 The Pu–Ce–Fe phase diagram.[23]

Plutonium Compounds

Harwell[25] has studied the thermal stability of plutonium oxycarbides in vacuo at 1500°C. The volatility as a function of oxygen content reaches a maximum at the approximate composition $PuC_{0.5}O_{0.5}$ due to its decomposition into plutonium metal and CO. As shown in Fig. I-6, the compound loses more than half its weight in 10 hr at 1450°C.

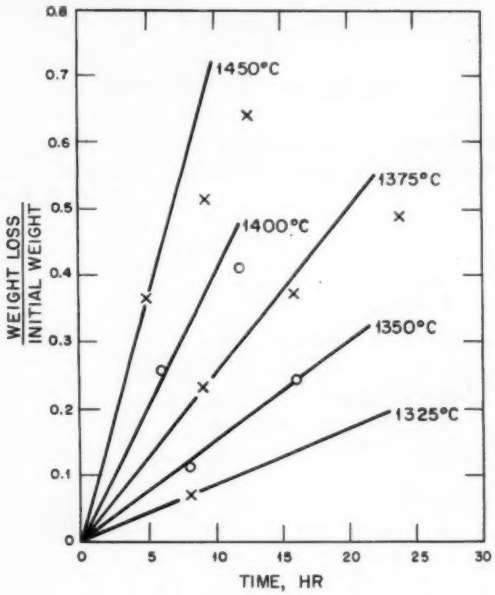

Fig. I-6 Effect of time and temperature of heating of ~$PuC_{0.5}O_{0.5}$ on its evaporation rate.[25]

A $BeO-UO_2-PuO_2$ ternary diagram has been proposed by Battelle–Northwest.[26] As expected, BeO did not form a ternary compound or solid solution with $(Pu,U)O_2$. The lowest solidus in the system is that of the $BeO-PuO_2$ binary (2135°C). The solidus can be expressed to about 2000°C if oxygen loss occurs from the PuO_2 phase. The proposed ternary is shown in Fig. I-7.

Preirradiation and postirradiation measurements on pneumatically impacted PuO_2 at Battelle–Northwest[27] indicate that the increase in thermal diffusivity observed after annealing in earlier studies was caused by irradiation self-damage and not by residual stresses incurred during the impaction process as originally speculated. The thermal conductivity of PuO_2 pneumatically compacted to 93.3% of theoretical density was calculated from the observed diffusivity measurements. The values are roughly 10% above those for UO_2 of comparable porosity, as shown in Fig. I-8. Figure I-9 shows that complete recovery

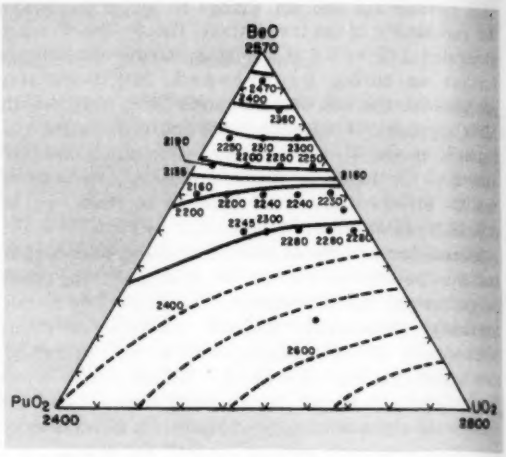

Fig. I-7 Proposed $BeO-PuO_2-UO_2$ ternary showing melting point corrected for oxygen loss.[26] *(Temperatures in °C; compositions in mole fractions.)*

of lattice expansion in irradiation-self-damaged PuO_2 upon annealing does not occur unless the annealing temperature is 1000°C or above.

Argonne reports[28] that iridium appears to be the least reactive refractory metal for containing PuO_2.

Plutonium arsenide, PuAs, has been prepared[29] by the reaction of decomposed PuH_{2-x} with arsine gas at 250 to 300°C. Preliminary studies indicate that this is the only compound in the Pu–As system and that its melting point is near 2450°C. In practice, plutonium hydride is not completely eliminated on the first cycle. Further cycles of decomposition and reaction with arsine are required until all the hydrogen is eliminated. Decomposition temperatures for successive cycles are 400, 600, and 700°C. The cycle with decomposition at 700°C is repeated several times. The temperature range for the arsine reaction is the same for each cycle.

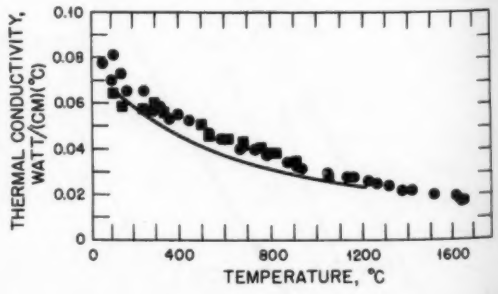

Fig. I-8 Calculated thermal conductivity[27] *for PuO_2. ●, PuO_2 sample 1, 83.3% theoretical density; ■, PuO_2 sample 2, 93.3% of theoretical density; —, UO_2 (ORNL data), 93.4% of theoretical density.*

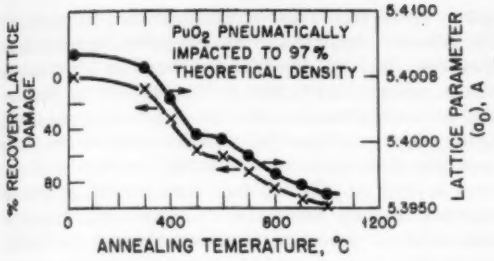

Fig. I-9 Recovery of alpha-self-irradiation damage in PuO_2 after isothermal anneals at several temperatures.[27]

Argonne[28] has measured the thermal diffusivity of pressed and sintered 93% dense PuC. The calculated thermal conductivity, shown in Fig. I-10, is considerably lower than that reported by earlier investigators between 200 and 400°C.

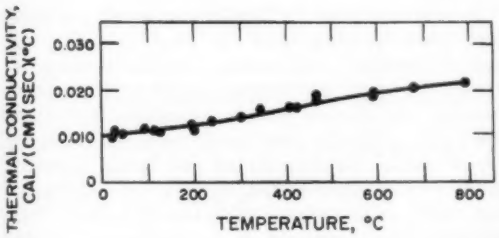

Fig. I-10 Thermal conductivity of plutonium monocarbide.[29]

The irradiation behavior of pneumatically impacted, physically mixed UO_2-PuO_2 fuel rods is being studied in the Plutonium Recycle Test Reactor (PRTR).[30] The results show that the power to produce melting in vibrationally compacted fuel (20 to 21 kw/ft for UO_2–2 wt.% PuO_2 fuel rods operating under PRTR operating conditions) is about 20% less than that for sintered-pellet fuel. Plutonium migration, as observed by alpha autoradiography, was observed in molten core defected rods, whereas no evidence of migration was noted in nondefected rods. Fission-gas-release results show a maximum of 92% (Xe + Kr) release from rods that operated at an average temperature of about 2200°C (60 to 65% of the radius molten) at a power of 27 kw/ft.

(D. F. Askey and W. M. Pardue)

Thorium

The postirradiation examination[16] of a Th–2.5 wt.% U–1 wt.% Zr fuel element (1.75 in. in outside diameter by 1.05 in. in inside diameter by 8 in. long and coextrusion clad with 0.025-in.-thick Zircaloy-2) at Battelle–Northwest revealed a change in volume of 1.6% with a burnup of 1.5 at.%. A substantial increase in the ^{233}U isotopic content of the fuel during irradiation demonstrated the attractiveness of thorium as a fertile material. Tests of fuel elements still in-pile show that a volume change of 2.5% is being realized at 1.74 at.% burnup for this same alloy.

(R. L. Martin)

Metal–Ceramic Fuels

Dispersion Fuels (Less Than 50 Vol.% Ceramic Phase)

The PM-1 type fuel elements have been characterized and evaluated at Oak Ridge National Laboratory[31] using spare nonirradiated elements to better define the as-manufactured physical characteristics for comparison. This study obtained information on cladding–fuel bonding, interface contamination, fuel-particle stringering and fragmentation, cladding grain size, fuel homogeneity, and dispersion density. The contamination found at the interface between the cladding and core prevented grain growth in some areas in these fuel elements.

Workers at Oak Ridge[32] have reported a swelling phenomenon that they found when fabricating Advanced Test Reactor (ATR) and High Flux Isotope Reactor (HFIR)-type fuel elements containing dispersed UAl_3 in aluminum. The cores for the ATR contain about 28 vol.% UAl_3 (–170 + 325 mesh) blended with aluminum powder and cold pressed at 22.5 tsi. The green-pressed 0.5-in.-diameter by 0.5-in. pellets were found to swell approximately 8% in height but only slightly in diameter when vacuum sintered at 590°C. Since very little volume change occurs when the UAl_3 particles convert to UAl_4, the swelling is thought to result from the particles changing shape during the conversion of UAl_3 to UAl_4, thus forcing the mechanically bonded aluminum grains apart in the pellet. This shape change and wedging process was observed by using a heated stage metallograph.

A new type of dispersion-fuel characterization is being initiated at Oak Ridge.[33] Although no correlation has been made with the subsequent irradiation performance of the fuel, a suitable method of quantitatively evaluating fragmentation and stringering in dispersion plates containing irregular as well as spherical fuel particles was established. In place of using the point count or line methods of evaluating particle stringers or fractures, a fragmentation ratio was measured by counting the small fragments generated from the original particle during fabrication. This technique was successfully demonstrated by evaluating the propensity of three different commercial grades of U_3O_8 powder to fragment and stringer during plate fabrication. It was found that the resistance of the oxide to fragmentation and stringering varied with oxide density, particle sphericity, surface area, and particle spacing. (D. E. Lozier)

Coated-Particle Fuels

Particle Coating

Workers at Oak Ridge are continuing the development of graphite-base fuel concepts involving pyrolytic carbon (PyC)-coated fuel particles for gas-cooled power-reactor applications. The effect of varying deposition conditions on coating properties with propane as the carbon source was studied systematically in a 1-in. fluidized-bed reactor provided with a stationary axial probe.[34-37] Coatings deposited at 1200°C, at a propane-supply rate of 3.2 cm^3/min per square centimeter of bed surface area, were comparable in density and anisotropy to coatings deposited from methane at temperatures in excess of 2000°C. The thicknesses of the coatings formed on the stationary probe were indicative of the coating deposition rates within the fluidized bed. In general, at low coating temperatures, the probe indicated a uniform deposition rate throughout the fluidized bed. At higher temperatures and low propane-supply rates, the coating formed primarily on particles in the lower part of the fluidized bed, whereas at both intermediate and high temperatures with the highest propane-supply rates, the zone of maximum deposition appeared to be shifted upward. The trends in coating thickness noted in the probe work emphasize the nonuniformity of coating rate in a fluidized bed under certain conditions.

Oak Ridge has also examined the deposition of SiC on fuel particles.[38] A series of coatings was prepared at 1500 and 1600°C with SiC deposited from hydrogen–methyl trichlorosilane mixtures at deposition rates of >2 μ/min and at deposition efficiencies of 70%. The dense SiC coatings (3.17 g/cm^3) protected fuel particles heated in air at 1000°C for at least 12 hr.

General Atomic has coated fuel particles with SiC to provide material for basic irradiation studies.[40] It was noted that the SiC deposition was easily accomplished at 1400 to 1800°C with hydrogen–methyl trichlorosilane mixtures to yield a beta SiC having moduli of rupture ranging from 70 to 120×10^3 psi in the as-deposited condition and a modulus of 140×10^3 psi for lapped samples. Deposition of ZrC is being investigated; however, the deposition rate has thus far not been reproducible. Development of the ZrC coating process is continuing since irradiation data on ZrC as well as SiC are encouraging. The fractional-release values for barium and strontium at 1400°C for the carbide-coated particles are typically 100 to 1000 times less than values obtained with PyC-coated particles (typical fractional-release values for PyC at 1400°C for 10 hr are in the range of 10^{-2} to 5×10^{-4}).

Workers at Battelle–Columbus[41] are continuing the development of the deposition of graphite on fuel particles by precipitation from carbon-saturated nickel baths. Some deposition of graphite on fuel particles has been accomplished by the precipitation technique. However, further development work is required to attain reproducibility and to circumvent the deposition of discontinuous coatings. Another approach to preparing a graphite-coated particle has shown some promise. A 3-layer coating of PyC–nickel–PyC has been applied to UO_2 and then heat-treated at a temperature slightly above the C–Ni eutectic. The purpose was to promote the dissolution by the nickel layer of the more soluble PyC and precipitate graphite. The X-ray diffraction patterns obtained on particles heat-treated for 40 min at 1340 to 1370°C and having the character of a considerable portion of both PyC layers altered showed them to be graphite with a crystallite size of about 500 A.

(N. D. Veigel)

Irradiation and Evaluation of Coated-Particle Fuels

A recent survey by General Atomic[42] has shown that coated-particle fuels are being used in all the high-temperature, gas-cooled, stationary power reactors (or major gas-cooled reactor experiments) in America and Europe. Briefly, monolithic PyC-coated $(Th–U)C_2$ particles are being used, with different Th–U ratios, for both fertile and fissile materials in the Peach Bottom HTGR, the first operating prototype power reactor to use coated-particle fuels. These particles are supported in a hot-pressed graphite matrix, which operates at an average temperature of 980°C (1330°C maximum).

The Public Service Company of Colorado HTGR will use BISO (Buffer-Isotropic) PyC-coated $(Th–U)C_2$ (fissile) and ThC_2 (fertile) particles. The fuel will be located in vertical channels dispersed within hexagonal graphite blocks. The average fuel temperature will be 815°C (1260°C maximum).

The Dragon experimental reactor (operated by the Organization for Economic Cooperation and Development) has used primarily (Zr–U)C particles with interrupted-laminar PyC coatings and UC-10 particles with PyC–SiC–PyC coatings. The particles are contained in resin-bonded graphite-fuel compacts and operate at a maximum temperature of 1250°C. The Ultra High-Temperature Reactor Experiment (UHTREX) is fueled with triplex-coated UC_2 particles supported in extruded graphite annular cylinders. The uranium from the damaged particles on the surface of these extrusions is removed by acid leaching. This fuel will operate at an average temperature of 1430°C (1590°C maximum). The German Arbeitsgemeinschaft Versuchsreaktor (AVR) is a prototype pebble-bed reactor. The fuel elements are machined graphite spheres (6 cm in diameter) filled with a dispersion of duplex PyC-coated UC_2 particles in a carbonaceous matrix. The maximum operating temperature of this fuel will be 1250°C. Plans are in progress for a

Thorium Hochtemperature Reaktor (THTR) of a similar concept using coated U–Th fuel. The UKAEA Advanced Gas-Cooled Reactor (AGR) is considering switching its design from stainless-steel-clad UO_2 fuel elements to SiC-matrix elements containing fuel particles with PyC–SiC–PyC coatings. This change would permit significantly higher operating temperatures for this reactor.

The experimental work in this country has been directed primarily toward evaluation of coated fuels for the General Atomic HTGR's and the German AVR (the first charge for the AVR is being produced in this country). A large number of irradiations conducted by Oak Ridge[38] and General Atomic[43,44] at temperatures to 1900°C, burnups to over 50% of the fissionable atoms, and fast-flux exposures to 2.7×10^{21} neutrons/cm^2 have produced data that permit design for specific environmental conditions and show that coated-particle fuels can perform within the HTGR specifications. Commercially prepared prototype AVR fuels spheres have been tested in-pile at Oak Ridge[45] at 1300°C to 10 at.% burnup with no observed coating failure and ^{88}Kr release fraction of 4×10^{-5}, well within the AVR design criteria.

The present emphasis is on optimizing the coated-particle fuels for specific applications, and the Prados–Scott mathematical model for predicting coated-fuel performance is being applied by Oak Ridge[34,46] for this purpose. For evaluating the model, a sample of coated-particle fuel which the model predicted would begin to fail at 15 at.% burnup at 1400°C showed coating failure to begin at slightly over 15 at.%. On continuing the exposure, the failure approaching 20 at.% burnup was found to be less severe than the model predicted, indicating it to be conservative. An addition has been made to the model to account for radiation-induced creep in the PyC coatings which will tend to offset the fast-neutron-induced shrinkage stresses which occur at high fast-neutron exposures such as will be undergone by the coatings on the long-residence fertile particles.

(N. E. Miller)

Uranium and Thorium Oxide Fuels

Properties and Behavior

Belle and coworkers[47] at Bettis Atomic Power Laboratory have reported results of thermal-conductivity measurements on ThO_2, UO_2, ThO_2–UO_2, ZrO_2–UO_2, and ZrO_2–CaO–UO_2. Some of these results are summarized in Table I-3. Figure I-11 shows various data for the UO_2–ThO_2–O_2 system, and Fig. I-12 shows the effect of composition and density on the thermal conductivity of ThO_2–UO_2 solid solutions.

Table I-3 THERMAL-CONDUCTIVITY CONSTANTS* FOR OXIDE FUELS[47]

Material	A_0, (hr)(ft)(°R)/Btu	$B_0 \cdot 10^4$, (hr)(ft)/Btu	N_0, (hr)(ft)(°R^2)/Btu	X_0, (hr)(ft)(°R^2)/Btu	Z_0, (hr)(ft)(°R)/Btu
UO_2	0.116	1.88	6.23	49.82	0.0139
ZrO_2–UO_2 (below 3000°F)	0.787	0	6.23	49.82	0.0139
ZrO_2–UO_2 (above 3000°F)	0.116	1.88	6.23	49.82	0.0139
ZrO_2–UO_2–CaO (below 2500°F)	0.666	0	6.23	49.82	0.0139
ZrO_2–UO_2–CaO (above 2500°F)	0.116	1.88	6.23	49.82	0.0139
ThO_2	0	2.21	6.23	49.82	0.0139
ThO_2 + 10 wt.% UO_2	0.0225	1.78	6.23	49.82	0.0139

*The given values represent the constants in the equation

$$K_P = \left(\frac{1-P}{1+\beta P}\right)\left[\frac{1}{A_0 + B_0 T + (N_0/T) + (X_0/T) + FZ_0\,(1386/T)}\right], \text{ Btu/(hr)(ft)(°R)}$$

where K_P is the thermal conductivity, at temperature T(°R) and fission depletion $F(10^{20}$ fission/cm$^3)$, of an oxide fuel having a fractional total porosity, P.

The ejection of uranium atoms from sintered UO_2 surfaces during neutron irradiation has been studied by Italian investigators.[48] It was found that an average fission fragment leaving the surface ejects from 7000 to 50,000 uranium atoms from sintered UO_2 with a grain size greater than 1 μ. Results obtained by other investigators are summarized in Table I-4 for

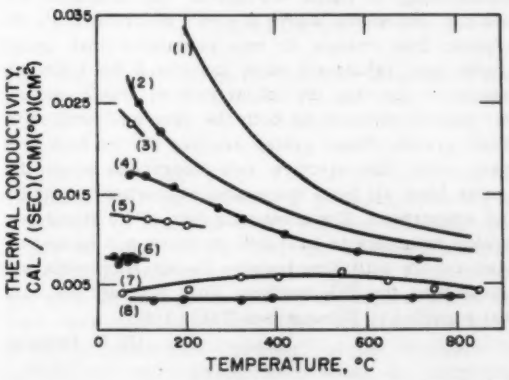

Fig. I-11 Thermal-conductivity data for various compositions in the UO_2–ThO_2–O_2 system.[47] (1) $ThO_{2.0}$, (2) $UO_{2.00}$, (3) UO_{2+x}, (4) $Th_{0.9}U_{0.1}O_{2+x}$, (5) $Th_{0.74}U_{0.26}O_2$, (6) $UO_{2.18}$, (7) $Th_{0.74}U_{0.26}O_{2+x}$, (8) $Th_{0.69}U_{0.31}O_{2+x}$

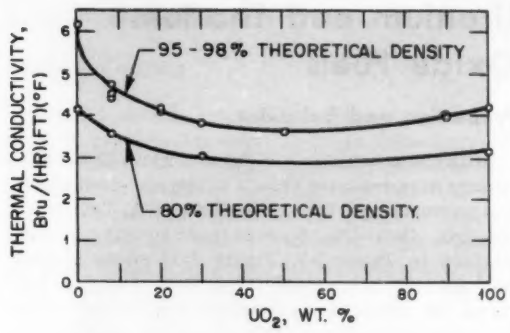

Fig. I-12 Effect of composition and density on the thermal conductivity of ThO_2–UO_2 solid solutions.[47]

very nearly theoretical densities and a wall thickness of the order of 0.6 mm. No data are available as to the deflocculents utilized or the slip *p*H values required in the process. From the high sintering temperature employed, one must assume that densification was accomplished in either a vacuum or reducing atmosphere. If this is the case, the final product probably does not contain a stoichiometric oxygen content.

Matzke at Chalk River[51] has studied the effect of TiO_2 additions on the sintering behavior of UO_2. Quantitative metallography and the measurement of the gas release following high-dose ion bombardment revealed that small amounts of titanium are soluble in UO_2. It was believed that reduction of TiO_2 and interstitial solutions of titanium ions resulted in disorder of the UO_2 lattice, thus increasing the diffusion rate of the uranium ion. Similar experiments are being conducted on $ThO_2 + TiO_2$. (T. R. Wright)

Table I-4 URANIUM EMISSION FROM URANIUM AND URANIUM DIOXIDE SURFACES BY NEUTRON IRRADIATION[48]

Emitting material	Atoms emitted/outgoing fission fragment	Investigation
Oxide-free uranium metal	1,200	Lapter and Ershler, *Soviet Journal of Atomic Energy*, 1: (1956)
Superficially oxidized metal	24	Lapter and Ershler, *Soviet Journal of Atomic Energy*, 1: (1956)
Oxide-free uranium metal	1,000	Rogers, British Report AERE-R-3908
Vacuum-deposited UO_2	50,000	Rogers, British Report AERE-R-4793
Sintered UO_2	5	Nilsson, Swedish Report AE-136

comparison purposes. Additional measurements by Rogers[49] in England have also been reported for sintered UO_2 pellets undergoing neutron irradiation. During the early part of the irradiation, about 110 uranium atoms were ejected for an average fission product leaving the surface. This then decreased continuously to about 4.5 atoms per fragment for neutron exposures above 5×10^{16} neutrons/cm^2. To explain this change it was postulated that small grains are vaporized when traversed by a fission fragment and that the initial rate of atoms ejected per fission depends on both the size and number of these grains. Small grains account for the high primary rate; the ejection rate decreases when the grains have all been traversed by fission fragments and evaporated. The continuing rate of 4.5 atoms per fission fragment is ascribed to knock-ons caused by hard-sphere collisions between fission fragments and atoms near the UO_2 surface. This rate agrees with that reported by Nilsson (see Table I-4).

(R. H. Barnes)

Fabrication

German investigators[50] are preparing thin-walled, vacuum-tight tubes of thorium dioxide by slip casting. Sintering at 2100°C results in bodies having

Uranium Carbides, Nitrides, Phosphides, and Sulfides

Properties and Behavior

The ternary system U–C–Si possesses quasi-binary ties[52] from SiC to U_2C_3, UC, USi_3, USi_2, and U_3Si_5 and from UC to SiC, U_3Si_5, U_3Si_2, and U_3Si. Ternary compounds or ternary eutectics exist at the approximate compositions $U_3C_3Si_2$ and $U_{20}C_3Si_{16}$. U_3Si_2 apparently dissolves up to 4 at.% carbon and this solvent phase is one product of a peritectoid reaction[53] between UC and U_3Si at 815°C:

$$U_3Si + UC \rightleftharpoons U_3(Si,C)_2 + U$$

This reaction eliminates the UC to U_3Si quasi-binary tie at temperatures above 815°C and introduces a new tie from U_3Si_2 to uranium metal.

Since it is well known that complete solution[54] exists between UC and UN and between UC and PuC, a re-

cent finding that complete solution exists between UN and PuN and between UC and PuN makes it virtually certain that the quasi-quaternary system UC–UN–PuN–PuC forms a continuous, complete solid solution (U,Pu)(C,N). The solubility of oxygen in UN is found to be 6 mole %, i.e., $U(N_{0.94}P_{0.06})$; the solubility of oxygen in PuN is found to be 16 mole %, i.e., $Pu(N_{0.84}O_{0.16})$. A thermodynamic analysis of the U–C–N–O system, including a comparison of thermodynamic predictions with data of the above type and source, has been published by Imoto and Stöcker.[55]

The reactions of refractory metals with UC and UC–ZrC have been studied at General Atomic.[56,57] Tungsten does not react with UC or UC–ZrC at 1800°C; but, after 1000 hr at 2000°C, UC–ZrC reacted in a limited fashion with tungsten to produce isolated tungsten-rich and uranium-rich phases in the carbide. No uranium or zirconium was detected in the tungsten. Rhenium did not react with hyperstoichiometric UC at 1800°C but did react with nominally stoichiometric UC. Reactions between rhenium and UC–ZrC were observed at 1400, 1600, and 1800°C. At 1800°C two layers, one rich in rhenium and uranium and the other rich in zirconium and uranium, were formed between rhenium and UC–ZrC. Tungsten–25 wt.% rhenium alloy was found to react in the same manner as rhenium. Molybdenum did not react with UC–90 mole % ZrC at 1800°C.

In agreement with the above compatibility data, General Atomic found that slightly hyperstoichiometric UC–90 mole % ZrC clad with vapor-deposited tungsten maintained stable electron-emission characteristics for at least 1000 hr at 1900°C but that emission characteristics degraded at 2000°C.

In the course of studies of the extrusion of UC at high temperatures, Accary, Magnier, and Marchal[58] have obtained elongation data that confirm the drastic weakening effect of liquid uranium on UC. Figure I-13 shows that at 1900°C and under a stress of 270 kg/cm^2, a large gap appears between the elongation-vs.-time curves of U–4.56 wt.% C and of U–4.72 wt.% C alloys. Assuming that (1) there is no free uranium in the 4.72 wt.% carbon alloy, (2) the alloy contains no oxygen or nitrogen, and (3) the carbon analysis is accurate, these data seem to provide a reasonably good measure of the limit of solubility of uranium in UC at 1900°C. Figure I-14 is a plot of the same data as a function of carbon content and includes data for a U–4.6 wt.% C alloy, thereby narrowing the unknown region slightly. Figure I-15 shows the creep (elongation vs. time) behavior of a U–5 wt.% C alloy at a stress of 270 kg/cm^2 at temperatures from 1600 to 2300°C.

Samples of hypostoichiometric UC showed essentially no change in the microstructure after an irradiation to 20,000 Mwd/metric ton of uranium at temperatures[59] of 870 to 980°C. However, after receiving this exposure, some of these samples were subjected to an excursion to 1650 to 2500°C for a

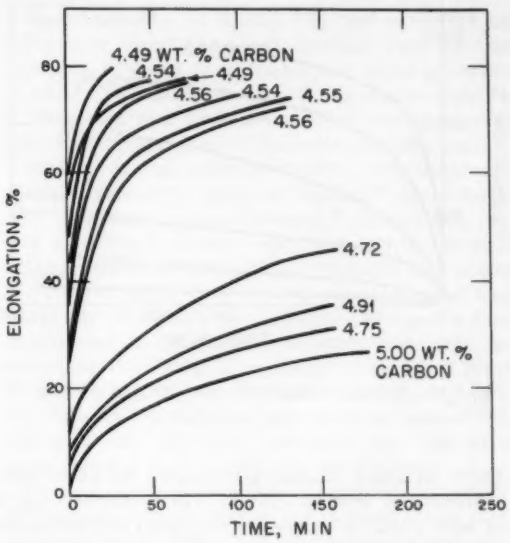

Fig. I-13 Elongation as a function of time for various U–C alloys.[58]

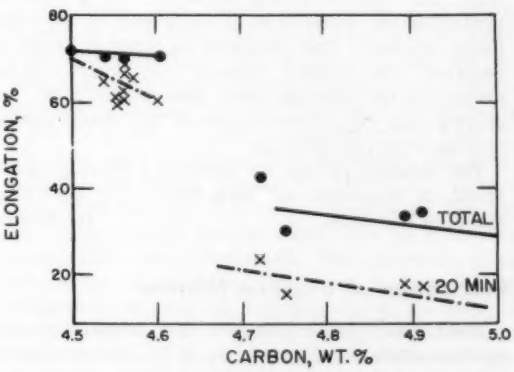

Fig. I-14 Effect of carbon content on the elongation of U–C alloys.[58]

period of less than 12 hr. The microstructure of the resultant material showed UC grains surrounded by a network of uranium metal; but each UC grain contained two regions. The majority of each grain contained fine porosity. A smaller region, generally on the side of each grain toward the center line of the fuel, was essentially void free. An irregular grain boundary suggested "pinning" of the boundary by bubbles or other precipitates while the nonporous zone was being formed.

The large, porous region of each grain is believed to represent that remnant or old part of the UC grains present during the irradiation at 870 to

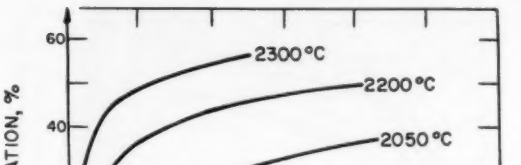

Fig. I-15 Effect of temperature on creep of U–5 wt.% C alloy.[58]

980°C in which bubbles grew during the 12-hr heat-treatment at 1650 to 2500°C. The nonporous region of each grain is believed to represent crystallization of new UC at 1650 to 2500°C. This new UC would contain essentially no fission gas. The crystallization of new UC occurred at 1650 to 2500°C as a result of the thermal gradient by solution of UC by liquid uranium from the outward-facing surfaces and growth of inward-facing surfaces by precipitation of UC from liquid uranium. The presence of liquid uranium is required. The bubbles "pinned" the boundaries by preventing the uranium from dissolving old UC, not by retarding the growth of new UC by crystallization on inward-facing surfaces.

The dilation of various refractory thorium compounds at temperatures[60] from 800°C up to 2100°C is shown in Fig. I-16. (W. Chubb)

Fabrication of Uranium Nitrides

Nishiyama[61] and coworkers have investigated the synthesization and the sintering of UN. The procedure utilized for the synthesization of UN powder was the standard hydride–dehydride gas reaction of uranium metal to produce uranium powder followed by nitriding with either nitrogen gas or ammonia to obtain the nitride powder. The effects of temperature and atmosphere on the sinterability of the UN power were examined, yielding the following results: (1) in vacuum, a density of 91.7% of theoretical could be obtained with no free uranium present, (2) at 1900°C in vacuum, free uranium was present, (3) under argon at 2200°C, a density of 89.6% of theoretical was achieved, (4) under nitrogen at 1900°C, a density of 86 to 88% of theoretical was attained, and (5) at 2200°C in a nitrogen atmosphere, densities of 91 to 93% of theoretical were obtained. The nitrogen content of the sintered UN pellets was less than that of the starting powder, and as the temperature was increased, the nitrogen content decreased. The highest

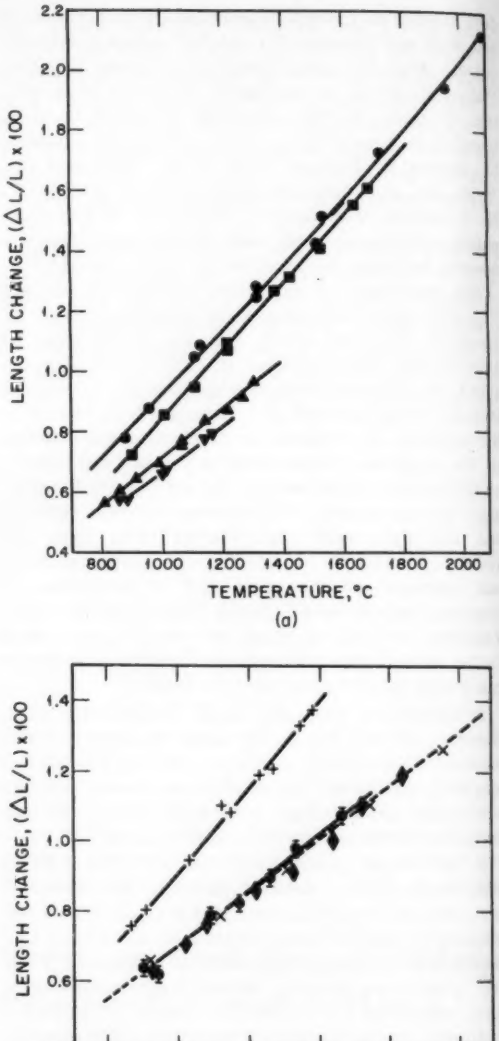

Fig. I-16 Thermal expansion of some refractory thorium compounds.[60] ●, ThO_2; ▲, ThN; ▼, Th_3P_4; ■, ThB_6; +, ThS; ×, $ThP_{0.91}$; ◆, $ThP_{0.71}$; ♣, $ThC_{0.84}$.

nitrogen contents were found in specimens sintered in nitrogen. At Battelle it has been observed that on sintering UN in vacuum at temperatures greater than 1500°C, UN decomposes; however, in a good vacuum the uranium vaporizes as fast as it forms, thus no free uranium is detected metallographically.

Workers at Oak Ridge[62] have been investigating several possible techniques for incorporating a fine

dispersion in UN that might enhance the irradiation performance of this nuclear fuel through the provision of nucleation and pinning sites for fission-gas bubbles. Molybdenum and thorium oxide are being considered as the potential dispersoids. Experiments are being conducted to define the solid-solubility relations below 2300°C that might lead to formation of a fine precipitate dispersion.

Uranium nitride containing a fine dispersant of thorium oxide has been prepared by internal oxidation of solid solutions of (U,Th)N. The (U,Th)N powder was synthesized by the standard technique by hydriding followed by nitriding with a final heat-treatment of 1800°C. This powder could be sintered to 91% of theoretical density by heating to 2300°C under 1 atm nitrogen. These specimens were observed to be single phase by metallographic examination and by X-ray diffraction. Similar powder, with 2 and 5 wt.% UO_2 additions, was sintered under the same conditions as the (U,Th)N powder. The addition of 2 wt.% UO_2 resulted in the oxidation of about 50% of the thorium in the nitride phase, whereas the addition of 5 wt.% UO_2 resulted in oxidation of about 80% of the thorium. The microstructure of sintered samples containing 2 wt.% UO_2 exhibited a small amount of white oxide phase well distributed within the nitride grains, whereas that of the specimen containing 5 wt.% UO_2 showed a greater concentration of the oxide phase throughout the specimen that sintered to 97.7% density. A large portion of these oxide dispersoids were fine. It was noted that the grain size of the specimens decreased with increasing UO_2 content. At a magnification of 2000×, the oxide can be seen as very fine particles and as platelets that seem to be crystallographically oriented with respect to the nitride subgrains. (D. S. Acuncius)

Fuel–Water Reactions

The reaction of molten UO_2 with water was investigated at Battelle–Northwest[63] by allowing melted UO_2 samples to fall into water heated to various temperatures. The UO_2 samples were analyzed for degree of oxidation following exposure by coulometric titration. Oxygen-to-metal ratios increased from an average initial value of 2.002 to values between 2.06 and 2.16, depending on the initial water temperature (30 to 250°C). Water temperatures were arbitrarily selected to determine the effects of water temperature on the final results; the temperatures selected were much below those required for oxidation of UO_2. The oxygen-to-metal ratios correspond to a maximum hydrogen generation of 12 ml (STP)/g of UO_2. The only oxidation product that could be determined from X-ray powder-pattern diffraction was U_4O_9. Attempts to measure simultaneous pressure transients, produced by water in contact with molten UO_2, were unsuccessful.

Rapid injection of molten UO_2 into water did not produce a powdered end product; however, the quenched UO_2 was very friable and could be readily reduced to a coarse powder. Tyler screen analyses on three different powdered samples gave essentially identical average particle diameters of 0.062 cm.

Studies of the reaction of UO_2 with water and steam reviewed by Baker of Argonne[64] agree fairly well with those described above.[63] Unclad UO_2 pellets submerged in water were exposed to transient neutron bursts in TREAT.[65] A transient that caused partial melting of UO_2 (2700°C) produced about 6 ml (STP) of hydrogen/g of UO_2 and produced a final composition of $UO_{2.07}$. More energetic transients that vaporized UO_2 (3300°C) produced about 17 ml (STP) of hydrogen/g of UO_2. In these latter experiments, the average composition of reaction product was $UO_{2.19}$. X-ray diffraction analyses gave support to the hypothesis that UO_2 reacted with the water.

General Electric Company[66] continued its investigation of the reaction between steam and UO_2 at temperatures near 1500°C. A thermobalance was employed to gravimetrically determine the extent of reaction. Specimens were solid cylinders (1.27 cm in length by 1.27 cm in diameter) of UO_2, sintered to about 95% of theoretical density at 1700°C for 5 hr in hydrogen. Tests were made in saturated steam flowing at a rate of about 100 mg/min at 1300, 1400, 1500, and 1600°C for 12.5 to 180 min. The test results indicate that the UO_2 remains intact and visually appears unchanged; however, there was approximately a 1 to 2% growth in length and diameter (3 to 6 vol.%). The data show an approximate agreement with parabolic kinetics when plotted vs. the square root of time. However, for long times, there was a leveling off of the weight gain-vs.-time plot as a limiting composition was approached. The parabolic rates determined from these data were plotted vs. the reciprocal of absolute temperature in the form of an Arrhenius plot to give a tentative experimental activation energy of about 65 kcal/mole. Equilibrium compositions for UO_{2+x} in steam at 1300, 1400, 1500, and 1600°C were 2.193, 2.183, 2.174, and 2.166, respectively. The controlling mechanism for the steam oxidation of UO_2 at these temperatures was hypothesized as being lattice diffusion of oxygen through the UO_2 lattice. (J. M. Genco)

Basic Studies of Irradiation Effects in Fuel Materials

Metals

Blackburn[67] has published an extensive review of inert-gas behavior with respect to metals. The general topics covered are adsorption on metals, solubility in metals, permeation through metals,

preparation of solutions of inert gases in metals, metallographic studies on nonfissile metals, metallographic and swelling studies on fissile metals, effects on physical properties, gas evolution on annealing, and miscellaneous aspects. A total of 331 references are listed.

At Harwell,[68] specimens of uranium 50 μ thick and of various compositions have been irradiated at ~400, ~500, 620, and 715°C under conditions in which induced stresses were small. The distribution of porosity was studied after irradiation using the electron-microscope transmission technique. The results showed that the preexisting precipitates did not affect the scale of the bubble distribution and that swelling due to bubbles within the grains was small. It was concluded, therefore, that, under stress-free conditions at burnups of less than 0.2%, there was no large swelling due to the evenly distributed gas bubbles within the grains. It was suggested that bubbles can nucleate homogeneously during irradiation and that observations in this experiment were not in contradiction. The fact that bubbles on dislocation lines and those close to grain boundaries were not larger indicated no shortage of vacancies to allow bubble growth. These results indicate that the bubble density saturates fairly early in the irradiation.

Raetskiy[3] has measured the electrical resistance of alpha-uranium crystals irradiated to 7×10^{18} neutrons/cm^2 (thermal) at about 50°C. The investigation was conducted on pseudosingle crystals, the disorientation angle of the subgrains being 2 to 3°. The electrical resistance was measured by a potentiometric method at −196 and +20°C. The difference in the electrical resistivities of the same crystal before and after irradiation is plotted against direction of the principal crystallographic planes in Fig. I-17. A symmetrical dependence of the change in electrical resistance upon the angle was assumed in the regions between experimental points.

Mass spectrometric techniques are being investigated at General Electric[69] to obtain accurate fuel-burnups analyses. The quantity of nonradioactive refractory fission products produced from a variety of fuels is being measured by using the isotope-dilution technique on stable fission products. In this manner, errors that limit the final accuracy of radiochemical analyses are eliminated. This work involved determination of the absolute ^{233}U thermal fission yields for stable neodymium fission products

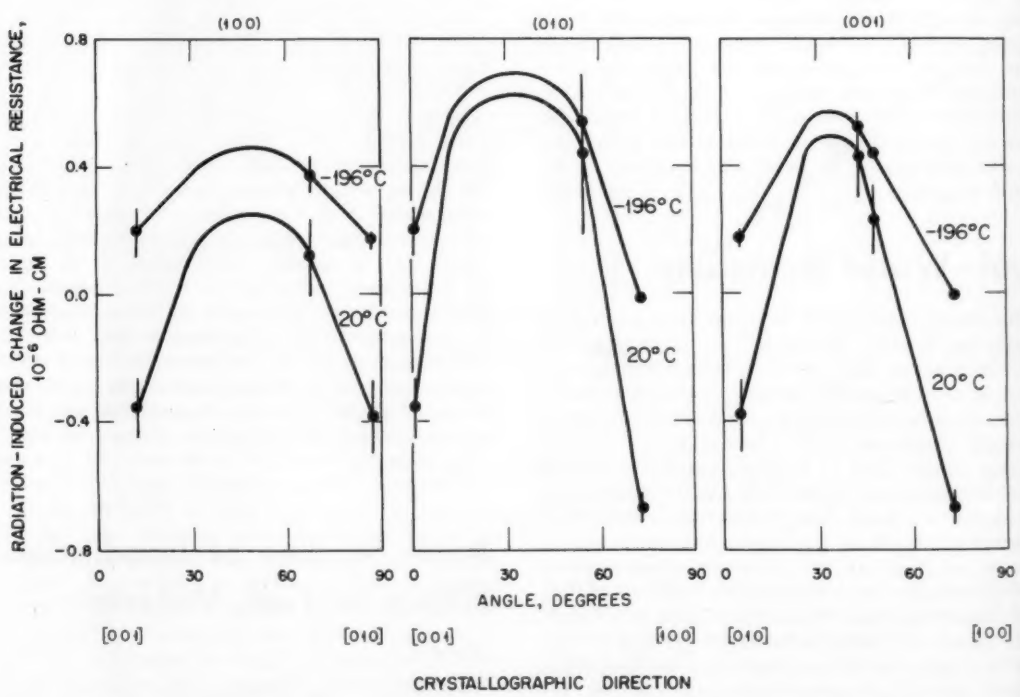

Fig. I-17 Angular dependence of the increase in the electrical resistance of alpha-uranium crystals after irradiation by 7×10^{18} neutrons/cm^2 (thermal).[3]

by isotopic-dilution mass spectrometry on an irradiated capsule containing a known amount of highly enriched ^{233}U. In addition, an eight-laboratory study of the precision of the ^{148}Nd procedure was made. A natural neodymium correction was also devised for application to the unspiked neodymium ratios.

Ceramics

A FORTRAN-IV computer program, FIGRO, has been developed at Westinghouse Electric Corporation[70] for the analysis of fuel volume swelling and the calculation of temperatures in bulk-oxide cylindrical fuel elements. The fuel pellet may be solid or annular, or may contain two radial zones. Oxide-fuel thermal conductivity is a function of temperature, depletion, and porosity; fuel swelling is a function of temperature, depletion, internal hydrostatic pressure, and fissioning rate. As a boundary condition for the heat-condition equation, either the clad surface or the temperature at the inside radius of the fuel may be specified.

Two fuel swelling models are available in FIGRO, although additional models can be programmed with relatively minor effort. The two available models are:

1. A model based on the assumption of a fixed number of fission-gas bubbles and spacing and the applicability of the ideal gas law utilizing a best-fit value for certain constants.

2. A model presented by Greenwood and Speight,[71] modified in FIGRO to utilize the van der Waals equation of state rather than the ideal gas law and to include the restraint of externally applied pressure in addition to the surface-tension restraint of the gas–solid interface. The effect of solid-fission-product formation is also included, as well as an optional provision for the reduction of fuel swelling due to release of fission gases from the matrix.

Chalk River[72] has reported that small additions of trivalent and pentavalent metals to UO_2 affect uranium self-diffusion, but not the release of xenon from lightly irradiated specimens. It appears, therefore, that xenon atoms do not diffuse via single vacancies but rather on interstitial sites or in vacancy clusters.

Optical and electron-microscopic examination[72] of UO_2 irradiated to nearly 1% burnup of the uranium has shown considerable porosity (up to 10 μ in diameter) in the hot regions but almost exclusively at grain boundaries. Electron-microscopic examination of irradiated UC showed considerable porosity within the grains, with the grain-boundary pores increasing in size and number as the irradiation temperature increased. The lower temperature gradients (due to higher conductivity) and larger grain size in the UC both contributed to this difference in behavior. In addition, the distribution of other fission products in irradiated fuels was studied by in situ gamma spectrometry ("gamma scanning") of intact elements, autoradiography of polished sections, and gamma spectrometry of samples taken by coring the fuel or swabbing the sheath.

Microcores from UO_2 fuel have been examined[73] by electron microscopy of direct carbon replicas, with a resolution of $\lesssim$75 A. The small size ($\lesssim$300 A) of intragranular pores in the microcores after a postirradiation anneal for 1 hr at 1750°C was consistent with observations by Whapham.[74] The intragranular pore size could be increased to 500 to 1500 A by annealing for 72 hr. However, in the as-irradiated microcores (irradiation time 3940 hr at a calculated temperature of 1750°C), intragranular pores were much fewer and smaller than those developed in the specimens annealed for 72 hr. Also, the pores were at least an order of magnitude smaller than those predicted from present theories of fission-gas-bubble swelling (e.g., Barnes and Nelson[75] and Gruber[76]).

MacEwan and Stoute[77] have studied the effect of irradiation on the thermal conductivity of UO_{2-x}, UO_2, and UO_{2+x} at 60°C. Equal conductivities were found for unirradiated $UO_{1.97}$ and UO_2 at 60°C, with both conductivities reduced by 30% following an irradiation exposure to 10^{17} fissions/cm^3 at a temperature below 150°C. The reduction in conductivity of $UO_{2.024}$ was less since this structure is already disordered by the presence of excess oxygen. The results indicate that UO_{2-x} and UO_2 are equally susceptible to irradiation damage below 150°C. It is argued that, on the basis of existing experimental evidence, there is an irradiation-induced enhancement of conductivity in UO_{2-x} above 400°C which may be associated with the solution of uranium in the lattice.

A theoretical analysis is being conducted at General Atomic[40] to find accurate values for the release rate of metallic fission products from the core of the HTGR reactors. The mathematical diffusion problem is formulated exactly using the phenomenological theory of thermodynamics of irreversible transport phenomena. The diffusion problem is solved taking into account the full time and space dependence of all variables. There are no restrictions other than those used in the thermodynamic–phenomenological theory of diffusion and those imposed by the accuracy of the input information. (A. J. Markworth)

References

1. H. E. Fotow and D. W. Osborne, Heat Capacity of Alpha Uranium from 1.7 to 25°K, *Phys. Rev.*, 151: 564-570 (Nov. 11, 1966).
2. V. M. Raetskiy, Electrical Resistivity of α-Uranium Crystals in the Temperature Range 67 to 293°K, *J. Nucl. Mater.*, 21: 105-108 (1966).
3. V. M. Raetskiy, Electrical Resistivity of Irradiated α-Uranium Crystals, *J. Nucl. Mater.*, 21: 109-111 (1966).
4. C. M. Walter and L. R. Kelman, The Interaction of Iron with Molten Uranium, *J. Nucl. Mater.*, 20: 314-322 (1966).

5. J. L. Bieber, J. M. Schreyer, and E. L. Williams, Purification of Uranium by Zone-Refining Techniques, USAEC Report Y-1564, Union Carbide Corporation, Nuclear Division, Feb. 7, 1967.
6. D. Duxbury, Improvements in or Relating to the Production of Uranium Metal, British Patent No. 1,033,223, June 22, 1966.
7. G. Ereztu and U. Even, The Wiedeman–Franz Ratio of Metallic Uranium at Elevated Temperatures, *J. Appl. Phys.*, 37: 4633-4634 (December 1966).
8. L. V. Pavlinov, A. I. Nakonechnikov, and V. N. Bykov, Diffusion of Uranium in Molybdenum, Niobium, Zirconium, and Titanium, *J. Nucl. Energy: Pt. A & B*, 20: 1027-1030 (November–December 1966).
9. S. Volman de Tanis and N. H. Ambrosis de Libanati, Strain-Anneal Method of Growing Crystals of Alpha Uranium, *J. Inst. Metals*, 94: 395-396 (November 1966).
10. J. Eisenblater, G. Haase, and F. Granzer, An X-Ray Study of the $\alpha \rightleftharpoons \beta$ Transformation in Uranium (in German), *J. Nucl. Mater.*, 21: 53-60(1967).
11. H. Buehler and H. W. Wagener, Compressive Behavior of Natural Uranium with the Aid of Upsetting Tests (in German), *Z. Metallk.*, 57: 825-830 (November 1966).
12. F. C. Duckworth and M. V. Speight, Evidence for a Helical Crystallographic Texture in Uranium Bars of Magnox-Clad Fuel Elements, *J. Nucl. Mater.*, 20: 307-313 (1966).
13. D. Lazarevic, The Effect of Small Aluminum Additions on the Structure of Uranium–Molybdenum Alloys (in Serbo-Croatian), *Tehnika (Belgrade)*, 3: 515-519 (1966).
14. D. Stewart and G. I. Williams, The Structure and Occurrence of the Metastable Monoclinic, α_b'', in Uranium–Molybdenum Alloys, *J. Nucl. Mater.*, 20: 262-268 (1966).
15. P. Guinet, H. Vaugoyeau, and P. Blum, The Uranium Dioxide–Uranium System at High Temperatures (in French), French Report CEA-R-3060, 1966.
16. F. W. Albaugh, S. H. Bush, J. J. Cadwell, D. R. deHalas, D. C. Worlton, unpublished, Battelle–Northwest, December 1966.
17. M. Myers and R. E. Edelman, Heat Treatment and Mechanical Properties of a U–2% Mo–2% Zr–2% Nb–0.5% Ti Alloy, Report AD-637777, July 1966.
18. Y. Seki and N. Mitamura, Production of Aluminum–Uranium Alloy Nuclear Fuel by Direct Reduction, *Genshiryoku Kogyo*, 11(9): 37-40 (September 1965).
19. A. Nyström, Radiation Effects on Solid, Uranium-Based Nuclear Fuel Materials, Vol. 6, No. 2, A Bibliography, AEC file No. NP-16522, December 1966.
20. L. E. Link, J. E. Ayer, D. K. Butler, K. A. Hub, W. B. Lowenstein, W. J. Mecham, D. Meneghetti, D. H. Thompson, V. G. Trice, Jr., and J. T. Weills, 1000-Mw(e) Metal-Fueled Fast Breeder Reactor, USAEC Report ANL-7001, Argonne National Laboratory, June 1966.
21. Argonne National Laboratory, Reactor Development Program Progress Report, October 1966, USAEC Report ANL-7267, Nov. 22, 1966.
22. Argonne National Laboratory, Reactor Development Program Progress Report, December 1966, USAEC Report ANL-7286, Jan. 26, 1967.
23. L. J. Wittenberg and G. R. Grove, Reactor Fuels and Materials Development Plutonium Research: 1965 Annual Report, USAEC Report MLM-1328, Mound Laboratory, Jan. 20, 1967.
24. D. F. Bowersox and J. A. Leary, Solubilities of Selected Elements in Liquid Plutonium: X, Thulium, USAEC Report LA-3623, Los Alamos Scientific Laboratory, Nov. 4, 1966.
25. P. E. Potter, The Volatility of Plutonium Oxycarbides, British Report AERE-R-5369, January 1967.
26. C. E. McNeilly, The Pseudo Ternary System BeO–UO_2–PuO_2, USAEC Report BNWL-350, Battelle–Northwest, January 1967.
27. F. W. Albaugh, S. H. Bush, J. J. Cadwell, D. R. deHalas, and D. C. Worlton, unpublished, Battelle–Northwest, March 1967.
28. Argonne National Laboratory, Reactor Development Program Progress Report, January 1967, USAEC Report ANL-7302, Feb. 24, 1967.
29. Argonne National Laboratory, Reactor Development Program Progress Report, February 1967, USAEC Report ANL-7308, Mar. 28, 1967.
30. M. D. Freshley and F. E. Panisko, The Irradiation Behavior of UO_2–PuO_2 Fuels in PRTR, USAEC Report BNWL-366, Battelle–Northwest, March 1967.
31. D. O. Hobson, V. O. Haynes, and R. S. Crouse, Characterization of Army PM-1 Type Reactor Fuel Elements, USAEC Report ORNL-TM-1676, Oak Ridge National Laboratory, December 1966.
32. J. L. Gregg, R. S. Crouse, and W. J. Werner, Swelling of UAl_3–Al Compacts, USAEC Report ORNL-4056, Oak Ridge National Laboratory, January 1967.
33. D. O. Hobson and C. F. Leitten, Jr., Characterization of U_3O_8 Dispersions in Aluminum, USAEC Report ORNL-TM-1692, Oak Ridge National Laboratory, February 1967.
34. J. H. Coobs and O. Sisman (Comps.), Coated-Particle Fuels Development at Oak Ridge National Laboratory for Period May 15, 1966–January 15, 1967, USAEC Report ORNL-TM-1772, Oak Ridge National Laboratory, March 1967.
35. A. W. Savolainen (Comp. and Ed.), Gas-Cooled Reactor Program Semiannual Progress Report for Period Ending September 30, 1966, USAEC Report ORNL-4036, Oak Ridge National Laboratory, February 1967.
36. Oak Ridge National Laboratory, unpublished, Jan. 6, 1967.
37. R. L. Beatty, Pyrolytic Carbon Deposited from Propane in a Fluidized Bed, USAEC Report ORNL-TM-1649, Oak Ridge National Laboratory, January 1967.
38. Oak Ridge National Laboratory, unpublished, Feb. 6, 1967.
39. Reference deleted.
40. General Atomic Division, General Dynamics Corp., HTGR Base Program Quarterly Progress Report for Period Ending November 30, 1966, USAEC Report GA-7553, February 22, 1967.
41. D. L. Keller, Progress Relating to Civilian Applications During October through December 1966, USAEC Report BMI-1791, Battelle Memorial Institute, Jan. 1, 1967.
42. W. V. Goeddel, Coated Particle Fuels in High-Temperature Reactors: A Summary of Current Applications, USAEC Report GA-7650, General Atomic Division, General Dynamics Corp., Feb. 3, 1967.
43. S. Jaye and W. V. Goeddel, High-Temperature Gas-Cooled Reactor Fuels and Fuel Cycles: Their Progress and Promise, USAEC Report GA-7482, General Atomic Division, General Dynamics Corp., Dec. 10, 1966.
44. C. S. Luby and A. S. Schwartz, Irradiation Tests of Pyrolytic Carbon-Coated ThC_2 and ThO_2 Particles, USAEC Report GA-7332, General Atomic Division, General Dynamics Corp., Oct. 8, 1966.
45. P. E. Reagan, Fission-Gas Release and Irradiation Damage to AVR Pyrolytic Carbon-Coated Thorium–Uranium Carbide Particles USAEC Report ORNL-4053, Oak Ridge National Laboratory, January 1967.
46. J. W. Prados and J. L. Scott, The Influence of Pyrolytic Carbon Creep on Coated-Particle Fuel Performance, USAEC Report ORNL-TM-1787, Oak Ridge National Laboratory, April 1967.
47. J. Belle, R. M. Berman, W. F. Bourgeois, I. Cohen, and R. C. Daniel, unpublished, Westinghouse Electric Corporation, Bettis Atomic Power Laboratory, February 1967.
48. S. Ferrari and G. J. Segre, Experiments on the Uranium Emission from Sintered Uranium Oxide Pellets, Italian Report RT-FI-(66)-18, 1966.
49. M. D. Rogers, Ejection of Uranium Atoms from Sintered UO_2, British Report AERE-M-1818, November 1966.

50. H. Ullmann, D. Naumann, and B. Werner, Preparation of Thin-Walled Thorium Oxide Ceramic Bodies of High Density by Slip Casting, *Silikat Tech.*, 17: 209-211 (July 1966).
51. Hj. Matzke, On the Effect of TiO_2 Additions on Sintering of UO_2, *J. Nucl. Mater.*, 20: 328-331 (September 1966).
52. P. Guinet and H. Vaugoyeau, La Coupe isotherme a´ Temperature Ordinaire du Diagramme Uranium–Carbone–Silicium, *Compt. Rend. Ser. C Chim. Sci.*, 262: 1856-1859 (June 27, 1966).
53. P. Guinet, H. Vaugoyeau, J. Laugier, and P. L. Blum, Etude d'un Equilibre a´ 4 Phases Solids dans le Systems Ternaire U–C–Si, *J. Nucl. Mater.*, 21: 21-31 (1967).
54. F. Anselin, Preparation and Study of Mixed Carbides–Nitrides of Uranium and of Plutonium, French Report CEA-R-2988, June 1966.
55. S. Imoto and H. J. Stöcker, Preparation of UN by the Reaction of UO_2 Carbon and Nitrogen, *Thermodynamics*, Vol. II, pp. 533-545, International Atomic Energy Agency, Vienna, Austria, 1966. Copies obtainable from National Agency for International Publications, Inc., 319 E. 34th St., New York, N. Y. 10016.
56. L. Yang, R. G. Hudson, and F. D. Carpenter, Some High Temperature Diffusion Studies of Materials of Thermionic Interest, Report NASA-CR-64768 (GA-6472), General Atomic Division, General Dynamics Corp., June 28, 1965.
57. L. Yang, R. G. Hudson, and F. D. Carpenter, Physico-Chemical Properties of Carbide Fuel for Thermionics, Report CONF-661003-11, presented at AIME Nuclear Metallurgy Symposium on High Temperature Nuclear Fuels, Delavan, Wis., October 1966.
58. A. Accary, P. Magnier, and M. Marchal, Mechanical Behavior of Uranium-Carbon Alloys Close to UC and Their Fabrication by Extrusion, *Rev. Hautes Temp. Refract.*, 3 (1): 59-77 (1966).
59. J. L. Arnold, Postirradiation Metallographic Examination of Arc-Cast Hypostoichiometric Uranium Monocarbide, in Advances in Metallography, Technical Papers of the Twentieth Metallographic Conference, USAEC Report REP-658, pp. 38-42, R. J. Jackson and A. E. Calabra (Eds.). 1966.
60. J. R. Weeks (Comp.), unpublished, Brookhaven National Laboratory.
61. A. Nishiyama, T. Kasamatsu, K. Itani, and H. Katsuya, Study of the Fabrication of Uranium Nitride Fuel, USAEC Translation UCRL-Trans-10074 [from *Sumitomo Denki*, No. 87: 123-130 (1965)].
62. P. Patriarca (Comp.), unpublished, Oak Ridge National Laboratory, March 1967.
63. R. L. Gibby, Reaction of Molten UO_2 with Water, USAEC Report BNWL-362, Battelle–Northwest, January 1967.
64. L. Baker, Metal–Water Reactions, *Nucl. Safety*, 8(1): 23-24 (Fall 1966).
65. Argonne National Laboratory, Chemical Engineering Division Semiannual Report, July–December 1964, USAEC Report ANL-6925, May 1965.
66. General Electric Company, Nuclear Materials and Propulsion Operation, High-Temperature Materials Program Progress Report No. 63, USAEC Report GEMP-63, Dec. 30, 1966.
67. R. Blackburn, Inert Gases in Metals, *Met. Rev.*, 11: 159-176 (1966).
68. B. Hudson, The Distribution of and Swelling Produced by Fission Gas Bubbles in Alpha and Beta Uranium Irradiated under Low Stress, British Report AERE-R-5039, January 1967.
69. B. F. Rider, C. P. Ruiz, J. P. Peterson, Jr., and F. R. Smith, Accurate Nuclear Fuel Burnup Analysis, Quarterly Progress Report No. 19, June–August 1966, USAEC Report GEAP-5270, General Electric Company, Nuclear Technology Department, Sept. 1, 1966.
70. I. Goldberg, L. L. Lynn, and C. D. Sphar, FIGRO: FORTRAN-IV Digital Computer Program for the Analysis of Fuel Swelling and Calculation of Temperature in Bulk-Oxide Cylindrical Fuel Elements, USAEC Report WAPD-TM-618, Westinghouse Electric Corporation, Bettis Atomic Power Laboratory, December 1966.
71. G. W. Greenwood, and M. V. Speight, An Analysis of the Diffusion of Fission Gas Bubbles and Its Effect on the Behaviour of Reactor Fuels, *J. Nucl. Mater.*, 10(2): 140-144 (1963).
72. Atomic Energy of Canada Limited, unpublished, September 1966.
73. Atomic Energy of Canada Limited, unpublished, December 1966.
74. A. D. Whapham, Electron Microscope Observation of the Fission-Gas Bubble Distribution in UO_2, *Nucl. Appl.*, 2(2): 123-130 (April 1966).
75. R. S. Barnes and R. S. Nelson, Theories of Swelling and Gas Retention in Reactor Materials, British Report AERE-R-4952, June 1965.
76. E. E. Gruber, Calculated Size Distributions for Gas Bubble Migration and Coalescence in Solids, *J. Appl. Phys.*, 38(1): 243-250 (January 1967).
77. J. R. MacEwan and R. L. Stoute, Effect of Irradiation on the Thermal Conductivity of UO_{2-x}, UO_2, and UO_{2+x} at 60°C, *J. Nucl. Mater.*, 20(1): 70-76 (1967).

Section II

Reactor Materials

Moderator Materials

Graphite

Dimensional and property changes of several graphites irradiated to high doses in the British Dounreay Fast Reactor have been reported.[1] Irradiation temperatures ranged from 380 to 750 °C, and total neutron doses were up to 3.3×10^{22} neutrons/cm^2. The graphites included anisotropic reactor-grade PGA, three high-thermal-expansion isotropic grades, and pyrolytic graphites. The nature of irradiation damage in graphite, based on a model developed from the accumulated data of prior studies, is discussed, and additional data are presented. According to the model, at irradiation temperatures in the range 150 to 1200 °C, damage in graphite proceeds in the following manner:

1. Collisions of neutrons with carbon atoms in the graphite crystals produce high-energy carbon atoms that collide with other carbon atoms to form single interstitials and vacancies.

2. Many of the interstitials and vacancies interact to destroy one another, but some interstitials quickly combine into small mobile groups. Most of these nucleate into large clusters on a scale which depends upon the irradiation temperature and flux and upon the perfection of the graphite crystals.

3. In addition to the large interstitial clusters, there remains a population of small clusters whose concentration depends upon the temperature and the neutron flux and dose.

4. The vacant lattice sites are initially isolated single sites that are not mobile at the lower temperatures, but they may move slowly above 350 °C. However, lines of vacancies can be formed by random juxtapostion, and each line collapses when its length exceeds a certain critical size; the collapsed lines continue to grow by the capture of further vacancies at their ends.

5. Above 300 °C the result of the formation of interstitial clusters and collapsed vacancies is that the crystals change shape without much change in volume. The interstitial clusters cause crystal growth in the c-axis direction, and the collapsed vacancies cause crystal shrinkage in the a-axis direction. Part of the c-axis crystal growth is accommodated in oriented microporosity in polycrystalline graphites; thus there is a bulk shrinkage in polycrystalline nuclear graphites at high irradiation temperatures, at least until they have received large neutron doses. When all the oriented microporosity has been filled, further crystal strain can be accommodated in most artificial graphites only by some degree of porosity generation, which causes the graphites to expand at large neutron doses. However, since isotropic graphites show little porosity generation at large doses, different crystal strain can be accommodated by irradiation-induced creep in the graphite.

6. The magnitude of the bulk dimensional changes induced in polycrystalline graphite by the crystal-shape changes depends upon the degree of preferred orientation of the crystals and the distribution of oriented microporosity in the graphite, together with the rate at which initial porosity is closed and new porosity is generated by differential strain in the crystals.

Typical properties of the four nuclear graphites irradiated are listed in Table II-1. No lattice parameters of these four graphites were determined, but measurements were obtained for the two pyrolytic graphites: (1) an alpha type with crystallite parameters L_c and L_a having values of < 200 and < 100 A, respectively, and a d-spacing of 3.425 A; and (2) a beta-type pyrolytic graphite with corresponding values of ~1000 and 3.356 A, respectively.

Table II-1 TYPICAL PHYSICAL PROPERTIES OF THE GRAPHITES BEFORE IRRADIATION[1]

	Anisotropic graphite	Near-isotropic graphites		
	PGA*	PH†	PO‡	PR§
Thermal expansion coefficient (20 to 120°C), 10^{-6}/°C				
Parallel	0.8	3.5	3.0	4.2
Perpendicular	2.8	3.9	3.6	4.4
Thermal conductivity, cal/(cm)(sec)(°C)				
Parallel	0.5	0.32	0.38	0.26
Perpendicular	0.3	0.28	0.36	0.23
Young's modulus, 10^6 psi				
Parallel	17	17	17	17
Perpendicular	8	15	14	15
Density, g/cm^3	1.7	1.85	1.8	1.8

*Pile Grade A (Shell H100 petroleum coke).
†Gilsocarbon coke.
‡Petroleum coke.
§Coal-tar pitch coke.

The dimensional changes observed for the anisotropic PGA graphite were significantly different from the isotropic types. In the direction perpendicular to extrusion, PGA contracted to slightly more than 1% at approximately 7.5×10^{21} neutrons/cm^2 and then expanded to reduce the total contraction to about 0.8% at 10^{22} neutrons/cm^2. The higher dosage was at irradiation temperatures in the 380 to 550°C range. In the direction parallel to extrusion, PGA contracted almost linearly to about 5% at 10^{22} neutrons/cm^2. In contrast, the isotropic graphites contracted continuously up to the highest exposure of approximately 1.7×10^{22} neutrons/cm^2 for both directions relative to extrusion. The rate of contraction decreased above exposure of about 10^{22} neutrons/cm^2. Maximum contractions were about 2.6% at 1.7×10^{22} neutrons/cm^2 by about 2.7% for the direction perpendicular to extrusion and about 3.2% for the direction parallel to extrusion. All three of the isotropic grades showed similar dimensional changes.

The bulk density of all of the graphites and the crystal strain rates were not very dependent on irradiation temperature in the range 380 to 750°C. In contrast, previous data for irradiation of PGA graphite in the lower neutron flux of the DIDO reactor showed considerable temperature dependence in the 450 to 650°C range. It was suggested that this disagreement in data must be related to the neutron-flux differences between the reactors.

The thermal-expansion coefficients of the isotropic graphites increased with exposure to about 5×10^{21} neutrons/cm^2 and then decreased to below the unirradiated values at exposures slightly in excess of 1.5×10^{22} neutrons/cm^2. No irradiation effect of PGA expansion coefficients was given.

Thermal-conductivity changes of the isotropic graphites tended to saturate below exposure of 5×10^{21} neutrons/cm^2, and the saturation level decreased with increasing temperature. It was believed that conductivity changes were mainly due to single vacancies and divacancies that reached a saturation concentration at relatively low exposures.

The irradiation increased Young's modulus of the isotropic graphites relatively slowly after the initial rapid rise at low exposure. The modulus at about 10^{22} neutrons/cm^2 was approximately 2.5 times the initial value.

The irradiation results for the pyrolytic graphite were particularly interesting. Table II-2 compares the strains for the two types of pyrolytics. These data show that the crystal strains in the poorly graphitized alpha-type sample was much larger than for the well-graphitized beta type. This supports the hypothesis that crystal strain rates increase as the crystallite size decreases and agrees with the generally observed more rapid shrinkage of poorly graphitized as opposed to well-graphitized materials at low radiation exposures and high temperatures.

Table II-2 COMPARISON OF DIMENSIONAL CHANGES IN BETA- AND ALPHA-TYPE PYROLYTIC GRAPHITE[1]

Specimen type	Exposure, 10^{20} neutrons/cm^2	Temp., °C	Strain, %	
			c-axis	a-axis
Beta	40	600	5.0	−1.2
	47	700	5.2	−1.9
Alpha	40	600	12.2	−5.1
	47	700	30.0	−10.5

Figure II-1 shows the observed strains for the well-graphitized beta-type pyrolytic graphite and also crystal strains calculated from the dimensional changes of the PGA graphite. The agreement between the calculated strains of PGA and observed strains of the well-graphitized pyrolytic provide good support of Kelly's theory.[2]

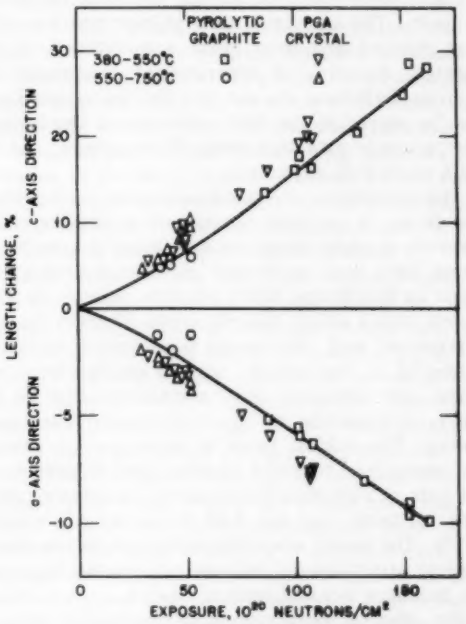

Temp., °C	Pyrolytic graphite	PGA crystal
380–550	□	▽
550–750	○	△

Fig. II-1 Dimensional changes observed in well-graphitized pyrolytic graphite and calculated in crystals of PGA graphite.[1]

The compatibility of BeO with graphite has been examined at Oak Ridge.[3] The test was designed to study irradiation effects at 1500°C on the chemical compatibility of graphite with BeO; to investigate the distribution of ^{6}Li formed in the BeO; and to deter-

mine weight, dimensional, and structural changes in the graphite and BeO. A BeO ring and a graphite ring were in close contact on flat surfaces and were nested over a solid BeO core within a graphite sleeve. The desired temperature was achieved for about half of the irradiation, and then it gradually fell to about 1280°C. The total irradiation exposure was 1.0×10^{21} neutrons/cm^2 ($E > 0.18$ Mev). There was no physical damage to the BeO or graphite during irradiation. Metallographic examination of selected surfaces showed no reaction products, and X-ray diffraction of the BeO ring showed no Be_2C. Microstructural changes were observed for the BeO, but not for the graphite. The irradiated BeO showed that the grain size doubled and each grain was outlined by gas bubbles. Analyses of experimental components for ^{6}Li concentrations showed that the major portion of the ^{6}Li stayed in the BeO core when it was formed. The graphite exhibited about 1% shrinkage, and the BeO, about 0.5% expansion.

The application of fracture-mechanics concepts to the design of graphite components to prevent brittle fracture is under study by Oak Ridge researchers.[4] Tests have been performed on notched-bend specimens of EGCR-type AGOT graphite. Specimens were beams with a single, lateral, artificial crack cut with a jewelers' saw. The results were used to determine values of G_c, the critical rate of strain-energy release, and relations were established both by the theory of elasticity and by experimental compliance testing. The critical rates of strain-energy release for specimens oriented parallel and transverse to the axis of extrusion were found to be approximately 0.39 in.-lb/sq. in. and 0.29 in.-lb/sq. in., respectively. The initial study indicated that the concept of critical strain-energy release rate applied to graphite, but more detailed study is needed.

The effect of degassing on the mechanical properties of graphites is being examined by British investigators.[5] Initial data show somewhat different effects of degassing on the parallel- and perpendicular-direction bend strengths. The breaking strain of parallel-cut specimens was little affected by vacuum degassing but the perpendicular-cut samples showed a pronounced effect. The data are of interest in view of the continuing uncertainty regarding the precise role played by adsorbed gases in the differences between room-temperature and high-temperature mechanical properties of graphites.

Additional data have been reported for long-term irradiation effects on graphite by Battelle–Northwest.[6] An exposure of 2.2×10^{22} neutrons/cm^2 ($E > 0.18$ Mev) at 800°C has been reached by CSF graphite samples. During the course of successive irradiations, a transverse-orientation sample contracted until it reached a maximum contraction of 0.9%. It then began expanding and continued until, at an exposure of about 2.2×10^{22} neutrons/cm^2, it had expanded 6.8%. For the same irradiation a parallel-orientation sample contracted, first at a rapid rate, then linearly, and finally at a lessening rate until the total contraction reached 7.7%.

Microstructural examinations of graphite samples under compressive and tensile loading have provided information on deformation mechanisms in polycrystalline graphite. Battelle–Northwest researchers[6] utilized a unique experimental technique. Ring-shaped samples were microscopically observed parallel to their cylindrical axis as the samples were diametrically loaded. This resulted in sample crack propagation (due to compressive or tensile stresses) in the plane of observation. The results of this study indicated that the inelastic behavior seen in stress-strain curves for graphite was related to interlayer crack formation in the crystallites. In the case of an applied tensile stress, the cracks occurred roughly perpendicular to applied stress, whereas for compression the cracks (propagating principally along the a-direction of suitably oriented particles) occurred in the direction of applied stress. (M. C. Brockway)

Beryllium and Beryllium Alloys

Metal Reduction

Nakamura[7] has invented a continuous process for the production of high-purity beryllium metal from $BeCl_2$ and $NaCl_2$. Electrolysis of the molten salts is conducted in nickel cells heated externally at 300 to 400°C. Beryllium flakes deposited on the nickel cathodes are scraped off and collected in porous nickel receivers that are removed at intervals with no interruption of the process. The beryllium content of the bath is maintained throughout the process by stoichiometric additions. Beryllium produced by this method is of higher purity than that produced by electrolysis of fused $BeCl_2$ or by magnesium reduction of BeF_2.

A U. S. patent has been granted Strohmeier for a method of electroforming beryllium.[8] The method described produces adherent polishable coatings of beryllium metal on substrates that would not take a high polish. The process consists of electrodeposition of the metal from organic beryllium compounds complexed with alkali-metal salts. These salts are taken from the group having atomic numbers 19 to 55. Deposition is conducted at a relatively low temperature, and coatings can be put on materials such as plastics or paper. Workers at the Bureau of Mines[9] reported on an exploratory study that was made to determine the feasibility of preparing beryllium by the metallothermic reduction of BeO. The procedure involves heating a nonvolatile metal reductant in contact with BeO in a vacuum. Beryllium vapors formed in the reaction are condensed as a coherent

deposit on a heated surface. Reductants tested include La, Y, Th, Th–Mg, and Zr–Ti alloys and the hydrides of La, Y, and Zr. Test temperatures ranged from 1350 to 1750°C, and reaction times ranged from 30 to 100 hr. In most cases, metal recoveries were low, although yields of 90% of theoretical were obtained with lanthanum, yttrium, and zirconium reductants. In most cases, deposits were contaminated by beryllides.

Mechanical Metallurgy

A study of the flow and fracture characteristics of beryllium has been undertaken at the Franklin Institute.[10] The objective was to study a means for producing an alloy or form of the purified metal having useful ductility in an engineering sense. The materials studied were 12-pass SR beryllium single crystals and the alloys Be–5.24 wt.% Ni and Be–4.37 wt.% Cu. The structure of these materials has been characterized by transmission-microscopy techniques. An unexpected nickel-rich grain-boundary precipitate was noticed and determined to be $Be_{21}Ni_5$ by microprobe analysis. Lattice parameter determinations made using the Kossel technique indicated $c = 3.5911\ A \pm 0.0001\ A$. These materials were tested by *c*-axis microstrain compression testing. The 12-pass SR single-crystal material was tested at room temperature, 220°C, and 333°C; Be–4.37 wt.% Cu at 364°C; and Be–5.24 wt.% Ni at room temperature, 177°C, and 354°C. The interesting result from these tests was that the high-purity material showed considerable microstrain plasticity at 333°C.

Samples of the SR materials being studied were explosively deformed at room temperature and then heat-treated at increasing temperatures for 30 min. Explosive loading produced heavily twinned structures. High-purity single crystals were loaded along the *c*-axis and at 45° to the *c*-axis. Heat-treatment at 400°C of the specimen loaded on the *c*-axis removed the heavily twinned regions. No recrystallization occurred at 400°C in the *c*-axis of the 45°C specimen. Rolled polycrystalline material was loaded parallel to the rolling plane. Heat-treatment of this specimen at 500°C produced no microstructural change. Twin-free grains were observed until the specimen was heated to 800°C for 1 hr. Texture determinations revealed that explosive forming and recrystallization could alter that texture because of the survival of specific twin orientations.

Rolled alloy material was given a recovery-type heat-treatment of 500°C for 1 hr and then bend tested. Both materials fractured after very small plastic strains. The surfaces of the broken specimens showed profuse pyramidal slip (nonbasal) traces in the vicinity of the fracture.

In a joint effort of Nuclear Metals and Franklin Institute, beryllium bicrystals were studied to evaluate the role of grain boundaries in the deformation and fracture behavior of beryllium.[11] Beryllium crystals were grown by a parallel-seed floating-zone technique, and orientation configurations believed significant in polycrystalline deformation were selected. In the first five configurations, the load was applied parallel to the grain boundary such that there was no tensile stress across the boundary. The last three configurations had the load applied across the boundary and, therefore, the boundary was under stress.

All of the asymmetric and modified symmetric configurations studied exhibited brittle behavior. This embrittlement was attributed to a lack of accommodation at the boundary of mixed dislocation interactions and to shearing at the boundary produced by incompatible rotation of the grains. As a comparison, appreciable ductility was observed in the basal/basal symmetric configuration. In this case, like dislocations could be accommodated at the boundary, and rotation of the grains was in harmony. On this basis, ductility might be expected in a symmetric configuration of the prism planes or in an antisymmetric configuration of either basal or prism planes.

Basal cleavage was the most common mode of failure, occurring in all grains where the basal planes were oriented at an angle greater than 20°. Specimens with basal planes oriented at angles less than 20° to the tension axis failed at considerably higher stresses by second-order prism-plane cleavage. For orientations close to 20°, competition between basal and prism cleavage was observed. For configurations having boundaries transverse to the loading axis, boundary cleavage always occurred. The origin of all basal- and prism-cleavage failures was traced to the grain boundary in all cases except the symmetric configuration. Cracks occurred at twins and bend planes and were associated with boundary shear, which developed as a result of incompatible rotations of the grains in nonsymmetric cases.

Electron-transmission microscopy of thin foils in as-grown bicrystals revealed a high density of dislocations and substructure at the boundary. Boundary restraint, which results from cooling during preparation, was believed to be responsible. As expected, dislocation pileups were observed at the boundary in deformed material.

The effects of prestraining under hydrostatic pressure on the mechanical behavior of polycrystalline beryllium are being studied at the Franklin Institute.[12] The forms of beryllium being investigated include hot-pressed rod, extruded rod, and hot-rolled sheet. Thus far these materials have been strained to fracture at room temperature under hydrostatic pressures up to 100 ksi. At hydrostatic pressures over 50 ksi, a significant increase in elongation and reduction in area occurred. These materials were also prestrained under a hydrostatic pressure of 100 ksi and then strained to fracture at ambient pressure. The prestraining produced increases in apparent

modulus, yield stress, and tensile strength but no significant increase in ductility. For example, one sheet specimen that was prestrained 12.5% at 100 ksi exhibited a yield stress 50% higher than that of the unstrained material with no loss in ductility.

Physical Metallurgy

Sibert and Hultquist have examined production techniques for beryllium alloys.[13] The methods investigated included aluminum reduction of beryllium compounds, electrolytic reduction of beryllium compounds, electrorefining crude beryllium ore, and electrolytic codeposition of beryllium and aluminum. It was concluded that an electrolytic process using a soluble beryllium-scrap anode and a liquid aluminum cathode showed the most promise.

Process Metallurgy

The Materials Advisory Board Committee on Beryllium Metallurgy has compiled the major process variables corresponding to the principal operations involved in the manufacture of a beryllium product.[14] The compilation comprises a checklist that should serve as a review of significant variables to be considered at the start of a research or development effort involving beryllium. The report describes suggested measurements that can be used to present a true characterization of the material. A flow sheet of processes and fabrication of beryllium as a framework and the principal steps involved are given in the report. However, it is unlikely that funds would be available to measure or describe all of the items listed or that all of the items would be pertinent to any specific program.

Chemical Analysis

Idaho Nuclear[15] reported on gas release and properties of beryllium irradiated at 600 and 750°C. Release of helium at these temperatures was related to a macrodiffusion coefficient, D. The value of D was 6.8×10^{-14} cm^2/sec at 600°C and 1.13×10^{-9} cm^2/sec at 750°C. The magnitude of the diffusion coefficient at 750°C agrees with that predicted for gas diffusion in beryllium. However, the value at 600°C agrees better with the self-diffusion in beryllium. The activation energy, G, for release of helium was found to be 5 ev, which is the order of magnitude normally expected for bulk diffusion at these temperatures. It was shown that the compressive yield strength for beryllium irradiated to 1×10^{21} neutrons/cm^2 ($E >$ 1 Mev) increased only slightly. Therefore it was concluded that most of the irradiation hardening was annealed out at the temperatures of irradiation. Fractographic studies indicated that helium-bubble formation generally occurred in the grain boundaries and the presence of these bubbles inhibited grain growth. (H. D. Hanes and F. T. Zurey)

Beryllium Oxide

Significant improvements in fission-product retention of BeO–UO_2 fuel compacts have been reported by General Atomic.[16] Hot-pressed fuel dispersions of UO_2 spheres in a BeO matrix have shown release fractions of xenon and krypton as low as 10^{-9} at 1400°C after a 1-hr collection time at the beginning of the fuel life. Other fission products such as barium, strontium, and iodine showed release fractions close to 10^{-6}. The improvement in retention characteristics, compared with earlier dispersions, was attributed primarily to the closing of pores so that the BeO matrix has a density greater than 99.3% of theoretical. (M. C. Brockway)

Solid Hydrides

Zirconium Hydride

Transport of hydrogen between porous beds of zirconium hydride under the influence of temperature transients was investigated at Martin.[17] A steady state was established between two beds of the hydride and then one bed was heated rapidly. Transients ranged in duration from 25 to 86 sec, and pressures varied from 0.1 to 1.0 atm. In a typical result the system pressure rose from 3.2 to 10 psia because of hydrogen evolution from the donor bed, which was heated from 800 to 1250°F (427 to 677°C) over a period of 45 sec. The acceptor-bed temperature increased from 1375 to 1420°F (746 to 771°C) as it absorbed hydrogen. Analysis revealed that the temperature increases were controlled by pressure drop with the beds rather than by diffusion within the particles. Thus the more permeable the bed, the faster was the absorption of hydrogen. The presence of a diluent gas was found to slow the absorption process.

Hydrided Zirconium Alloys

The microindentation properties of hydrided Zircaloy-2 were studied in the temperature range 25 to 225°C at Chalk River.[18] These measurements showed that above 50°C the hydride can deform plastically by at least 8%. This observation supports the idea that the restoration of the tensile properties of zirconium alloys containing oriented hydrides is due to the plasticity of the hydride flakes. The results indicate an ultimate tensile strength of 146,000 psi at 25°C, falling to 111,500 psi at 225°C, as calculated from Knoop hardness values of 321 at 25°C and 245 at 225°C. The plot was nonlinear between 25 and 60°C but then became linear to 225°C.

Yttrium Hydride

A patent has been granted to the AEC for a method of cladding yttrium hydride and yttrium-base alloy

hydrides.[19] This patent is based on work done at General Electric and involves cladding with chromium. A layer of metallic chromium from 1 to 10 mils thick is applied to the metal, and the composite is heated at 2000 to 2260°F (1093 to 1238°C) in a nonoxidizing atmosphere to bond the chromium to the base material. Hydriding is then carried out at 1800°F (982°C).

Lithium Hydride

The compressibility of lithium hydride and lithium deuteride has been measured at Lawrence Radiation Laboratory.[20] Subjected to pressures up to 40 kbars at 25°C were ^{7}LiH, ^{7}LiD, ^{6}LiH, and ^{6}LiD. Extrapolated values of the compressibility to zero pressure were in good agreement with other reported values. However, simple ionic models for these compounds did not predict the observed variations in compressibility, and a partial covalent character was indicated.

Titanium Hydride

The lattice parameters of titanium hydride have been measured both by Debye–Scherrer and diffractometer methods at Aldermaston.[21] An fcc structure with $a_0 = 4.405$ A up to a composition of H/Ti = 1.37 ± 0.03 was observed. At higher hydrogen contents, a_0 increased rapidly, indicating that the above composition marks the phase boundary between single-phase and two-phase material. The value of a_0 increased to 4.413 A at $TiH_{1.5}$ and eventually to 4.452 A at TiH_2. A bct phase, which is a distorted form of the fcc type, was found also for the composition TiH_2. For this phase, $a_0 = 3.165$ A and $c_0 = 4.368$ A. The lattice parameters measured for the fcc phase are in reasonable agreement with those reported by previous investigators. (H. H. Krause)

References

1. P. T. Nettley and W. H. Martin, The Irradiation Behaviour of Graphite, British Report TRG-Report-1330, Sept. 12, 1966.
2. B. T. Kelly, W. H. Martin, and P. T. Nettley, Dimensional Changes in Polycrystalline Graphites Under Fast-Neutron Irradiation, *Phil. Trans. Roy. Soc. London, Ser. A*, 260 (1109): 51-71 (June 16, 1966).
3. Oak Ridge National Laboratory, Reactor Chemistry Division Annual Progress Report for Period Ending December 31, 1966, USAEC Report ORNL-4076, March 1967.
4. J. M. Corum, Determination of the Fracture Toughness of EGCR-Type AGOT Graphite, USAEC Report ORNL-4030, Oak Ridge National Laboratory, December 1966.
5. D. H. Logsdail, An Apparatus for the Measurement of the Flexural Strength of Degassed Graphite in High Vacuum at Elevated Temperature, British Report AERE-R-5136, October 1966.
6. F. W. Albaugh, S. H. Bush, J. J. Cadwell, D. R. deHalas, and D. C. Worlton, Battelle–Northwest, unpublished, December 1966.
7. T. Nakamura, Method of Continuous Production of High-Purity Beryllium Metal, U. S. Patent 3,278,402, to NGK Insulators, Ltd., Oct. 11, 1966.
8. W. Strohmeier, Electroforming of Beryllium, U. S. Patent 3,278,400, to Ethyl Corp., Oct. 11, 1966.
9. T. T. Campbell, R. E. Mussler, and F. E. Block, Metallothermic Reduction of Beryllium Oxide, *Trans. Met. Soc. AIME*, 236: 1456-1461 (October 1966).
10. V. Damiano, G. London, and F. Witt, Flow and Fracture Characteristics of Beryllium, First and Second Quarterly Reports, April 5–July 4, 1966, and July 5–October 4, 1966, The Franklin Institute Research Laboratories.
11. L. R. Aronin, D. F. Kaufman, J. J. Pickett, V. V. Daminano, G. J. London, and R. Pyle, Beryllium Bicrystal Studies, Report AFML-TR-65-252(Vol. II), Nuclear Metals, Inc., and Franklin Institute, June 1966.
12. N. Inoue, F. Cooke, and H. Conrad, Effects of Prestraining Under Hydrostatic Pressure on the Mechanical Behavior of Polycrystalline Beryllium, Interim Progress Report, June 11–September 30, 1966, Franklin Institute.
13. M. E. Sibert and A. E. Hultquist, Production of Beryllium Alloys, *J. Metals*, 18: 1215-1222 (November 1966).
14. Materials Advisory Board, National Academy of Sciences–National Research Council, Characterization of Beryllium, Report MAB-226-M, August 1966.
15. J. M. Beeston, Gas Release and Compression Properties in Beryllium Irradiated at 600 and 750°C, USAEC Report IN-1057, Idaho Nuclear Corp., February 1967.
16. R. A. Meyer, Status of Development of Dispersed Fuel Particles in a Beryllium Oxide Matrix, USAEC Report GA-7069, General Atomic Division, General Dynamics Corp., April 1966.
17. R. G. Lightner and D. Duffey, Absorption of Hydrogen in Porous Beds of Zirconium Hydride, *Trans. Amer. Nucl. Soc.*, 9: 404 (October–November 1966).
18. J. F. R. Ambler, The Effect of Temperature on the Microindentation Properties of Zirconium Hydride, Canadian Report AECL-2538, March 1966.
19. K. M. Bohlander, E. S. Funston, and J. A. McGurty, Method of Cladding Yttrium Hydride and Yttrium Base Alloy Hydrides, U. S. Patent 3,277,565, to USAEC, Oct. 11, 1966.
20. D. R. Stephens, Compression of Lithium Hydride, USAEC Report UCRL-12386, University of California Lawrence Radiation Laboratory, Feb. 4, 1965.
21. P. M. S. Jones, P. Ellis, J. R. Smith, T. Aslett, and C. G. Hutcheson, An X-Ray Examination of Titanium Hydride, British Report AWRE-O-60/66, August 1966.

Section III

Reactor Materials

Cladding and Structural Materials

Corrosion by Aqueous and Gaseous Media

Zirconium Corrosion

OXIDATION

The epitaxial nature of the oxidation of zirconium has been studied by the Air Force Materials Laboratory.[1] Preferred oxidation nucleation on the (0 0 0 1) and (2 $\bar{1}$ $\bar{1}$ 0) planes of zirconium was observed at 100 and 170°C. Random oxidation was observed at temperatures ranging from 200 to 700°C. The preferential oxidation was directly related to dislocation sites which acted as nuclei for the emerging oxide phase along the principal crystallographic directions.

Oxygen-saturated zirconium has been oxidized at temperatures to 1300°C by Kennecott Copper.[2] In the range 840 to 975°C, a rapid initial film growth was followed by a parabolic film-growth rate more rapid than that observed during oxidation of oxygen-free metal. In the range 1100 to 1300°C, a parabolic film-growth rate was obtained which was also more rapid than that observed in oxygen-free metal.

AQUEOUS CORROSION

The influence of various surface conditions on the corrosion and hydrogen absorption of Zircaloy-4 in 680°F (360°C) boronated water has been reported by Babcock & Wilcox.[3] Of the surface pretreatments studied, pickling produced the lowest weight gains, whereas sanding (or sanding followed by ultrasonic cleaning) produced the highest weight gains. All contaminants studied had an adverse effect on weight gain, with fluorides having a greater effect than perspiration, oil, and metal contaminants.

The corrosion behavior of Zircaloy-2 fuel cladding after up to 875 days in boiling-water reactors has been reported by Vallecitos.[4] The in-reactor corrosion rate corresponded to that obtained in 700°F (371°C) steam in ex-reactor tests. Hydrogen pickup was 0.0635 ppm/day, or less than 7% of that produced by the corrosion reaction. The low hydrogen pickup was attributed to the presence of dissolved oxygen (0.3 ppm) and the absence of dissolved hydrogen in the water.

Bettis has described the corrosion behavior of Zircaloy-2 cladding on the blanket rods of the first Shippingport core.[5] After 1885 days in hot water (posttransition conditions), the Zircaloy tubing exhibited a mottled appearance, an oxide thickness averaging 2.4 μ, and a hydrogen content averaging 70 ppm. These values compared well with out-of-pile results obtained under similar exposure conditions.

IRRADIATION

Bombardment with 65-kev neon ions has been used in an attempt to simulate the effects of high neutron exposures on oxidized zirconium in research conducted at Harwell.[6] Exposures of 1 μa-min and above increased the subsequent corrosion rate of anodically or thermally preoxidized zirconium in 250°C steam at 1 atm. The effect was independent of exposure rate and was an increasing function of exposure. The effect did not occur when the oxide film was thick enough to prevent damage to the underlying metal. Increased corrosion also occurred in steam for bare zirconium and Zircaloy-2, which were irradiated prior to the film formation in air. It was concluded that increased corrosion of zirconium and Zircaloy-2 caused by very high neutron exposures could be the result of damage to the metal rather than to the oxide film.

Oak Ridge researchers[7] have examined the effect of hydrogen peroxide on the corrosion behavior of Zircaloy-2 in high-temperature water. Exposure conditions were 297 hr in a refreshed autoclave with 280°C water containing $10^{-5}M$ H_2O_2 [$10^{-5}M$ H_2O_2 is the steady-state concentration estimated in water at 280°C under reactor irradiation of moderate intensities by a fast-neutron flux of 10^{13} neutrons/(cm^2)(sec)]. Corrosion rates in H_2O_2-treated water were found to be 7 to 8 μg/(cm^2)(day), compared with observed corrosion rates of 70 μg/(cm^2)(day) for the flux conditions described above. Thus it was concluded that hydrogen peroxide in solution was not responsible for the accelerated corrosion of Zircaloy-2 which results on irradiation by fast neutrons.

ANODIZING

The incorporation of anions in the oxide film on zirconium during anodizing is being studied at Oak

Ridge.[8] Anions from the following anodizing solutions were found in the oxide film: 0.5*M* H_2SO_4, 0.5*M* citric acid, 0.5*M* lactic acid, 0.5*M* oxalic acid, and 0.5*M* H_3PO_4. No anions were incorporated in the oxide film from the following anodizing solutions: 1% KOH, 0.5*M* $(NH_4)_3BO_3$, saturated H_3BO_3, 0.5*M* K_2CrO_4, 0.5*M* $K_2Cr_2O_7$, 0.5*M* KNO_3, and 0.25*M* Na_2MoO_4. Films with incorporated anions were found to be thinner and possessed lower electrical conductivity than those that did not contain ions but were formed at the same voltage. The lower oxidation rate due to incorporated ions was related to their large size which held them in a fixed position in the oxide lattice where, because of their negative space charge, they served as a barrier to the diffusion of both oxygen ions and electrons through the oxide film.

Steel Corrosion

The internal corrosion of high-pressure boilers is being studied by Combustion Engineering.[9] This research has been concerned with the effect of water treatment (ammonia, phosphate, or caustic), boiler conditions (clean or dirty), and boiler-water contamination on corrosion and deposition on SA-192 carbon-steel tubes at heat fluxes of 110,000 and 150,000 Btu/(hr)(sq ft). No corrosion occurred under any conditions when the tube surfaces were clean, or with NH_3 or phosphate treatment when the surfaces were dirty. High rates of corrosion occurred under nucleate-boiling conditions, under the combination of fouled tube surfaces and caustic water treatment. Deposition of contaminants occurred on heat-transfer surfaces and was greater at the higher heat flux. Silica deposited out of NH_3-treated water, and copper deposited out of NH_3 and caustic-treated water.

Stainless-Steel Corrosion

GENERAL

Excellent corrosion resistance for chromized metals in steam at 500°C is indicated in corrosion studies[10] at SERAI. The base metal apparently had little effect on the corrosion of the chromized zone in 1000-hr tests. The corrosion film was identified as rhombohedric chromium oxide. A spinel oxide on cold-worked 304 stainless steel and an alpha Fe_2O_3 film on electrolytically polished material have been revealed by 24-hr tests in 500°C steam containing 20 ppm oxygen. Longer exposures are planned for these latter specimens.

CRUD

Examination of selected fuel elements from the Saxton Nuclear Facility by Westinghouse[11] workers indicated that the amount of crud deposition was small and there was no significant difference between amounts deposited on stainless steel and Zircaloy fuel cladding. It appeared that the controlling factors for crud deposition were heat flux and crud-source strength. Deposition was observed to occur at a minimum heat flux of about 300,000 Btu/(hr)(sq ft).

The effects of a crud test on core reactivity and boric acid distribution have been studied by Westinghouse in the Saxton reactor.[12] A ferrous hydroxide slurry was injected into the operating reactor to produce Fe_3O_4 crud. The results of the test indicated no boron hideout either in the form of absorbed or power reversible boron following crud injection. With no boron in the main coolant, the injection of crud resulted in a 0.15 to 0.3% loss in reactivity in the core. Changes in reactivity also occurred with change in *p*H of the coolant, i.e., reactivity increased with increasing *p*H.

STRESS–CORROSION CRACKING

The effect of surface condition and sensitization on the stress–corrosion cracking behavior of stainless steels has been studied at Combustion Engineering.[13] Exposure conditions were water at 316°C containing approximately 1000 ppm chloride (as NaCl) and >40 ppm dissolved oxygen at startup. On the basis of results obtained for pressurized tubular specimens, it was concluded that 304 stainless steel was more susceptible to stress–corrosion cracking than 347 stainless steel, regardless of surface condition. With 304 stainless steel, a nickel surface layer provided the highest resistance to attack, followed by swaged (15% reduction in area), solution annealed, as-drawn, swaged (10% reduction in area), and sensitized material in that order. Little difference in behavior was noted for 347 stainless steel, regardless of surface condition.

Transgranular cracks found in the BONUS dryer–preheater piping (304 stainless steel) after operation from August 1965 to April 1966 have been attributed to stress–corrosion cracking in a report issued by Puerto Rico Water Resources Authority.[14] Inconel components did not exhibit cracking. The stainless-steel piping was repaired by grinding out the cracks, which did not penetrate the component, and buttering the area with weld metal, or by replacing the cracked section with Inconel.

Stress–corrosion cracking failures of 304 stainless-steel piping in organic coolants have been reported by Chalk River.[15] The transgranular-cracking failures occurred in a zone near a weld after 50 ppm chlorine was added, as trichloroethylene, to HB-40 coolant. No carbide precipitation and no other unusual features were found in the microstructure of the stainless steel in the vicinity of the crack. Up to 18% chlorine was found in the corrosion product in the failed area. The cracks were located in an area with intermittent or no coolant flow which was considerably colder than the rest of the loop.

IRRADIATION AND OXIDATION

The effect of fission-fragment irradiation on the oxidation of 20 wt.% Cr–25 wt.% Ni–Nb stabilized stainless steel has been studied by Harwell.[16] Exposure time ranged to 3700 hr in oxygen at 650°C with a fission-fragment flux of 7×10^8 fission fragments/(cm^2)(sec). Comparison with unirradiated controls showed that the oxidation was accelerated by the fission fragments, but was not influenced by the associated incident reactor radiation (neutrons and gamma rays). Carefully conceived experiments showed that contamination of the oxide film with uranium and fission products apparently had no influence on the oxidation. Thus the accelerated attack was probably the result of displacement damage in the oxide film as a direct result of fission-recoil bombardment.

Corrosion of Nickel-Base Alloys

Several nickel-base alloys and stainless steels have been evaluated in the High Temperature Gas Cooled Reactor coolant in research conducted by General Atomic.[17] Specimens were exposed for up to 3000 hr to 1650 and 1850°F (899 and 1010°C) helium containing 3000 ppm CO and H_2. René 41 and Inconel X exhibited severe intergranular attack and carburization followed by oxidation. Type 304 stainless steel showed grain growth at 1650 and 1850°F and intergranular attack at 1850°F. Incoloy 800 showed grain growth and intergranular attack at both temperatures. On the basis of mechanical-property measurements and metallographic examination, Hastelloy X and 430 stainless steel were the materials least affected by the exposure conditions, and, of the two materials, Hastelloy X was least affected at 1850°F.

Intergranular modifications in Nickel 200 and Nickel 201, exposed to the fluidized-bed fluoride-volatility process, have been studied at Battelle–Columbus.[18] The modifications, which were detected only with a nitric acid–acetic acid etch, were found to adversely affect tensile properties. The modifications were related to the pickup of small quantities of sulfur, presumably from impurities in the Al_2O_3 fluidized beds, during exposure at temperatures of about 500°C.

Corrosion of Other Metals

The corrosion behavior of Be–Al alloys in flowing water at 163°C has been reported by Phillips Petroleum.[19] Weight-loss results for the two alloys were approximately 450 mg/dm^2 after 1300-hr exposure. Posttest metallographic examination revealed selective removal of aluminum to a depth of ~1.5 mils in the 38 wt.% aluminum alloy and to a depth of ~2 mils in the 48 wt.% alloy.

The air oxidation of iridium and a Rh–Ir alloy has been reported by Thompson Ramo Wooldridge.[20] The key parameters in the oxidation of pure iridium in the temperature range 1050 to 1500°C were velocity and temperature of the air. As air velocity increased and air temperature decreased (iridium at constant temperature), it appeared that gaseous diffusion of reaction products became less important and surface reactions became more important in determining the overall oxidation rate. Alloying with rhodium reduced the oxidation rate of iridium. The high-temperature oxidation of Ir–Rh alloys was characterized by the formation of internal porosity at the grain boundaries. It was concluded that the porosity was the result of solid-state diffusion and subsequent oxidation of rhodium in the grain boundaries. The penetration of porosity decreased with time, indicating that, as oxidation proceeded, the tendency for individual voids to grow larger was more predominant than the tendency for the pores to penetrate deeper into the metal.

The oxidation behavior of praseodymium in oxygen has been studied by the UKAEA at Aldermaston.[21] After the initial parabolic-reaction stage, it was found that the reaction rate was proportional to the logarithm of the oxygen pressure. This was interpreted to show that the oxide reached a limiting thickness and became porous in the outer layers at the same rate as that at which fresh oxide was produced at the metal–oxide interface. The activation energy calculated from the temperature-dependency plots of the logarithmic rates was 27 kcal/mole, which was comparable with the value for the diffusion of oxygen through the oxide in the parabolic stage of the reaction. (W. E. Berry)

Corrosion of Refractory Metals

In a study of the oxidation of niobium,[22] the growth rate of the first layer of gamma Nb_2O_5 was measured in dry oxygen at 720 to 825°C as a function of oxygen pressure. This layer, which accounted for the major proportion of oxygen uptake during formation, was found to obey parabolic growth kinetics in which the dominant diffusing species was oxygen. The growth rate was highly sensitive to oxygen pressure, but the layer was not permeable to molecular oxygen.

In an investigation of tantalum oxidation at Oak Ridge,[23] it was found that anodic films retard oxidation in the range 425 to 575°C. For example, a 1000 A film reduced oxygen consumption by a factor of about 10 at 525°C. The activation energy for oxygen permeation was 45 kcal/mole. The film appears to reduce oxidation by (1) reducing oxygen flux which was related inversely to the film thickness and (2) postponing suboxide nucleation to higher oxygen levels. Protection by the anodic film eventually was lost by localized failure. In the oxidation of tantalum and niobium at 350 to 550°C, stresses on the order of the yield stress arose in the surface layer owing to the solution of oxygen in the metal and oxide-film ef-

fects.[24] Stresses were characterized by a flexure technique. As thicker oxide layers developed, the film stress substantially controlled gross flexure behavior.

In simulated reentry conditions the characteristics of tantalum ablation in O_2-N_2 mixtures has been studied by Sandia using a hyperthermal-arc-tunnel facility.[25] Tantalum melted at reduced temperatures of approximately 1800°C in the high-velocity gas stream. This phenomenon was attributed to oxide formation which was controlled by oxygen diffusion across the boundary layer. The melted material was identified by X-ray diffraction as alpha Ta_2O_5 + Ta. No nitrides or intermediate oxides were found. Neutron-activation analyses established an overall composition approximating TaO. Calculation of reaction rates based on TaO (not Ta_2O_5) gave good agreement with experimental data.

The oxidation of arc-melted and homogenized niobium containing 10 to 90 wt.% chromium was studied[26] at 500 to 900°C. Chromium increased oxidation resistance, especially at temperatures up to 800°C. The addition of 10 wt.% chromium promoted the formation of beta Nb_2O_5 and shifted the upper limit of alpha-phase stability from 900 to 600°C. In the presence of chromium, another oxide, apparently $CrNbO_4$, formed and slowed down oxygen diffusion through the scale.

The oxidation rate of vapor-deposited tungsten[27] has been studied in wet (1 to 2 vol.% H_2O) and dry air (−79°C dew point) at 600 to 1000°C. In wet air the tungsten initially exhibited parabolic oxidation with an activation energy of 48.2 kcal/mole, and then linear oxidation with an activation energy of 25.6 kcal/mole. At 1000°C the oxidation rate for vapor-deposited tungsten was essentially the same as that for powder-metallurgy tungsten. The rate was unchanged in dry air.

The Martin Company[28] conducted simulated hypersonic, low-altitude performance studies of tungsten (95 to 99% dense), Durak B-coated tungsten, ZrB_2-coated tungsten, and composites of W−2 wt.% ThO_2, W−8 wt.% Ag, W−10 wt.% Cu, and W−Sn−Al. These materials were exposed to heat fluxes of 1015 to 4160 Btu/(sq ft)(sec) at air-stagnation pressures of 21 to 70 atm and at stagnation temperatures of 2750 to 3500°C. Stagnation pressure and surface temperature largely governed the behavior. In general, at stagnation pressures up to about 50 atm and surface temperatures up to about 2600°C, surface recession rates were on the order of 0.01 to 0.02 in./sec for all materials and appeared to be controlled by the oxidation of tungsten which, in turn, was limited by gaseous diffusion of oxygen. At higher temperatures and/or pressures, the test specimens failed structurally, with pieces being fractured off. Average surface recession rates up to about 0.1 in./sec were noted. Little difference in behavior was observed among the various materials tested.

Russian workers[29] have studied the oxidation of arc-melted and homogenized tungsten containing up to 50 wt.% niobium at 900 to 1300°C. Alloying reduced the oxidation rate by a factor of up to 10, with 30 wt.% niobium being the most effective. From X-ray and metallographic tests, three types of scale, three types of subscale, and an embrittled diffusion zone were found. During oxidation, the metal-scale interface became enriched with niobium.

The corrosion behavior of arc-cast Mo−0.1 wt.% Ti−0.1 wt.% Zr and sintered alloys designated as Mo−Zr and Mo−W−Y−C in various acids heated in an autoclave has been reported.[30] The results can be summarized as follows:

	Corrosion rate, mm/year, and acid concentration	
Acid	At boiling point of acid	At 185°C
H_2SO_4	< 1 (0−70%)	< 1 (0− ~85%)
HCl	< 0.1 (0−20%)	< 0.3 (0−35%)
H_3PO_4	< 0.1 (0−90%)	< 0.4 (0−90%)

In H_2SO_4 the corrosion rate increased rapidly above about 80%. Alloy composition, method of preparation, and structure (wrought or recrystallized) had little effect on corrosion rate.

COATED REFRACTORY METALS

Sylcor is continuing studies of fused-slurry silicide coatings for protecting D-43 niobium-alloy sheet.[31] On the basis of 1-hr cyclic oxidation tests between 800 and 2500°F (427 and 1371°C) in air, coating compositions were optimized from the 25 initially chosen from the Cr−Ti−Fe−V−Si system. Compositions containing 20 wt.% chromium or 10 wt.% VSi_2 and without titanium addition resulted in significantly better performance than did compositions with higher concentrations. The effect of iron was not as conclusive. Optimum compositions found were Si−20 wt.% Cr−20 wt.% Fe−10 wt.% VSi_2 and Si−20 wt.% Cr−20 wt.% Fe, which survived about 30 and 50 cycles, respectively, at 99% reliability. Several compositions were characterized by using X-ray diffraction and electron-microprobe analysis and by noting wettability, faying surface penetration, and coating repair.

Iridium-base alloys have been explored by Solar[32] for use on tantalum alloys above 3500°F (1930°C). In coating-alloy development, Ir−30 wt.% Rh had the lowest surface recession rate, 1 to 4 mils/hr, in plasma-arc heats at 3850°F (2120°C). Additions of 15 wt.% osmium, 5 vol.% ThO_2−5 vol.% Ta_2O_5, 10 vol.% HfO_2, 10 vol.% SiO_2, 10 vol.% Al_2O_3, 10 vol.% ThO_2, or 10 vol.% MgO to iridium by arc melting or powder metallurgy offered no improvement. In other work, iridium and Ir−30 wt.% Rh were electrodeposited on 125-mil-diameter tungsten rods. Pinholes

developed in both coatings and caused premature failure during self-resistance heating in air at 3500°F.

Texas Instruments[33] is investigating the chemical vapor-deposition process for coating refractory metals and has demonstrated the feasibility of coating B-66 niobium alloy with Cr–Ti–Si of controlled composition. On the basis of air oxidation tests at 2300 and 2500°F (1260 and 1371°C), the performance of the coating appeared comparable to that of the Cr–Ti–Si coatings produced by other methods.

Electrophoretic coatings for Ta–10 wt.% W have been investigated by Vitro.[34] ZrB_2, ZrB_2–10 wt.% $MoSi_2$, and $TaAl_3$ coatings were unsatisfactory because of interdiffusion and substrate embrittlement at 3100°F (1700°C). Satisfactory adherence and minimum contamination were obtained with $TaSi_2$, $MoSi_2$, and WSi_2 when the average particle size was under 10 μ. After application of a dense, gradated, binary oxide overlayer, a typical oxidation life of 15 min at 3500°F (1930°C) was obtained with WSi_2/Al_2O_3–4 wt.% MgO, WSi_2/ThO_2, WSi_2/ZrO_2–2 wt.% TiO_2, and WSi_2/MgO coatings. Failure was due to either edge and corner defects or interaction with the setter material.

In a companion study, Vitro[35] investigated other coatings for protecting T-222 tantalum alloy. On the basis of cyclic oxidation tests from room temperature to 1500 or 2400°F (816 or 1316°C), Hf–27 wt.% Ta, $TaAl_3$, ZrB_2, and $ReSi_2$ coatings were eliminated. Work was concentrated on single-phase and binary silicides. When postsiliconized and preoxidized, the WSi_2–$MoSi_2$, $MoSi_2$–3 wt.% VSi_2, and $MoSi_2$–3 wt.% $TiSi_2$ coatings behaved erratically and were susceptible to pest fracture at 1500°F. The concentration of second phases VSi_2, $CrSi_2$, and also $TiSi_2$ was then increased to 10 to 30 wt.%. $MoSi_2$–30 wt.% VSi_2 gave the best performance. Two specimens survived 600 hr (including 30 cycles to room temperature) at 1500°F and at 2500°F (1371°C) without failure, whereas others failed at 12 to 100 hr. WSi_2–30 wt.% VSi_2 behaved well at 2400°F but failed at 1500°F.

Protection offered by a series of coatings on Nb–1 wt.% Zr was evaluated at Jet Propulsion Laboratory in 4 cu ft/hr STP argon (containing 1 to 3 ppm O_2, and < 10 ppm H_2O for this first 24 hr with 1 to 3 ppm thereafter) at 2000°F (1093°C) for 500 hr (Ref. 36). The coatings consisted of Sylcor Sn–Al, Chromizing Corporation Durak KA, Pfaudler single- and double-cycle silicides, Vitro Cr–Mo–Si, and $MoSi_2$ with a 5-mil-thick molybdenum barrier layer. The coatings were evaluated by metallography, hardness measurements, bend tests, and electron-microprobe analysis. $MoSi_2$/Mo gave the best protection. Tin and aluminum offered adequate oxidation resistance despite spalling. The other coatings were less satisfactory since Cr–Mo–Si allowed chromium diffusion into the substrate and the Pfaudler and Chromizing coatings permitted some substrate oxidation.

The Russians have developed a hot-dip method of applying aluminum-alloy coatings on niobium and molybdenum.[37] The surface was activated by dipping in a fluoride-base flux and by preoxidizing in air at 480 to 660°F (249 to 349°C) for niobium and 660 to 840°F (316 to 449°C) for molybdenum. Complex aluminum-alloy coatings were much more oxidation resistant than unalloyed aluminum. Aluminum on 99.5% niobium spalled after 50 hr at 1560 to 1650°F (849 to 899°C) in air, and an Al–Si–Mo coating (composition not given) was protective for 100 hr at 1850 to 2010°F (1000 to 1100°C) and Al–Si–Mo–Cb–Cr was protective for 200 hr at 2280 to 2370°F (1250 to 1300°C). An Al–Si–Mo–Cr coating protected 99+ % molybdenum at 2730°F for at least 30 hr.

(B. C. Allen)

Corrosion by Nonaqueous Liquids

Steels in Sodium

In the Atomics International Sodium Components Test Facility, thermal expansion is accommodated by 304 stainless-steel bellows expansion assemblies. Three such bellows that failed after relatively short periods of service were found[38] to be sensitized and corroded intergranularly. After much study it was concluded that the sensitization had occurred during a 700°C baking operation performed to remove volatile materials between the two plies of the bellows. Further, the intergranular attack was judged to have stemmed from atmospheric moisture in contact with the sensitized steel during the 30-month period between fabrication and installation. Subsequently, multiple cracks occurred in the corroded areas when the bellows were flexed during operation. Thus the exposure to sodium was apparently in no way responsible for the failures. A reduced bellows baking temperature (425°C) and close control of storage conditions have been instituted to prevent similar failures in the future.

Tubing materials for sodium-heated steam generators must be compatible with boiling water on one side and high-temperature sodium on the other. For water and steam service, ferritic steels are preferred over austenitic steels because of their low cost and superior resistance to stress–corrosion cracking. For high-temperature sodium containment, on the other hand, austenitic steels are preferred because of their greater strength and indifference to decarburization. If a compromise is attempted by utilizing an austenitic steel for high-temperature regions and a ferritic steel for lower temperature zones of the same boiler, there is danger that the ferritic steel will be weakened by decarburization and the austenitic steel embrittled by carburization. On the basis of results of an 8000-hr test of a single-tube steam generator modeled after one tube of a bimetallic 1000-Mw(e) sodium-heated steam genera-

tor, workers at Babcock & Wilcox[39] concluded that a 316 stainless-steel hot zone (600°C, maximum) followed by a Croloy 2¼ steel cold leg (340°C, minimum) was satisfactory. During the test the oxygen in the sodium had been maintained below 30 ppm by hot and cold trapping. The partial decarburization of the Croloy 2¼ to depths up to 25 mils, the depletion of chromium and nickel and enrichment of iron in a thin surface layer of the 316 stainless steel, and the complete sensitization of the latter were apparently not serious enough to rule out this combination of materials. However, because of the tempering effects of the high-temperature exposure, it was not possible to get an accurate picture of the influence of the sodium on the mechanical properties of either the austenitic or the ferritic steel.

On the basis of a series of "see-saw" capsule tests (up to 20,000 ½-hr cycles with hot end at 650°C and cold end at 500°C), workers at Brookhaven[40] concluded that adding 15 at.% hot-gettered lithium to hot-gettered sodium had no adverse effect on its corrosiveness toward 304, 316, 321, or 410 stainless steel. No hot-zone penetration or cold-zone deposition could be detected. Posttest analyses for oxygen in the alkali metals showed that there was substantially less Na_2O in the capsules containing lithium than in those without lithium. Most of the oxygen in the former was tied up as Li_2O.

Vanadium Alloys in Sodium

Table III-1 shows some results of Argonne's corrosion tests[41] on specimens of several vanadium alloys being considered as fuel claddings for sodium-cooled fast reactors. Significant conclusions from these are as follows:

1. If the oxygen level in the sodium is too low for the formation of a vanadium oxide phase, corrosion of these vanadium alloys is manifested by slow weight gains [on the order of 1 mg/(dm²)(day)].

2. Increasing the oxygen level in the sodium by just a few parts per million causes the corrosion to appear as relatively rapid weight losses [from ~13 to ~60 mg/(dm²)(day)], apparently stemming from the loss of the nonadherent vanadium oxide phase which can form at the higher oxygen level. This suggests that, as suspected, stringent restriction of oxygen in the sodium to very low values is vital to the successful use of these vanadium cladding alloys.

3. At the higher oxygen level, the V–20 wt.% Ti alloy showed much slower weight losses than the others [~13 mg/(dm²)(day) compared with ~60]. Such a large difference had not been found in earlier tests at 650°C (100°C higher).

4. The earliest tests on V–20 wt.% Ti at 650°C gave a weight-loss rate of ~100 mg/(dm²)(day), compared with the rate of ~13 mg/(dm²)(day) for the same alloy at 550°C and similar oxygen conditions. This shows the sensitivity of corrosion to temperature when the vanadium oxide corrosion product can form.

Preliminary examinations of 12 samples of assorted potential cladding materials after 14 months' exposure to sodium in the Experimental Breeder Reactor (EBR-II) core at temperatures to 530°C showed essentially no weight changes for 304 stainless steel and nickel-base alloys, small weight losses for V–20 wt.% Ti and V–40 wt.% Ti, and severe attack (~50% weight loss) for unalloyed vanadium.[41] The poor performance of the latter specimen is probably not attributable to the radiation exposure. More likely, there was enough oxygen in the sodium to permit vanadium oxide to form and accelerate the loss in weight. In an earlier 70-day ex-pile exposure of unalloyed vanadium to 650°C sodium with oxygen below the oxide-formation threshold, the specimen did not lose weight at all; instead, it gained weight at an average rate of about 0.3 mg/(dm²)(day).

Table III-1 CORROSION OF VANADIUM ALLOYS[41] IN COLD-TRAPPED SODIUM AT 550°C

Time:	1 week		2 weeks		6 weeks	
Cold-trap temp., °C:	170	120	170	120	170	120
Oxygen in sodium,* ppm:	13.7		13.1	9.1	11.0	8.6
Alloy, wt.%	Weight change, mg/cm², at indicated time					
V–5 Ti–15 Cr (cold rolled)	−4.25	+0.15	−9.80	+0.27	−27.0	+0.42
V–5 Ti–15 Cr (1250°C HT)	−4.09	+0.12	−9.55	+0.23	−27.1	+0.43
V–5 Cr (annealed)	−3.73	+0.08	−9.24	+0.23	−26.0	+0.59
V–20 Ti (annealed)	−0.75	+0.25	−1.80	+0.29	−5.52	+0.55

*Measured at indicated time by mercury-amalgamation technique.

Demonstrating that the V–20 wt.% Ti alloy is inert to high-temperature sodium with sufficiently low oxygen content, Brookhaven researchers[40] found no attack or deposition in a thermal-convection loop of this material after 5000 hr of operation with hot-trapped sodium (4 ppm oxygen) between 825 and 665°C. The only effect noticed was a slight increase in the oxygen content of the V–20 wt.% Ti tubing throughout the loop.

To get an idea of what would happen to a V–20 wt.% Ti cladding on the fuel in a sodium-cooled-reactor

system made of stainless steel, Brookhaven workers[40] ran a 316 stainless-steel "see-saw" capsule with a V–20 wt.% Ti tubular insert for 3060 hr at 760°C (hot end) and 500°C (cold end). The results indicate that material transfer may be a problem in such a system. For instance, a reacted hard layer was found on the surfaces of the insert. Its carbon content increased from 270 to 4700 ppm during the test, but the measured weight gain indicated that other species transferred as well. The carbon content of the hot end of the 316 stainless-steel capsule was reduced from 530 ppm (as received) to 460 ppm after the test.

Refractory Metals in Sodium

The French conducted a study[42] of the corrosion of niobium by 400 to 600°C sodium flowing at ¼ to 2 m/sec for periods up to 3000 hr. The vital role of oxygen in the sodium is demonstrated by the following tabulation.

Method of sodium purification (in order of increasing effectiveness)	Test temp., °C	Velocity of sodium, m/sec	Corrosion rate, mg/(cm²)(month)
Diffusion cold trap	550	1.8	45–49
Circulating cold trap	550	1.8	28
Hot trap	550	1.7	0.1–0.2

The corrosion rate was quite sensitive to temperature, as shown in Fig. III-1. It obeyed an Arrhenius law with an activation energy of 34.5 kcal/mole. Very little difference was observed between the rate of attack of cold-worked niobium and that of annealed material. The addition of 5 wt.% vanadium to the niobium had no significant effect on its corrosion. However, the alloy Nb–7.5 wt.% Ti–0.75 wt.% Zr showed a markedly reduced corrosion rate. These effects are illustrated in Fig. III-2.

Hydronautics, Inc., has published a summary report[43] on their investigations of cavitation damage, high-frequency fatigue, and stress corrosion of five alloys in liquid sodium up to 815°C. As can be seen in Fig. III-3, the ultrasonic vibrations produced a high rate of damage at first, followed by a reduced steady-state rate. Stellite 6B was found to be most resistant to cavitation damage, followed in order by Cb-132M, T-222, TZM, and 316 stainless steel. It was noted that the amount of oxygen in the sodium (in the range 35 to 100 ppm) had no effect on the 14,000-cps fatigue behavior of TZM alloy or of 316 stainless steel. Further, the 14,000-cps fatigue characteristics of 316 stainless steel in 815°C sodium were comparable with those in vacuum at 4 to 5 cps. No stress–corrosion cracking could be found in highly stressed TZM or 316 stainless steel following 60-hr exposures to 540 and 815°C sodium of various oxygen contents.

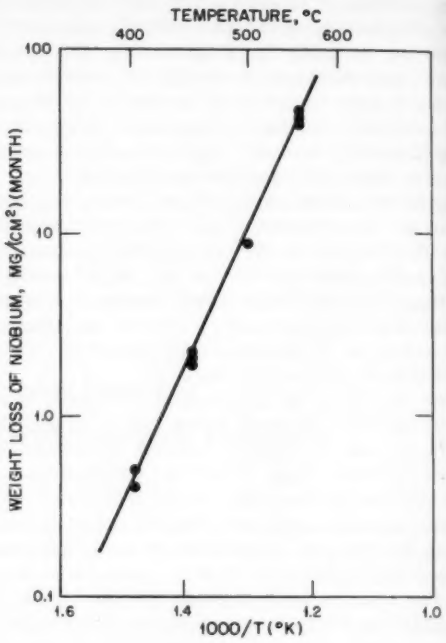

Fig. III-1 Effect of temperature on the corrosion rate of niobium by flowing sodium cold trapped[42] at 110°C.

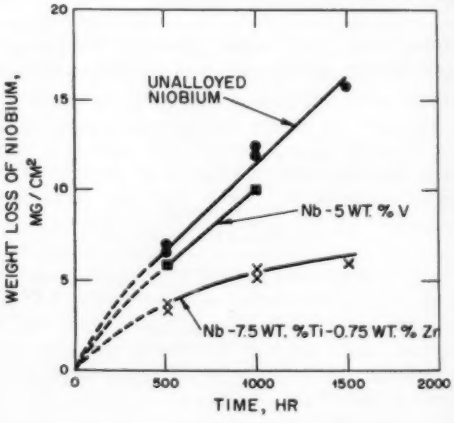

Fig. III-2 Comparison of the corrosion of unalloyed niobium with that of two of its alloys in 500°C sodium cold trapped[42] at 110°C.

It was reported previously that Oak Ridge workers had examined a capsule in which sodium had been boiled at 1230°C and condensed at 1190°C for 5000 hr and found that the Nb–1 wt.% Zr sleeve-type inserts had altered their oxygen content in a very nonuniform manner. Metallography of a specimen taken from the bottom or boiler end-plug weld revealed spongy gray

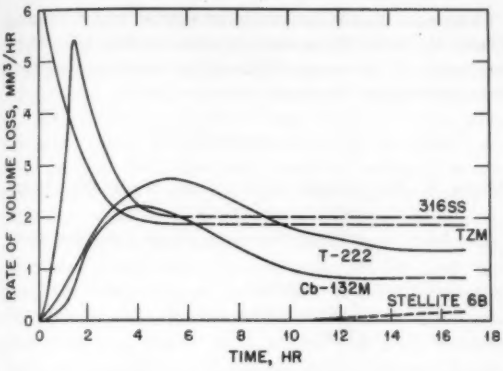

Fig. III-3 Relative cavitation-damage resistance of five metals tested at 14 kc/sec (1.36 mils double amplitude) in 400°F (205°C) sodium containing ~35 ppm oxygen.[43]

nonmetallic deposits several mils thick on the surface and a light etching diffusion zone about 0.5 mil thick below the surface.[44] The results of microprobe analyses of these layers are shown in Fig. III-4. Note that the zirconium concentration in the nonmetallic deposit corresponds closely to that in ZrO_2. According to the investigator, the presence of ZrO_2 can be explained plausibly in terms of several alternative mass-transfer sequences.

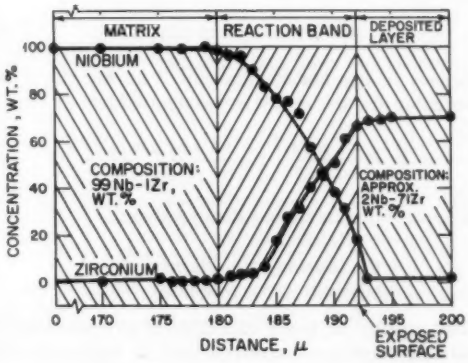

Fig. III-4 Concentration profiles of niobium and zirconium in Nb–1 wt.% zirconium capsule insert just above liquid level after 5000-hr exposure of surface to 1230°C boiling, refluxing sodium.[44]

Corrosion by Molten Potassium

Workers at the Allison Division of General Motors conducted an extensive program to determine the effects of velocity, heat flux, area ratio, residence time, and oxygen contamination on the behavior of bimetallic (316 stainless steel and Nb–1 wt.% Zr) potassium loops operating between 1200 and 1500°F (650 and 815°C) for periods up to 8000 hr. Subsequently, they made detailed examinations and analyses of materials from various parts of these loops to better define the long-life design limits. Results of the latter studies are summarized in a final report on the project.[45] Highlights are as follows:

1. The microstructure of 316 stainless steel showed complex carbides (mainly $Cr_{23}C_6$) after exposure to flowing potassium at 1200°F. In 1500°F portions of the same loops, chi phase appeared in addition to the complex carbides. Here, the relative amount of chi phase increased with exposure time. No sigma phase was found.

2. Heat-treating 316 stainless steel in air at 1500°F for as long as 8000 hr prior to testing had little or no effect on its 1500°F stress-rupture life. However, samples exposed to flowing potassium prior to testing showed a continuous reduction in 1500°F stress-rupture life up to about 3000 hr of preexposure and a leveling off thereafter, as illustrated in Fig. III-5.

3. Exposure of 316 stainless-steel specimens to molten potassium at 1350 and 1450°F (730 and 790°C) caused a small, but consistent, decrease in fatigue life, as determined by low-frequency (20 cycles/min) strain-cycling tests.

4. Calculated diffusion coefficients for carbon in 316 stainless steel (based on kinetics analysis from chemical and metallurgical studies of a loop) were orders of magnitude greater than those in the Nb–1 wt.% Zr alloy. Carbon transport from the high-temperature portion of the loop was limited only by solid-state diffusion in the stainless steel and not by surface reaction or solubility in potassium.

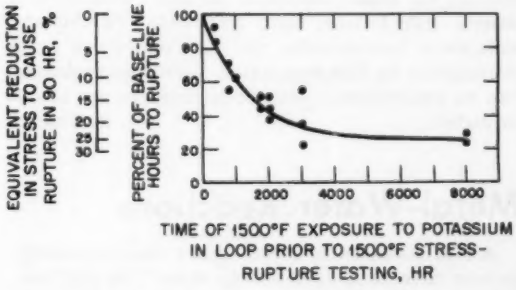
EQUIVALENT REDUCTION IN STRESS TO CAUSE RUPTURE IN 90 HR, %
PERCENT OF BASE-LINE HOURS TO RUPTURE
TIME OF 1500°F EXPOSURE TO POTASSIUM IN LOOP PRIOR TO 1500°F STRESS-RUPTURE TESTING, HR

Fig. III-5 Effect of preexposure to flowing potassium on stress-rupture characteristics of 316 stainless steel.[45] *(Base-line data = ASTM values for 316 stainless steel.)*

Fouling by Organics

The impurities in organic coolants which affect the fouling of Zr–2.5 wt.% Nb clad fuel have been described by Chalk River.[46] It was found that the fouling potential increased with chlorine contents greater than 0.5 ppm, oxygen at low levels, and water content

less than 100 ppm. The fouling potential was also related directly to radiation dose.

Containers for Molten Uranium

Of a half-dozen metals tested by workers at Ames Laboratory,[47] tungsten was found to be the only one that can be used successfully to enclose yttrium capsules containing molten uranium up to 1400°C. This setup is being used to test the corrosion of yttrium by molten uranium. In tests at 1300°C for up to 250 hr, a solution-type attack was observed, with yttrium precipitating at the uranium meniscus level. Also, traces of uranium were found on the outer surfaces of the capsules as a result of diffusion along the boundaries of the large yttrium grains. The amount of solution attack was about the same after 250 hr as it was after 50 hr.

Embrittlement by Liquid Metals

The phenomenon of embrittlement of some solid metals by simple contact with certain liquid metals (e.g., copper with mercury) has been studied extensively. Most explanations are based on action at a surface imperfection like the tip of a scratch or crack, where it is postulated that the liquid metal causes a great reduction in the energy needed to break atomic bonds. Robertson[48] has presented a somewhat different approach, by assuming that capillarity causes the liquid metals to extend to the very tip of the crack and that under an applied stress there is an increased solubility of the solid in the liquid at the crack tip. The rate of crack propagation would then be governed by the rate of diffusion of solute through the liquid away from the tip. On the basis of sample calculations, using realistic parameters, Robertson demonstrated that the velocity of crack propagation by this dissolution–diffusion mechanism can be appreciable—tens of centimeters per second or higher. (E. M. Simons)

Metal-Water Reactions

Recent advances in metal–water reaction investigations have been reviewed by Baker[49] for the reactor metals zirconium, stainless steel, and aluminum. Testing of Zircaloy-4-clad UO_2 was continued at General Electric[50] to define the melting behavior of the metal at various stages of cladding oxidation. The experimental techniques and samples employed were the same as those described in a previous review.[51] The cladding was oxidized by heating the sample in an atmosphere of water vapor at rates of 0.3, 0.6, 1.0, and 3.0°C/sec to temperatures of 1200 to 1600°C. The rates of heating, the maximum temperature attained, and the estimated oxide-film thickness are shown in Table III-2.

A comparison of dynamic and isothermal corrosion rates has been presented by General Electric.[50] The corrosion of zirconium in steam at constant temperature follows the parabolic law:

$$W^2 = K_0 \exp(\Delta H/RT)t \quad (1)$$

where W = the weight of zirconium reacted/cm^2 area
K_0 = a constant, mg^2/(cm^4)(sec)
ΔH = the activation energy of the reaction, kcal/mole
R = the gas constant
T = absolute temperature, °K
t = time, sec

Three experimentally determined equations are available, those of Baker and Just,[53] Lemmon,[54] and General Electric.[52] Constants of these equations are

	K_0, mg^2/(cm^4)(sec)	ΔH, kcal/mole
White	4,073,460	−40,025
Baker and Just	33,300,000	−45.5
Lemmon et al.	468,000	−34.0

The expected extent of corrosion under conditions of steadily rising temperature was calculated from the isothermal data presented above. These calculations were performed when Eq. 1 was first differentiated with respect to time to obtain the corrosion rate at constant temperature:

$$d(W^2)/dt = K_0 \exp(\Delta H/RT) \quad (2)$$

After $a + bt$ was substituted for T in Eq. 1, it was integrated and the result approximated by

$$W^2 = \frac{K_0 M}{be^x}\left(1 - \frac{x^2 + a_1}{x^2 + b_1}\,\frac{x + a_2}{x + b_2}\right) \quad (3)$$

where M = the maximum temperature
$x = -\Delta H/RM$
b = the heating rate, °K/sec
a_1, a_2, b_2 = approximating constants

The results of these calculations are presented in Table III-2 and are compared with the experimentally

Table III-2 PREPARATION OF PARTIALLY OXIDIZED CLADDING[50]

Heating rate, °C/sec	Max. temp., °C	Oxide-film thickness, μ			
		Estimated	Calculated by equation of		
			General Electric[52]	Baker[53]	Lemmon[54]
3.0	1400	40	54	64	49
0.3	1200	40	67	71	69
1.0	1400	120	94	111	85
0.6	1350	120	98	113	91
1.0	1550	200	167	212	140
0.3	1450	200	210	255	184
0.3	1500	320	254	316	218
0.6	1600	320	256	332	209

determined estimated oxide thicknesses. In general, reasonable agreement is obtained, with Baker's data[53] being perhaps the most consistent.

Meltdown experiments at Argonne[55] were continued in TREAT with Zircaloy-2-clad, UO_2-core fuel rods. The purpose of this research was to obtain information on the chemical and physical changes which occur upon meltdown of the fuel cluster during a loss-of-coolant accident. Specific emphasis was placed on determining the extent of metal–water reaction, the temperature and pressures produced, and the final distribution of particle size of the fragmented fuel. Three experiments were performed, each on a progressively longer time scale. The experimental technique consisted of loading a "scaled-up" autoclave with a fuel-rod cluster and water and exposing the assembly to a neutron flux in TREAT. In these experiments, three fuel rods were used in each test and were located above the pool of water instead of being submerged in it. Each fuel rod consisted of 10 sintered, fired UO_2 pellets clad with Zircaloy-2. The fission heat generated in the 10% enriched UO_2 during the TREAT transient caused meltdown of the fuel rods. In each experiment the TREAT reactor power level, i.e., the neutron flux, was held constant to more realistically simulate a loss-of-coolant accident.

Results from these three experiments are summarized in Table III-3. The runs are arranged from the shortest time of fission heating (12 sec) to the longest (50 sec). The most significant feature of the experiments was the appearance of the residues; portions of the cladding were present that retained their original cylindrical form. Consequently, considerable quantities of molten UO_2 emptied from the Zircaloy cladding before melting of the cladding occurred. A very significant observation, based on the distribution of the residues, was the absence of large quantities of very fine particles. This suggests that molten UO_2 and molten UO_2–Zr–ZrO_2 mixtures do not exhibit a marked tendency for spontaneous subdivision on being quenched in water. As seen in Table III-3, the total extent of metal–water reaction for the three experiments varied from 30 to 44%.

(J. M. Genco)

Irradiation Effects in Nonfuel Materials

Zirconium Alloys

A summary on the effects of irradiation on the mechanical properties of Zircaloy-4 has been compiled at Westinghouse.[56] The data include tensile properties and in-pile collapse of cladding. Another summary on the behavior of zirconium alloys in nuclear applications has been issued by Bement.[57] Burst tests performed on irradiated Zircaloy-2 tubing at Phillips Petroleum indicate that the hoop strength

Table III-3 SUMMARY OF RESULTS OF LOSS-OF-COOLANT EXPERIMENTS[55] IN TREAT WITH ZIRCALOY-2-CLAD, UO_2-CORE FUEL CLUSTERS*

	Experiment number		
	CEN-217S	CEN-220S	CEN-223S
Transient			
Location of fuel cluster	Above 30°C H_2O	Above 100°C H_2O	Above 100°C H_2O
Duration of flat-top transient, sec	12	32	50
Average heat-generation rate in UO_2,† kw/ft	40	20	11
Average reactor power level,† Mw	40	20	11
Fission-energy input, cal/g UO_2	560	770	630
Results			
Metal–water reaction, %	40	44	32
Peak pressure rise, psig	87	750	220
Maximum rate of pressure rise, psig/sec	45	76	3
Final appearance of UO_2 fuel	Complete destruction; fragments and particles; ~½ of cluster dropped into water	Complete destruction; fragments and particles; whole cluster dropped into water	Complete destruction; fragments and particles; whole cluster dropped into water
Average particle size of residue (d_{sv}),‡ mils	91	83	

*Ten sintered pellets of UO_2 (10% enriched in ^{235}U) per rod. Overall rod dimensions: 5.62 in. long by 0.42 in. in diameter; 25-mil-thick cladding; 3-mil gap between core and cladding; helium bonded. Three rods with a weight of 254 g of UO_2 and 82 g of Zircaloy-2 per cluster; 750 g of water in autoclave.

†The identical values of heat-generation rate and reactor power level are coincidental.

‡$d_{sv} = \dfrac{1}{\sum \frac{w_i}{d_i}}$ where w_i = fraction by weight of particles with diameter d_i as determined by sieve screen analysis.

required for fracture was increased.[19] The results of these tests are given in Table III-4.

Specimens of Zr–2.5 wt.% Nb–0.5 wt.% Cu, which had received different preirradiation heat-treatments, were tested[58] at room temperature and 300°C. The results of these tensile tests are given in Table III-5, and the preirradiation properties are given in Table III-6. The specimens that had been aged for 6 hr at 535°C after quenching from the alpha-plus-beta phase showed the smallest changes in yield strength and reduction in area after irradiation.

Table III-4 BURST STRENGTH OF UNIRRADIATED AND IRRADIATED ZIRCALOY-2 TUBES[19]

Sample	Exposure, 10^{21} neutrons/cm^2	Burst pressure		Ultimate hoop stress	
		Psi	Kg/cm^2	Psi	Kg/cm^2
2	1.7	17,250	1,214	119,800	8,430
4	2.35	15,650	1,100	108,000	7,600
6	1.4	15,750	1,108	109,500	7,700
8	Nil	15,075	1,060	97,300	6,850
10	Nil	13,750	966	88,800	6,250
12	Nil	13,900	978	89,900	6,325

In-pile creep tests on zirconium, annealed Zircaloy-2, cold-worked Zircaloy-2, and Zr–2.5 wt.% Nb in various conditions are continuing at Chalk River. The results of these tests were summarized by the Canadians as follows:[59]

1. Irradiation enhances the creep rate of cold-worked Zircaloy-2 at all stresses tested (up to 45,000 psi) in the temperature range 220 to 400°C, but has little effect on heat-treated Zr–2.5 wt.% Nb at 300°C and possibly reduces the creep rate in annealed crystal-bar zirconium at 200°C.

2. At a stress of 20,000 psi, preirradiation has little or no effect on the creep rate of Zircaloy-2 at 300°C, but, at 45,000 psi, the creep rate is lower by approximately one order of magnitude when under irradiation and by two orders of magnitude when out of flux.

3. At 3000°C and 45,000 psi, cold-worked Zircaloy-2 shows no onset of tertiary creep in the reactor up to at least 1.95% strain. This compares well with out-reactor test where the onset of tertiary creep has been determined to lie between 1 and 2% strain.

4. At 350°C and high strain rate, onset of tertiary creep was observed at approximately 1.4% strain, i.e., comparable to the behavior in the laboratory, but when the strain rate was reduced, steady creep conditions persisted up to at least 2.58% strain.

5. The temperature dependence of creep rate in cold-worked Zircaloy-2 and heat-treated Zr–2.5 wt.% Nb is similar both in and out of flux. There is a marked change in the slope of log (creep rate) vs. log (1/temperature) curve around 350°C. The values for the activation energy of creep obtained from the Arrhenius-type plot are 50,000 to 60,000 cal/mole above 350°C and 15,000 to 25,000 cal/mole below 350°C.

6. At creep rates of 10^{-7}/hr and lower, it takes at least 3000 hr to reach a steady creep rate under irradiation.

Table III-5 EFFECT OF NEUTRON IRRADIATION ON THE TENSILE PROPERTIES OF THE Zr–2.5 WT.% Nb–0.5 WT.% Cu ALLOY[58]

Metallurgical condition	Irradiation temp., °C	Integrated flux, neutrons/cm^2 (E > 1.0 Mev)	Test temp., °C	Change in property,* %			
				Yield stress (0.2% offset)	Fracture stress	Uniform elongation, %	Reduction in area, %
Quenched from (α + β) phase and aged 6 hr at 535°C	<100	5.3×10^{19}	RT	+17	0	−80	0
	<100	5.3×10^{19}	300	+25	+13	−55	0
	250 to 325	6.2×10^{19}	RT	+14	0	−66	0
	250 to 325	6.2×10^{19}	300	+16	−20	−28	0
	375	1.2×10^{20}	RT	+10	0	−25	−12
	375	1.2×10^{20}	300	+20	+13	−18	0
Slow cooled from (α + β) phase (850°C)	250 to 325	6.0×10^{19}	RT	+70	0	−73	−36
	250 to 325	6.0×10^{19}	300	+129	+11	−82	−20
	375	1.2×10^{20}	RT	+58	0	−31	−30
	375	1.2×10^{20}	300	+62	+14	−51	−21
Slow cooled from β phase (880°C)	<100	5.7×10^{19}	RT	+62	+11	−90	0
	<100	5.7×10^{19}	300	+83	0	−90	−11
	250 to 325	3.0×10^{20}	RT	+68	0	−91	−58
	250 to 325	3.0×10^{20}	300	+144	+17	<95	−35
Rapidly cooled from β phase (1000°C)	<100	5.7×10^{19}	RT	+46	0	−82	0
	<100	5.7×10^{19}	300	+74	−23	−91	−25
	250 to 325	4.4×10^{19}	RT	+59	0	−73	−80
	250 to 325	4.4×10^{19}	300	+102	−27	−82	−50
Quenched from β phase and aged 24 hr at 400°C	250 to 325	3.0×10^{20}	RT	+23	0		0
	250 to 325	3.0×10^{20}	300	+20	+25	−25	0

*Changes measured at <10% are recorded as zero.

Table III-6 PREIRRADIATION TENSILE PROPERTIES OF THE Zr–2.5 WT.% Nb–0.5 WT.% Cu ALLOY[58]

Metallurgical condition	Alloy	Test temp., °C	Tensile property			
			Yield stress (0.2% offset), 1000 psi	Fracture stress, 1000 psi	Uniform elongation, %	Reduction in area, %
Quenched from (α + β) phase and aged 6 hr at 535°C	AS	RT	110	188	5.5	54
		300	73	160	4	73
Slow cooled from (α + β) phase (850°C)	AS	RT	55	130	14.5	51
		300	29	93	16.5	67
Quenched from β phase and aged 24 hr at 400°C (880°C)	AM	RT	141	167	1.5	5
		300	116	154	2	28
Slow cooled from β phase (880°C)	AM	RT	62	110	11	41
		300	29	77	10	62
Rapidly cooled from β phase (1000°C)	AS	RT	69	141	10	50
		300	38	132	10	80

Mild and Alloy Steels

The recovery of irradiation-induced increase in yield strength of A-302B steel by annealing was shown to depend on both the annealing temperature and exposure of the specimen.[60] It was noted that at higher exposures a higher annealing temperature is required to obtain a similar reduction in the yield strength. The influence of annealing time was shown to decrease with increasing temperature. The effect of microstructure on the fracture toughness of irradiated A-302B steel has also been determined.[61] Three different microstructures were obtained by (1) quenching and tempering, (2) normalizing, and (3) annealing. The effect of irradiation on the ductile-to-brittle transition temperatures of the different microstructures is shown in Table III-7. It can be seen that the quenched-and-tempered structure was the most resistant to irradiation embrittlement and that the structure resulting from annealing is the least resistant. A similar order of irradiation-embrittlement performance by the different microstructures is exhibited when the measurement criterion is plane-strain fracture toughness (K_{Ic}). These results support the findings at the Naval Research Laboratory,[62,63] where it was noted that the tempered martensitic structure was the most resistant to irradiation embrittlement, whereas an annealed ferritic structure was most easily embrittled by irradiation. Reduced ductile-to-brittle transition temperatures can be obtained by intermediate annealing of mild steel between irradiation which results in removal of a portion of the irradiation effects before further irradiation commences.[40] Figure III-6 compares the effect of continuous irradiation and intermediate annealing during irradiation on the impact strength of A-212 steel.

The effect of irradiation on axial fatigue behavior of A-302B and A-212B steels was determined[64] after exposure to 4×10^{17} neutrons/cm^2. The results indi-

Table III-7 IRRADIATION EFFECTS ON CHARPY IMPACT PROPERTIES AND HARDNESS FOR FOUR CONDITIONS OF A-302B STEEL[61]

Heat-treatment	Neutron exposure, 10^{18} neutrons/cm^2 (>1 Mev)	Transition temp.,* °F	Change in transition temp., °F	Full shear Charpy energy		Hardness	
				E_s, ft-lb	ΔE_s, ft-lb	R_B	ΔR_B
Normalized	Control	0		130		84.8	
	Thermal control	0	0	130	0	85.3	+0.5
	7.0	90	+90	100	−30	90.1	+5.3
	13.5	115	+115	95	−35	92.9	+8.1
	15.0	130	+130	85	−45	93.4	+8.6
Annealed	Control	130		75		87.9	
	Thermal control	110	−20	80	+5	86.0	−1.9
	9.0	255	+125	63	−12	92.5	+4.6
	13.5	300	+170	60	−15	94.1	+6.2
Annealed and normalized	Control	10		140		80.2	
	Thermal control	10	0	140	0	77.7	−2.5
	6.5	85	+75	102	−38	85.6	+5.4
	13.0	120	+110	100	−40	88.2	+8.0
	15.0	150	+140	97	−43	88.7	+8.5
Quenched and tempered	Control	−210		125		102.4	
	Thermal control	−210	0	125	0	112.2	−0.2
	14.0	−115	+95	100	−25	103.6	+1.4

*Transition temperature for 30 ft-lb.

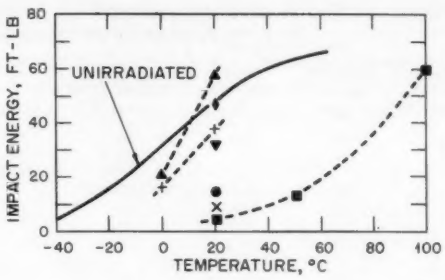

Fig. III-6 Impact properties of A-212 steel irradiated to a total accumulated exposure of 8×10^{18} neutrons/cm² and given intermediate and final annealing treatments.[40] Four hours after each 1×10^{18} neutrons/cm²: ●, 200°C anneal; +, 300°C anneal; ▲, 350°C anneal. ■, 8×10^{18} neutrons/cm², no annealing. Four-hour anneal: ×, 8×10^{18} neutrons/cm² + 200°C; ▼, 8×10^{18} neutrons/cm² + 300°C; ◆, 8×10^{18} neutrons/cm² + 350°C.

cated that irradiation had only a minor effect on fatigue life, increasing it at low strains and decreasing it at high strains.

Stainless Steel and Nickel Alloys

Irradiation studies on 0.15 wt.% titanium-modified 304 stainless steel have shown that the preirradiation heat-treatment significantly affects the postirradiation mechanical properties.[65] The results in Tables III-8 and III-9 indicate that the higher annealing and irradiation temperatures result in lower postirradiation ductility. This was attributed to two possible factors: (1) that the anneal at 900°C resulted in fine intergranular dispersions near the grain boundary which acted as traps for the helium atoms; and (2) that the higher temperature anneal resulted in a larger grain size which has previously been shown to be a structure more susceptible to elevated-temperature embrittlement.[66]

Helium that was injected into 304 stainless steel by cyclotron bombardment causes the steel to behave similarly to neutron-irradiated material at elevated temperatures.[65] A moving tapered moderator was constantly moved back and forth across the beam of accelerated alpha particles to obtain uniform helium distribution in the material. Results of tensile tests at 500 to 900°C indicate that the effect of helium (10^{-7} atom fraction) does not become significant until 700°C, and, at higher temperatures, it tends to affect the necking strain considerably more than the uniform strain. Another interesting experiment to investigate the cause of irradiation-induced embrittlement has been performed by the Germans.[67] An Fe–11.3 wt.% Cr alloy was irradiated to 1.6×10^{19} neutrons/cm² and tested at temperatures of 500 to 880°C. Irradiation had no effect on the postirradiation ductility of the alloy until the crystal structure of the alloy transformed from body-centered cubic to face-centered cubic at 825°C. The phase transformation was determined by measuring the change in specimen length by a dilatometer. This finding indicates that the elevated-temperature embrittlement in irradiated materials is characteristic of face-centered cubic materials. Irradiations of an Fe–14 wt.% Cr–4 wt.% Al–1 wt.% Y alloy have shown that no elevated-temperature embrittlement is caused by irradiation.[68,69] However, aluminum is a strong alpha stabilizer and the 4 wt.% addition prevents a phase transformation from taking place. Therefore the behavior of the Fe–Cr–Al–Y alloy would tend to support the hypothesis that the embrittlement is characteristic of only face-centered cubic materials.

Table III-9 EFFECT OF IRRADIATION* ON THE POSTIRRADIATION DUCTILITY OF 304L STAINLESS STEEL CONTAINING 0.14 WT.% TITANIUM[65]

Preirradiation annealing temp., °C	Irradiation temp., °C	Total elongation, % 600°C	700°C	800°C
900	650	29.0	18.7	20.9
900	800	34.8	24.6	19.0
1215	650	14.0	11.8	7.4
1215	800	12.4	5.0	3.8

*Specimens irradiated to 1.3×10^{21} neutrons/cm² (thermal) and 1.0×10^{21} neutrons/cm² ($E > 1$ Mev).

Table III-8 EFFECT OF PREIRRADIATION HEAT-TREATMENT ON THE TENSILE PROPERTIES OF TITANIUM-MODIFIED 304 STAINLESS STEEL[65] TESTED AT 871°C

Alloy	Annealing temp., °C	Yield strength, 1000 psi Unirradiated	Irradiated	Total elongation, % Unirradiated	Irradiated*
304 stainless containing 0.014 C and 0.14 Ti (wt.%)	900	10.1	11.0	64.7	34.1
	1036	8.7	9.4	75.5	17.7
304 stainless containing 0.05 C and 0.15 Ti (wt.%)	900	11.5	12.6	60.9	28.1
	1036	10.8	9.4	71.5	23.7

*Irradiated at 50°C to an exposure of 1×10^{20} neutrons/cm² (thermal).

However, it is noted that, in previous work at Hanford, copper (face-centered cubic) has not shown any irradiation-induced embrittlement at elevated temperatures. A 5- to 10-μ-thick layer, at the inside diameter of 304 stainless-steel cladding, has been found in areas which were adjacent to UO_2 during irradiation.[71] The duplex layer was found to be completely austenitic, with considerably higher microhardness and with distinctly different etching characteristics from the rest of the cladding. The formation of this zone was attributed to fission fragments originating from the adjacent fuel.

Further data are becoming available on the effects of predominantly fast flux on the mechanical properties of stainless steel. Burst tests of irradiated 304 stainless-steel claddings of EBR-II fuel elements are continuing at Argonne.[72] Irradiated claddings were annealed for 1 hr at 900°C in argon and subsequently burst tested at 500°C. Results of these tests show that the annealed tubes exhibited a tangential rupture strength slightly higher than that of the irradiated tubes at 500°C. The ductility of the annealed irradiated material was found to be considerably higher than that for the unirradiated material at 500°C. Tensile tests have been performed on specimens irradiated by the British at Dounreay.[73] The results show that the ultimate strength of these materials is not significantly affected by fast-neutron irradiation. However, the ductility is decreased by irradiation as a function of exposure as shown in Fig. III-7. The slope of ductility reduction is approximately the same for both the solution-annealed and prestrained material. The decreased ductility is attributed to helium formation by fast neutrons from the matrix materials of iron, nickel, and chromium. The effect of annealing for 1 hr at various temperatures on the microhardness was determined for 316 stainless steel irradiated to a total neutron accumulation[74] of 1.3 × 10^{22} neutrons/cm^2. It was noted that the greatest change occurred between 400 and 700°C, in which range the hardness decreased from approximately 360 to 150 VHN.

Postirradiation creep-rupture tests are being performed on Hastelloy N (INOR-8) at both General Electric[50] and Oak Ridge.[75] The results of creep-rupture tests performed at General Electric on irradiated Hastelloy N at 650 and 760°C are summarized in Fig. III-8. The creep-rupture data from Oak Ridge indicate that there may be a stress below which the stress-rupture curves for irradiated and unirradiated materials come together. This lends support to the theory which requires a minimum stress for the movement of helium bubbles to grain boundaries in an irradiated material. Therefore below the stress required for movement of helium bubbles, one would not expect any difference between the irradiated and unirradiated creep-rupture behavior. Attempts to correlate the elongation at rupture

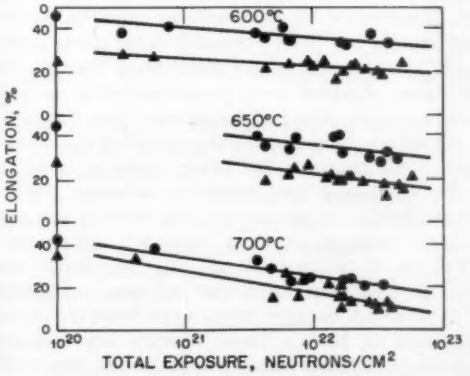

Fig. III-7 Ductility of solution-treated and 17% prestrained 316 stainless steel at temperatures of 600, 650, and 700°C after irradiation in the fast reactor[73] at 250 to 350°C. ●, solution treated; ▲, 17% prestrained.

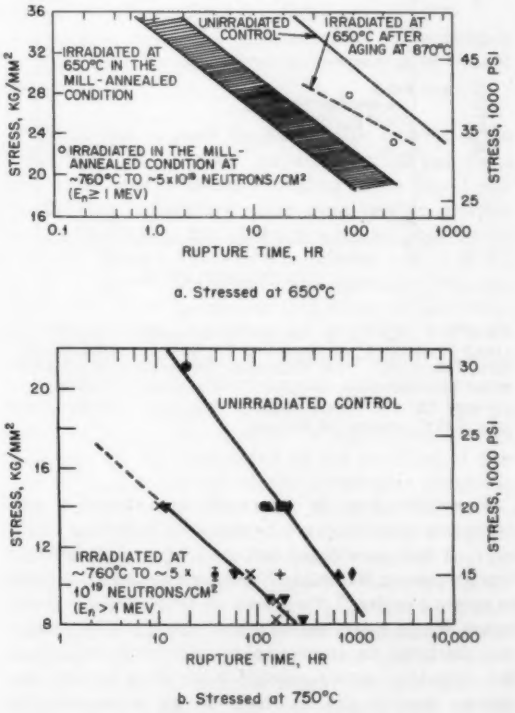
UNIRRADIATED CONTROL
IRRADIATED AT 650°C AFTER AGING AT 870°C
IRRADIATED AT 650°C IN THE MILL-ANNEALED CONDITION
IRRADIATED IN THE MILL-ANNEALED CONDITION AT ~760°C TO ~5×10¹⁹ NEUTRONS/CM² (Eₙ≥ 1 MEV)
STRESS, KG/MM²
STRESS, 1000 PSI
RUPTURE TIME, HR
a. Stressed at 650°C
UNIRRADIATED CONTROL
IRRADIATED AT ~760°C TO ~5 × 10¹⁹ NEUTRONS/CM² (Eₙ > 1 MEV)
STRESS, KG/MM²
STRESS, 1000 PSI
RUPTURE TIME, HR
b. Stressed at 750°C

Fig. III-8 Stress–rupture properties[51] of irradiated and unirradiated Hastelloy N. ●, unirradiated control (mill annealed); ■, unirradiated control (aged 4 hr at 870°C prior to testing); ▲, unirradiated control (mill annealed and aged 410 hr at 700 to 750°C); ◆, unirradiated control (aged 4 hr at 870°C + 410 hr at 700 to 750°C); ▼, irradiated in mill-annealed condition; ×, irradiated after aging 4 hr at 870°C; +, mill annealed + irradiation + 4 hr at 870°C; ✦, 4 hr at 870°C + irradiation + 4 hr at 870°C.

of irradiated Hastelloy N with the helium generated by (n,α) reactions from the boron were somewhat successful for most test results. Vacuum melting of the Hastelloy N resulted in reduction of the boron content from 20 to 40 ppm to 7 to 9 ppm, and the low-boron alloys exhibited significantly better postirradiation ductility if all specimens were irradiated at low temperatures. However, if the irradiation temperature was the same as the testing temperature (650°C), no difference in postirradiation ductility was found between the low- and high-boron Hastelloy N specimens. It was further found that the addition of titanium to Hastelloy N results in significant improvement in rupture life when tested at 650°C with a load[75] of 32,500 psi. This improvement in rupture life is illustrated in Fig. III-9.

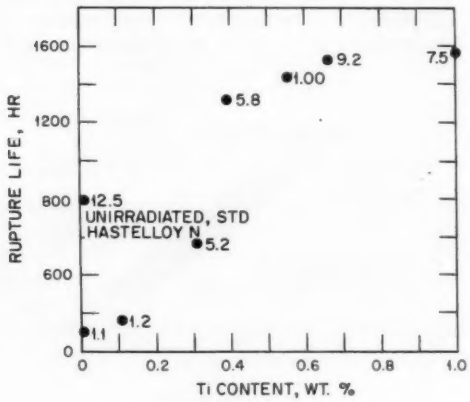

Fig. III-9 Influence of titanium on the postirradiation creep properties[75] of Hastelloy N. Numbers indicate fracture elongations. Test conditions: annealed 1 hr at 1177°C prior to irradiation; irradiation temperature, 650°C; exposure, 2.5 × 10^{20} neutrons/cm² (thermal); test temperature, 650°C; stress, 32,350 psi.

A tensile test is generally considered a good screening test for creep behavior of materials. However, it has been found that the trends indicated by a tensile test on Hastelloy N may not necessarily apply to creep results.[75] Two sets of tensile tests at different strain rates had indicated that the postirradiation ductility is improved by zirconium additions. But long-time creep-rupture tests showed that zirconium content had no effect on the postirradiation ductility of Hastelloy N. The effect of irradiation on the mechanical properties of the high-strength nickel-base alloy PDRL-120 (Ni–21 wt.% Cr–14 wt.% Co–4 wt.% Mo–2 wt.% Nb–2.5 wt.% Ti–0.25 wt.% Al) has been determined at Battelle–Northwest.[76] These test results were observed to follow the general trends of irradiated nickel alloys. The preirradiation yield strength is completely restored at a testing temperature of about 550°C, whereas the ductility remains significantly reduced.

The effect of irradiation and postirradiation annealing on room-temperature tensile and microhardness properties of molybdenum has been determined.[50] The results show that an annealing temperature of 1200°C is necessary for restoration of preirradiation mechanical properties. However, the effects of irradiation seem to be annealed out by lower annealing temperatures if long times are used. For example, it was noted that the 700, 850, and 980°C long-time creep-rupture properties of irradiated molybdenum were essentially the same as those of unirradiated specimens. The twinning transition temperature of Nb–40 wt.% V alloy was found to be increased[77] by fast-neutron irradiation at 43°C. The twinning transition temperature increased about 60°C after an exposure of 3.2 × 10^{18} neutrons/cm².

Basic Studies of Irradiation Effects

A large number of papers on defect clusters were presented[74] at the Consultants Symposium held at Harwell, England, in July 1966. A significant number of these papers dealt with defect clusters that resulted from neutron and charged-particle irradiation. Most of the experimental work consisted of observing the irradiated material with the transmission-electron microscope, measuring the size of clusters, and establishing whether the clusters were made up of vacancies or interstitials. Also studied were the dependence of the final cluster size and distribution on material purity and irradiation temperature. The kinetics of cluster removal and agglomeration by annealing at various temperatures were also determined for the various materials. Most of the papers pertaining to neutron irradiation will be discussed in this section.

Molybdenum containing 20 and 60 ppm carbon was irradiated[74b] at 60 and 200°C to 5 × 10^{19} neutrons/cm². Observation by transmission-electron microscopy showed the defect clusters in the purer molybdenum to be more coarsely distributed. This suggests that these clusters were heterogeneously nucleated on the impurity atoms or fine precipitates. Irradiation at the higher temperature also resulted in a coarser cluster distribution. The purer material irradiated at 200°C showed two distinctly different types of defect clusters: irregular dislocation lines and small vacancy clusters of 50 A diameter. Annealing at 900°C for 1 hr resulted in only interstitial loops being present in material that had been irradiated at 60°C, whereas vacancy loops were found in material irradiated at 200°C. These results are consistent with the belief that vacancy migration is responsible for the 170°C recovery stage in molybdenum. Another study on irradiated molybdenum by transmission-electron microscopy and field ion microscopy substantiated the finding that the defect structure con-

sisted primarily of interstitial loops with a few large vacancy clusters.[78] The size of these defects was about 100 A in the as-irradiated material, and they grew to about 200 A upon annealing for 1 hr at 760°C.

The importance of the impurity atoms on irradiation hardening has also been shown to be significant for tantalum.[79] Additions of 10^{-3} and 10^{-4} atom fraction of oxygen to tantalum were found to result in increased irradiation hardening at 4.5°K. This was especially significant for the low-temperature recovery stage at 9°K as measured by electrical-conductivity changes. The recovery of irradiation-induced change in electrical conductivity in tungsten has been found to be dependent on carbon.[80] This was illustrated by irradiating a tungsten specimen without any carbon and another tungsten specimen that contained 0.01 at.% carbon. Both were irradiated at 4.5°K to 7×10^{17} neutrons/cm^2 and then annealed. The specimen containing a significant amount of carbon did not show any recovery until 400°K, whereas the tungsten without carbon showed continuous recovery with increasing annealing temperature from 4.5°K. The onset of recovery at 400°K for the carbon-containing tungsten was attributed to the mobility of carbon atoms at that temperature, thereby causing a breakup of the carbon-anchored irradiation defect cluster.

Single crystals of niobium were irradiated to exposures[81] of up to 2×10^{18} neutrons/cm^2. It was found that irradiation limits the number of slip planes and thus causes the room-temperature deformation to be more heterogeneous. The upper yield strength was found to increase with increasing exposure and depended on a relation of total exposure to the 0.07 power.

Researchers at Brookhaven have concluded that there are at least three distinctly different types of defects which contribute to the irradiation hardening of relatively pure iron.[40] The characteristics and behavior of these are listed below.

Type I:

1. Rapidly removed by postirradiation annealing at 400°C
2. Form transient aggregates during annealing
3. Cannot be converted to Type II defects by adding oxygen during annealing
4. Responsible for irradiation hardening at exposures up to 2×10^{18} neutrons/cm^2
5. May include more than one species
6. May be related to the available carbon and nitrogen impurities

Type II:

1. Aggregate during postirradiation annealing at 300 to 500°C forming spots and loops visible by electron transmission microscopy
2. Form some small aggregates during irradiation because of thermal spikes
3. Affect hardness after relatively long annealing at 400°C
4. Appear to be a single species consisting of one or more oxygen atoms combined with one or more vacancies
5. Require exposures of less than 2×10^{18} neutrons/cm^2 for formation
6. Can be detected by hardness measurements or electron transmission microscopy when produced at exposures above 1×10^{19} neutrons/cm^2
7. Appear to increase the hardness linearly as a function of concentration.

Type III:

1. Rapidly removed by postirradiation annealing at 400°C without forming visible structures
2. Can be converted to Type II defects by adding oxygen during postirradiation annealing
3. Are presumably vacancies or small vacancy aggregates
4. Appear to be generated at the same rate as Type II defects, but only after available oxygen is used up in forming Type II defects
5. Appear to have a greater effect in increasing hardness than an equivalent concentration of Type II defects

Irradiations of pure copper[74c] were carried out at 4 and 293°K to 7.2×10^{17} neutrons/cm^2. It was found that the defect clusters resulting from the lower temperature irradiation were considerably smaller and the density of the clusters could be given by the $N = Ke^{-bd}$ relation, where N is defects/cm^3, d is the defect diameter, and K and b are constants. This relation applied to specimens irradiated at both temperatures. Further irradiations at 77 and 378°K on identical material, but in a different reactor, resulted in deviation of the defect density and diameter relation for the material irradiated at 378°K. The irradiation at 378°K resulted in significantly more large defects than predicted by the relation. It was also observed that the higher irradiation temperatures resulted in considerably more interaction between the irradiation-induced defect clusters and the dislocations which were originally present in the copper. Single crystals of copper[74d] were irradiated to 2.5×10^{18} neutrons/cm^2 and examined by transmission-electron microscopy after annealing at 270, 306, and 336°C. Figure III-10 shows that a relation exists between the critical shear stress at different testing temperatures and the square root of the density of clusters less than 50 A in diameter. No such relation was found with clusters larger than 50 A, which are believed to be interstitial loops. Therefore it was concluded that the small vacancy clusters are responsible for irradiation hardening. It was also found that the temperature where comparable results are obtained by identical annealing times is significantly increased by further irradia-

Fig. III-10 The critical shear stress as a function of the square root of the density of clusters less than 50 A in diameter.[74d] The density of clusters is varied by thermal annealing for various times material irradiated with 2.5 × 10^{18} neutrons/cm². ●, annealed at 275°C; ×, annealed at 306°C; ■, annealed at 336°C.

tion.[74d] The irradiation-induced increase in critical shear stress of nickel is attributed to the interaction of defect clusters by the moving dislocation lines.[74e] These defect clusters in nickel which had been irradiated to 3 × 10^{18} neutrons/cm² at 80°C and deformed at 90°C were found to contain about 10 vacancies. The disintegration of these vacancy clusters during annealing took place by splitting off of divacancies.

The defect clusters, as observed by transmission-electron microscopy, in irradiated materials are produced directly by energetic heavy particles or their cascade effects.[74f] In bombarding gold it was found that 3.4 × 10^4 ev was required to produce a 20 A-diameter cluster. The size of the defect cluster increased with increasing particle energy. However, when copper was bombarded under similar conditions, it was noted that each bombarding particle did not create a defect cluster. However, invisible clusters smaller than 20 A may be formed by particles with lower energy, and these defects will combine with other small clusters to form observable clusters by means of temperature activation. Irradiation of iridium to low exposures of 10^{14} neutrons/cm² resulted in the formation of three different types of defect clusters, as observed by field ion microscopy:[74g]

1. Clusters made up of about 200 vacancies
2. Dislocation loops that had originated from the collapse of large vacancy clusters
3. "Dispersed" clusters where 30 to 40% of lattice sites in a small volume are unoccupied

However, no dislocation loops have been observed for tungsten[74g] irradiated up to 1 × 10^{17} neutrons/cm².

Irradiation-induced changes in yield strength of platinum recover[40] at two different temperature ranges: 200 to 300°C and 500 to 600°C. The first-stage recovery is attributed to removal of single vacancies from vacancy clusters, and the second-stage recovery is believed to be due to motion of interstitials. The irradiation-induced increase in yield strength of platinum has been found to obey the exposure to the 0.5 power law and reaches saturation at about 1 × 10^{18} neutrons/cm².

Transmission-electron microscopy was performed on stainless-steel cladding materials[74a] after a total flux of 6 × 10^{22} neutrons/cm² at irradiation temperatures of 270 to 500°C. Irradiation below 350°C was found to produce defect clusters which were formed into dislocation loops by annealing and completely disappeared at 700°C. These defect clusters were believed to be responsible for the irradiation hardening, and the temperature of their disappearance coincides with the restoration of preirradiation microhardness. At irradiation temperatures above 350°C, spherical voids of up to 500 A were formed which accounted for 1 to 2% of the metal volume. These voids were removed by annealing at 900°C but migrated to grain boundaries and left a residual volume that was equivalent to the predicted helium volume produced by (n,α) reactions. These large voids are believed to be due to stabilization of vacancy clusters by the transmuted helium atoms. Attempts to identify, by electron transmission microscopy, helium bubbles in 348 stainless steel irradiated at 650°C and annealed at 1200°C after irradiation resulted in observance of light spots on the grain boundaries.[82] These spots had previously been identified by other investigators as helium bubbles but are believed to be polishing pits formed at the intersection of a dislocation and the grain boundary. In another study,[83] transmission-electron microscopy was performed on 348 stainless steel which had been irradiated to 8 × 10^{21} neutrons/cm² at 650°F (343°C). Defect clusters about 100 A in diameter were observed but no evidence of helium bubbles in the grains or grain boundaries was found. Irradiations of 348 stainless steel to 1 × 10^{20} neutrons/cm² at 60°C resulted in the following sizes and distributions of point-defect clusters as observed by transmission-electron microscopy.[76]

Condition	Cluster size, A	Cluster concentration
As irradiated	60–100	2 × 10^{16}/cm³
1 hr anneal at 450°C	Slight increase	1 × 10^{16}/cm³
1 hr anneal at 500°C	No increase	4 × 10^{15}/cm³
1 hr anneal at 600°C	Complete removal of clusters	

Since the annealing out of irradiation-induced changes in mechanical properties generally takes place in the 400 to 600°C range, it was suggested that these defect clusters may be responsible for changes in mechanical properties. (M. Kangilaski)

Selected Metallurgical Aspects of Cladding and Structural Materials

Zirconium Alloys

A total of 43 papers pertaining to research on zirconium and its alloys for nuclear application were published in a book by the Electrochemical Society.[84] The topics covered in these papers include corrosion, fabrication, hydride orientation, mechanical properties, irradiation effects on mechanical properties, and phase transformations in Zr–Nb alloys. These papers were originally presented at the Electrochemical Society Meeting in Buffalo, N. Y., Oct. 10–14, 1965. Another comprehensive evaluation of zirconium alloys for cladding applications in nuclear reactors was prepared by Bement.[57] Also, a thorough report has been issued by Bettis which summarizes all variables related to Zircaloy-4 tubing.[56] The areas that are most completely covered are those relating to effects of heat-treatment, annealing kinetics, and fabrication procedures as related to texture and consequent hydride orientation.

Three different methods were used to produce Zircaloy-2 single crystals.[85]

1. Cycling the specimen between 840 and 1200°C. This resulted in large beta grains which transformed to alpha grains with low-angle boundaries. Sigma phase was precipitated along these low-angle boundaries, and this phase could not be removed by subsequent annealing.

2. Heating of as-cast Zircaloy-2 for 33 days at 840°C resulted in 12-mm grains at the edge of the material. Subsequent heating for 20 days resulted in similar sized grains throughout the specimen.

3. Annealing of a specimen for 30 min at 1200°C and quenching it to room temperature resulted in formation of subgrain boundaries. Subsequent annealing at 840°C resulted in nucleation of alpha grains and their subsequent growth. Annealing for 12 days at 840°C resulted in 2- to 4-mm-diameter grains that were somewhat larger than the beta subgrains resulting from quenching.

Considerable effort is still directed toward the study of hydride formation and orientation in Zircaloy-2. The effects of hydrogen and strain rate on impact properties of Zircaloy have been determined by the British.[86] The results obtained by slow bending and impact tests are shown in Fig. III-11. These results indicate that hydrogen is considerably more embrittling (as measured by ductile-to-brittle transition temperature) in impact tests than in slow bend tests at equivalent high hydrogen contents. However, at low hydrogen contents (10 ppm), the slow bend test resulted in lower impact values. The effect of cooling rate on hydride orientation during stressing of Zircaloy-2 was studied at Oak Ridge.[8] The specimens were cooled from 400°C under a load of 20,000 psi, at cooling rates of 4, 12, and 170°C/min. The cooling rate had no effect on the orientation of the hydrides. However, the slower cooling rate resulted in larger hydride particles and the particles were preferentially located at the grain boundaries; the fast cooling rate resulted in smaller hydride particles being located within the grains. A novel approach for alleviating the hydride embrittlement of Zircaloy-2 cladding has been initiated by the Canadians.[87] This approach is based on the migration of hydrogen from the hot part of the cladding to the cold part owing to thermal gradients. When fins were placed on the tubular cladding, thermal gradients of the order of 30°C were established between the fins and most of the cladding. The fin as well as the tubular cladding contained 521 ppm hydrogen before irradiation. After 302 days of irradiation, the hydrogen content in the cladding was reduced to 120 to 140 ppm, whereas sections of the fin contained up to 2300 ppm hydrogen.

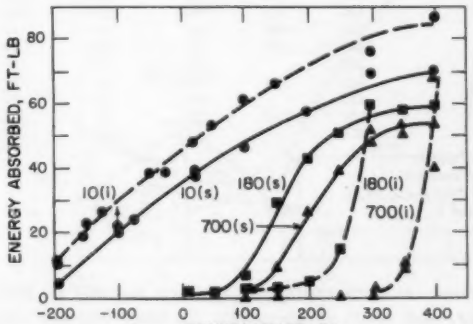

Fig. III-11 Energy transition curves obtained in impact and slow bend.[86] ●, hydrogen free; ■, 180 ppm hydrogen; ▲, 700 ppm hydrogen. ——, slow bend (s); - - -, impact (i); numbers refer to hydrogen content in parts per million.

Table III-10 illustrates the relative movement of the hydrogen in the finned Zircaloy-2 cladding. The effect of 170- to 2000-ppm oxygen additions on the mechanical properties of Zr–2.5 wt.% Nb were determined[88] at room temperature and 300°C. For the material that had been quenched from the beta phase and aged 24 hr at 500°C, the increased oxygen content resulted in increases in strength and decreases in ductility at room temperature. At 300°C the strength was found to increase with oxygen content up to 800 ppm oxygen, after which it decreased. Oxygen content had no significant effect on ductility at 300°C. Material that had been quenched from the alpha-plus-beta phase and aged for 24 hr at 500°C exhibited the same strength variations, as a function of oxygen

Table III-10 HYDROGEN TRANSFER IN A ZIRCALOY-2, FINNED PRESSURE TUBE DUE TO A MAINTAINED THERMAL GRADIENT[87]

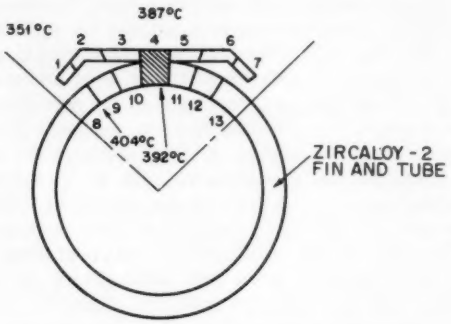

Zone	Hydrogen content, ppm				
	Start	After 43 days	After 106 days	After 168 days	After 302 days
1	521	1420	2140	1800	2222
7	521	1260	2095	2790	2384
2	521	1220	1660	1414	1686
6	521	1080	1515	1678	1711
3	521	752	773	224	267
5	521	755	756	325	169
4	521	488	250	157	141
10	521	320	179	155	132
11	521		175	160	135
9	521	225	179	155	130
12	521		164	158	131
8	521	220	195	162	124
13	521		167	162	127
Calculated values for zones 6 and 7		1040	1790	2540	4100

content, at both room temperature and 300°C. However, the room-temperature ductility showed considerable fluctuations with increasing oxygen content. The 300°C ductility was found to increase with oxygen content. These test results suggest that the mechanical properties are determined by the interplay of solution and precipitation-hardening processes which are governed by niobium and oxygen. It was shown that increasing the aging time at 500°C before testing a Zr–2.5 wt.% Nb specimen in creep at 300°C at 70,000-psi stress increases the creep rate.[59] This is illustrated in Fig. III-12. The higher creep rate for the longer annealed material is attributed to the increased particle diameter and consequently decreased precipitate density.

Stainless Steel and Nickel Alloys

Considerable interest has been shown in the possible improvement of creep strength of austenitic stainless steels by additions of refractory metals. The effect of 1 to 15 wt.% molybdenum additions to Fe–18 wt.% Cr–15 wt.% Ni on the elevated-temperature strength has been determined.[89] These alloys also contained zirconium and titanium as carbide formers. It was found that an optimum strength increase was obtained by molybdenum additions of 5 to 7 wt.%. This strength increase was found to be a result of solid-solution hardening as well as dispersion hardening due to the Ni_3Mo phase. Considerable age hardening was also found to result from the precipitation of the Fe_2Mo phase after long heat-treatments. If higher molybdenum contents were used, detrimental effects were observed because of the loss of dispersion strengthening and the formation of chi phase ($Fe_{36}Cr_{12}Mo_{10}$) at the grain boundaries. The loss of dispersion strengthening was due to the coarsening of the TiC and ZrC particles.

The effect of tantalum additions on the hardness of high-nickel austenitic stainless steels was also determined.[90] It was found that the precipitation hardening was caused by platelike precipitates of Ni_3Ta. Varying the carbon content from 0.01 to 0.15 wt.% was found to have a minor effect on hardening. Overaging of the alloy at 650°C was observed to take place by coarsening of the platelike Ni_3Ta particles; at 850°C and above, the Ni_3Ta dissolved and the tantalum precipitated as Fe_2Ta. The optimum tantalum additions for increased hardness were found to be 4 wt.% with 25 wt.% nickel and 8 wt.% with 35 wt.% nickel. It was concluded that the tantalum additions to the stainless steel did not improve the resistance of the dispersion-hardened steel over that of stainless steel containing aluminum and titanium.

The precipitation characteristics during long-time aging of titanium- and aluminum-containing precipitation-hardening stainless steels (A-286) at 700°C have been studied.[91] Hardening during aging at 700°C, due to Ni_3Ti formation, was slower if the material had been solution annealed at 1250°C rather than at

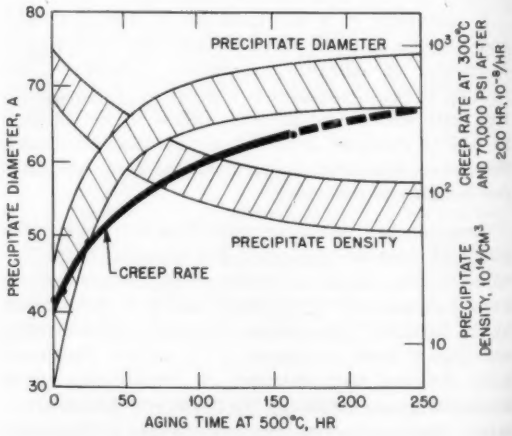

Fig. III-12 Observed creep rates and precipitate distribution for Zr–2.5 wt.% Nb as a function of aging time[59] at 500°C.

980°C. This behavior was attributed to the rapid precipitation of the Ni_3Ti particles. Prestraining (5 to 10%) of the material solution annealed at 980°C increased the rate of hardening, whereas prestraining of the material solution annealed at 1250°C decreased the rate of hardening during aging. The overaging of the steel solution annealed at 1250°C was somewhat slower than overaging of that annealed at 980°C. However, the high-temperature solution anneal resulted in large grains that impaired the tensile properties, especially after intermediate aging treatments (120 hr at 700°C). Longer aging treatments were found to improve the ductility.

In another study on Fe–18 wt.% Cr–12 wt.% Ni–0.9 wt.% Nb, the precipitation of carbide particles on stacking faults had considerably more effect on mechanical properties than did precipitation of these NbC particles on extended dislocations.[92] High stacking-fault concentrations were obtained by fast quenching, and increased strength was observed after aging at various temperatures. The addition of 1 wt.% yttrium to the British 20-25-Nb stainless steel was found to result in $Y(Fe,Ni)_9$ particles at the grain boundaries.[93] These particles prevented grain growth at annealing temperatures up to 1200°C. Annealing at temperatures above 1200°C resulted in redistribution of the intermetallic phase which allowed grain growth to take place. The addition of nitrogen to 304 stainless steel was found to increase the proportional limit and work-hardening characteristics.[94] The largest increase in work-hardening coefficient was observed when the nitrogen additions exceeded their solid solubility in the stainless steel.

In recent years, some attempt has been made to replace the nickel in austenitic stainless steels with manganese. The earlier attempts proved unsatisfactory but, by the addition of up to 0.4 wt.% nitrogen, a stable austenitic stainless steel was obtained. Compared with the nickel-containing austenitic stainless steels, the Mn–N austenitic stainless steels exhibited superior tensile and creep-rupture properties[95,96] and comparable or superior corrosion resistance but inferior impact properties and oxidation resistance. Long-time aging of these manganese stainless steels resulted in precipitation of $Cr_{23}C_6$ at the grain boundaries and Cr_2N in the matrix with the amount of $Cr_{23}C_6$ precipitation depending on carbon content.[97]

Additions of 0 to 15 wt.% tungsten to precipitation-hardened nickel alloys (Ni–Cr–Al–Ti) have been studied.[98] Generally, the strengthening in these alloys resulted from small particles of gamma prime (fcc Ni_3Al) and eta (hcp Ni_3Ti). However, the addition of tungsten results in an alpha phase (bcc) which is basically a tungsten solid solution and is stable at 850°C. The presence of tungsten also changes the shape of gamma-prime particles from cubic to spheroidal if the Ti/Al ratio is greater than 1. At Ti/Al ratios of less than 1, tungsten has negligible effect on the shape of gamma-prime particles. The equilibrium diagram[99] of Ni–Nb has been determined by use of thermal analysis, metallography, and X-ray diffraction techniques. Previously, only the high-nickel end of the equilibrium diagram had been studied. Both of the intermetallic phases (Ni_3Nb and NiNb) were found to exhibit large limits in stoichiometry as illustrated in Fig. III-13.

Cold-rolling and annealing studies have been performed on Ni–2.5 vol.% ThO_2 sheet.[100,101] The texture was found to be the same as that of pure metal, and the amount of cold work necessary for changing this texture was found to vary with fabrication procedures. The degree of particle breakdown as a function of cold work is illustrated in Fig. III-14. The annealing characteristics of the cold-worked sheet are compared with those of pure nickel in Fig. III-15.

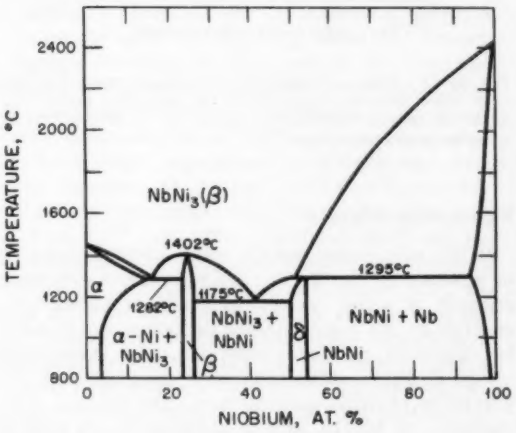

Fig. III-13 Equilibrium diagram of the Nb–Ni system.[99]

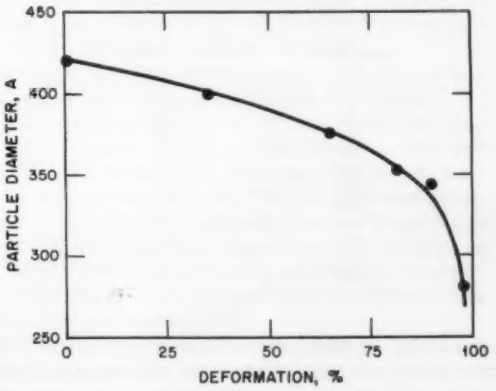

Fig. III-14 Variation of particle-size with percentage deformation in cold-rolled Ni–ThO_2 alloy.[100]

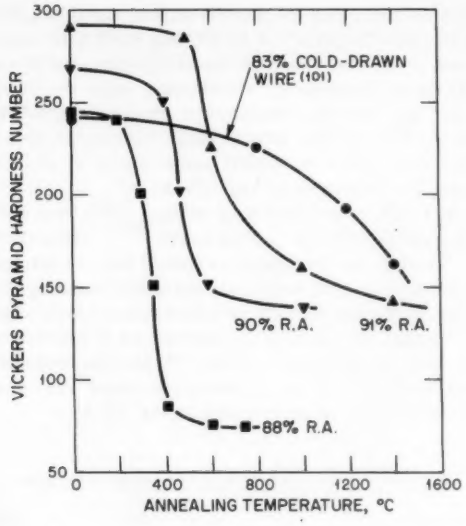

Fig. III-15 Effect of heat-treatment temperature on hardness. Heat-treatment time 1 hr. ▲, fine ThO_2 milled for 32 hr; ●, coarse ThO_2 milled for 16 hr; ▼, Ni–2½% ThO_2 wire; ■, pure nickel sheet.[100]

Refractory Metals

It has been shown that the solid-solution hardening of niobium by Ta, V, Zr, and W is linear with composition at small concentrations.[102] At higher concentrations the solid-solution hardening was found to be dependent on atomic-size mismatch rather than on the elastic-modulus difference which has been reported by previous investigators. The thermal conductivity of Nb–10 wt.% W between 50 and 1000°C has been determined, and the values are given[44] in Table III-11.

Table III-11 SMOOTHED THERMAL-CONDUCTIVITY VALUES FOR Nb–10% W ALLOY[44]

Temperature, °C	Thermal conductivity, watts/(cm)(°C)
50	0.4700
100	0.4844
200	0.5099
300	0.5307
400	0.5468
500	0.5625
600	0.5782
700	0.5920
800	0.6062
900	0.6175
1000	0.6264

Annealing studies on T-111 were performed[44] at 1260, 1370, and 1480°C after the material had been cold worked 50, 75, and 90%. The times necessary for 60% recrystallization at various temperatures are illustrated in Fig. III-16. A U. S. patent has been granted on a fine-grained tantalum alloy which resists grain growth at elevated temperatures.[103] The grain growth is minimized by small additions of yttrium and other rare earths.

Vibration of molybdenum during solidification at 1000 cycles/min reduced the grain size[104] substantially from a range of 3 to 5 mm to a range of 2 to 3 mm. The grain size was found to be affected considerably more by vibration in the transverse direction than in the longitudinal direction. Cold-rolled sheet from the vibrationally solidified metal exhibited higher strength and ductility than did conventionally electron-beam-melted metal. Vacuum annealing at temperatures of 500 to 1400°C for 1 hr was found to have less effect on the mechanical properties of the vibrationally solidified metal. It was noted that the room-temperature strength and ductility of molybdenum is continuously improved as the surrounding pressure is reduced[105] from atmospheric to 10^{-10} torr. However, only insignificant differences in mechanical properties are evident when different atmospheres like air, dry nitrogen, and purified argon are used during testing. The improvement of mechanical properties by testing in vacuum is attributed to a stress-induced desorption of interstitial-impurity atoms. Large grain size was observed to increase the thermal conductivity of arc-cast molybdenum[106] by up to 25%. Similar grain-size dependence was found for sintered molybdenum, with the sintered material exhibiting significantly lower thermal conductivity than the arc-cast materials. A U. S. patent has been issued for a precipitation-hardenable molybdenum alloy[107] which contains titanium, zirconium, and carbon. The addition of optimum amounts of titanium and zirconium prevents the formation of the embrittling Mo_2C during aging.

The effect of C, O, N, and H additions on the room-temperature mechanical properties of tungsten was determined.[108] Carbon was found to have the greatest effect on mechanical properties with the increase in carbon content from 12 to 540 ppm resulting in doubling the yield strength, halving the reduction of area, and increasing the ductile-to-brittle transition

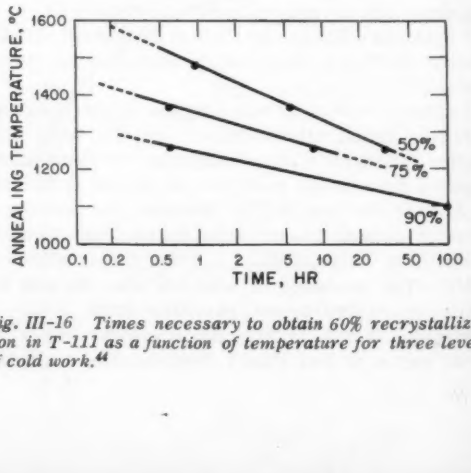

Fig. III-16 Times necessary to obtain 60% recrystallization in T-111 as a function of temperature for three levels of cold work.[44]

temperature from −196 to 0°C. Oxygen was found to have a minor effect on mechanical properties, whereas nitrogen and hydrogen had no measurable effect.

Considerable development work has been performed by General Electric[50] on W−Re−Mo alloys. It was found that W−30 wt.% Re alloys containing up to 55 wt.% molybdenum did not undergo significant aging when annealed in the 1400 to 1600°C range for up to 100 hr. Metallographic examination of the heat-treated alloys revealed that the W−30 wt.% Re alloys containing 10 and 20 wt.% molybdenum formed more sigma phase than did alloys containing either more or less molybdenum. However, the sigma-phase formation did not result in any measurable hardness changes. The morphology of 50% reduced W−25 wt.% Re−30 wt.% Mo after annealing in the 1200 to 2600°C range was studied. The 50% total reduction was obtained by reducing the material 4 to 5%, annealing it at 1400°C in hydrogen for 15 min, and then repeating the procedure until the 50% reduction was obtained. It was found that aging at 1200°C had no effect on the grain size but that annealing at 1600°C resulted in some tendency toward equiaxed grains. At 1800°C the material recrystallized into equiaxed grains of 40 to 45 μ which was the approximate grain size before mechanical working. Annealing at 2600°C for up to 1000 hr increased the recrystallized grain size about 20 to 30%. The W−30 wt.% Re−30 wt.% Mo specimens underwent a little more grain growth than did the specimens containing 25 wt.% rhenium.

Miscellaneous Materials

Addition of more than 5 wt.% titanium to vanadium and V−Nb alloys results in a yield point which exists in the 750 to 850°C range.[109] The disappearance of the yield point above 750 to 850°C is explained by the assumption that the strain rate must exceed the value of $D \times p$, where D is the diffusion coefficient of titanium and p is the dislocation density.

The strain hardening of SAP alloys (Al−Al_2O_3) at low temperatures is attributed to intersection of dislocations in the aluminum matrix.[110] The large number of dislocations found to be present (~10^{11} dislocations/cm^2) is due to the presence of alumina particles. The role of atomic impurities in strain hardening is believed to be insignificant.

(M. Kangilaski)

Diffusion Studies

Layer growth of refractory-metal carbides and the diffusivity of carbon through these layers were studied by several investigators. The reactions of niobium and graphite were investigated[111] in the temperature range 1700 to 2300°C. Parabolic growth behavior was observed for NbC and Nb_2C. The diffusivity of carbon into the carbide layers was shown to be much greater than the niobium diffusion into the carbide. The diffusion coefficient of carbon into NbC was given as $D = 7.6 \exp[-88.2 \text{ kcal/(mole)}(RT)]$ cm^2/sec. The corresponding equation for carbon into Nb_2C could not be determined because of a possible error in available phase equilibrium diagrams. In a previously reviewed article on this system by Resnick, Steinitz, and Seigle,[112] the diffusion of carbon into NbC was described by the equation $D = 1.2 \exp[-79.0 \text{ kcal/(mole)}(RT)]$ cm^2/sec. The two diffusion equations agree well at the higher temperatures but show some divergence at the lower temperatures. A study of carbon diffusion in TaC and Ta_2C was reported in Germany.[113] The mutual influence of the two layers during growth at temperatures between 2215 and 2745°C was taken into consideration. The activation energies determined were 98 kcal/mole for carbon diffusion into TaC and 85 kcal/mole for carbon diffusion into Ta_2C. The values are comparable to those determined by Resnick et al.[112] except for the activation energy of 98 kcal/mole which was higher by about 15%. Reports of carbon diffusion in Mo_2C and in ZrC are also available in the Russian literature. Diffusion in Mo_2C was determined[114] by carbon diffusion in previously formed Mo_2C and also by the layer-growth method. The temperature dependence of diffusion was given by the equations $D = 0.3 \exp[-67.0 \text{ kcal/(mole)}(RT)]$ cm^2/sec as determined from the first method, and $D = 3.17 \times 10^3 \exp[-78.0 \text{ kcal/(mole)}(RT)]$ cm^2/sec as determined in the layer-growth experiments. Diffusion of carbon into previously formed Mo_2C was about three orders of magnitude slower than into Mo_2C formed by layer growth. This difference is considered a consequence of the higher carbon-concentration gradient existing in the layer-growth system. Carbon diffusion in ZrC was studied[115] by condensing zirconium onto a graphite surface heated to temperatures of 1650 to 2000°C. This technique appears to be highly dependent on the rate of deposition, at least in the early stages of reaction. A temperature-dependent coefficient of $5 \times 10^2 \exp[-79{,}000 \text{ kcal/(mole)}(RT)]$ cm^2/sec for carbon diffusion into zirconium carbide was noted.

Diffusion studies on body-centered cubic metals and alloys are being continued at Oak Ridge.[68] Included are the diffusion of ^{51}Cr in chromium, Cr−20 wt.% Ni, and Cr−40 wt.% Ni between 1000 and 1850°C; the diffusion of ^{110}Ag and ^{46}Sc in beta titanium; the self-diffusion of ^{54}Mn in alpha manganese from 1170 to 1210°C; and diffusion of ^{44}Ti and ^{48}V in Ti−V alloys. Significant results in the diffusion in the Ti−V alloys are given in Fig. III-17. The coefficients are shown at fractions of the absolute melting point of the particular alloy.

The rates of diffusion of chromium in TD nickel were examined[116] in connection with attempts to provide oxidation protection for TD nickel. Chromium was electrodeposited on Ni−5 wt.% ThO_2 and studied at various temperatures. Rates of diffusion of chro-

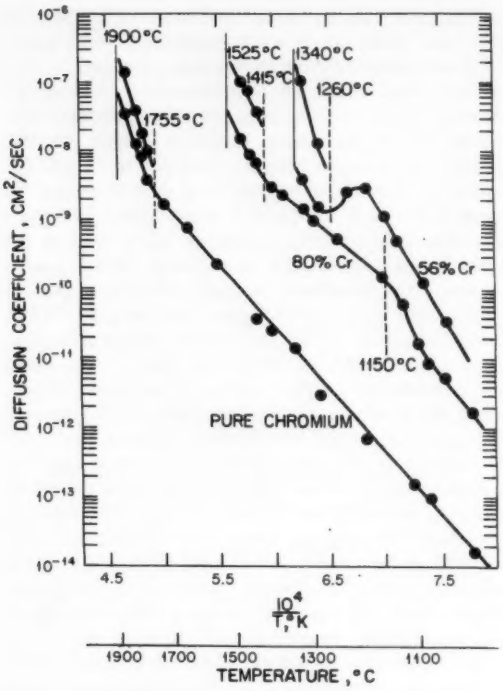

Fig. III-17 Diffusion of ^{51}Cr in Cr–Ni alloys.[68]

mium into TD nickel were measured by electron-beam-microprobe analysis, and the changes in surface concentration were determined as functions of time and temperature. Compared with published data, the diffusion coefficients for chromium into nickel were higher and the activation energies were lower. The high dislocation density in subgrain boundaries was the suggested cause. The high diffusivity of chromium into TD nickel possibly limits the use of chromium in protecting TD nickel at temperatures above 800°C.

Studies of diffusion in refractory-metal systems have been reported from several sources. Niobium self-diffusion was examined[117] in Nb–Mo alloys prepared by arc melting in argon and annealing in vacuum for 10 hr at temperatures near the alloy melting points. Grain sizes after this treatment were approximately 3 to 5 mm. Diffusion was investigated at temperatures between 1600 and 2100°C by using ^{95}Nb. Values for the diffusion coefficients were determined from frequency factors and activation energies which were given as functions of the molybdenum concentration. Increasing values of D, D_0, and E (the activation energy) with increasing amounts of molybdenum up to 8% were observed. These values then decreased with higher molybdenum concentrations.

Surface diffusion of tungsten isotopes in tungsten was studied[118] at temperatures of 1700 to 2300°C, yielding results which were described by an Arrhenius-type equation. The frequency factor, D_0, was determined to be 1.1×10^{-3} cm²/sec, and the activation energy was 31.6 kcal/mole. The result of ^{185}W diffusion in polycrystalline tungsten having a grain size of 0.1 to 0.2 mm has also been reported.[119] Diffusion at 1740 to 2100°C was primarily by grain-boundary diffusion and was described by the relation $D = 1.8 \times 10^{-3} \exp[-93.1 \text{ kcal/(mole)}(RT)]$ cm²/sec. Diffusion coefficients were determined[120] for the Nb–W system after diffusion between 1700 and 2300°C. The coefficient was found to decrease exponentially as the tungsten concentration increased from 0 to 50 wt.%; at higher concentrations the coefficient decreased abruptly. The activation energy at Nb–20 wt.% W was given as 60.5 kcal/mole, which is much lower than the activation energy for volume diffusion and indicates that other modes of diffusion are contributing significantly to the interdiffusion of niobium and tungsten. A technique for the diffusion bonding of tungsten to tungsten is described in a U. S. Patent.[121] The method involved forming layers of intermediate materials of WO_3, Mo, W, Mo–W, C, Ni, or Ni–Re on the tungsten surface. The bond was formed at pressures over 1000 psi and at temperatures greater than 1700°C. Best results were obtained by direct surface oxidation and by depositing Mo–W from carbonyl decompositions. The resulting diffusion bond gave tensile strengths which were about 50% of that for solid tungsten. The interdiffusion of iridium and tantalum was determined[122] in connection with the protection of refractory metals against oxidation in slow-moving air. Iridium coatings were electrodeposited onto tantalum and pressure bonded. The interdiffusion of iridium and tantalum was examined between 1200 and 1600°C. An apparent activation energy of 53.5 kcal/mole was obtained for the overall process. A 5-mil iridium coating on tantalum completely protected tantalum at 1850°C for 51 hr. The recession rate was about 0.02 mil/hr, and no internal oxidation was observed.

Several reports are available which describe diffusion processes involving fissionable materials. Included are studies from Germany[123] of the system UO_2–CeO_2 and a study of U, Pu, and Th compatibility with Al, Zr, Mg, Be, Ti, and several refractory metals.[124]

(A. N. Ashurst)

Selected Mechanical Properties of Cladding and Structural Materials

Iron-Base Alloys

The fracture toughness of A-302B steel was investigated by researchers at Materials Research

Laboratory.[125] The values of K_{Ic} from several tests are plotted as a function of the time interval over which the load increased from zero to the fracture load in Fig. III-18. The data represent fracture initiation both from fatigue cracks and from arrested fast cracks. The values of K_{Ic} were not dependent on the type of starting crack. The K_{Ic} values were obtained for specimens with three different thickness and side-groove-depth combinations, and no variation in the values was observed. Although the data in Fig. III-18 represent a relatively narrow range of strain rate (or loading time), a systematic decrease in K_{Ic} with increasing strain rate is clearly indicated. Cracks were not arrested in all the specimens tested, and in many, vibration following rapid cracking contributed to the uncertainty in reading the load corresponding to the crack arrest. The K_{Ic} values for crack arrest which were obtained ranged from 65 to 80,000 psi $\sqrt{\text{in.}}$

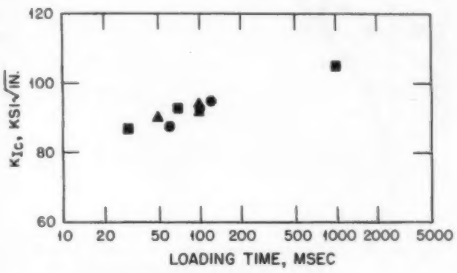

Fig. III-18 Dependence of room-temperature K_{Ic} on loading time and specimen design for A-302B steel.[125] ●, b = 2.0 in., b_n = 1.0 in.; ■, b_n = 1.0 in., b_n = 0.75 in.; ▲, b = 1.0 in.; b_n = 0.50 in.

The flat fracture surfaces and the fact that the K_{Ic} determinations showed no dependence on thickness and side-groove depth was evidence that the values were valid plane-strain-toughness measurements. For strain rates in the range used, a 1-in.-thick specimen with b_n/b = 0.50 provided valid K_{Ic} measurements. If these thickness parameters placed the specimen in the plane strain to plane stress transition region, a decrease in measured toughness with increasing section thickness would be expected. The arbitrary criterion that the calculated plastic zone should be small relative to the width across the crack plane could not be applied until yield-stress measurements at appropriately high strain rates were made. It is to be expected that the yield stress at the high strain rates is much greater than the 65,000-psi stress measured at low strain rates.

Tube-burst tests of 0.74-cm-OD × 0.04-cm-wall tubing of 304 stainless steel and V–15 wt.% Ti–7.5 wt.% Cr were made at Argonne.[126] The stainless-steel tubes were tested at both room temperature and 650°C in an as-drawn condition (~40% cold work) and in an annealed (15 min at 1090°C and rapid cool) condition. Tubes of V–Ti–Cr alloy were tested at room temperature in the as-drawn condition (~40% cold work) and in the annealed condition (1 hr at 850°C). The V–Ti–Cr tubes were also tested at 650°C in an as-drawn condition and two annealed conditions: the standard anneal of 1 hr at 850°C, and a high-temperature anneal of 1 hr at 1250°C.

The results of the tube-burst tests are summarized in Table III-12, which gives the burst pressures, calculated hoop stresses, and approximate elongations. The range is given along with the average values. The V–15 wt.% Ti–7.5 wt.% Cr alloy proved significantly stronger than 304 stainless steel for all cases except the room-temperature tests with the materials in an as-drawn condition. In this case the

Table III-12 RESULTS OF TUBE-BURST TESTS AT ROOM TEMPERATURE AND 650°C ON 304 STAINLESS STEEL AND V–15 WT.% Ti–7.5 WT.% Cr TUBING[126]

Material and condition*	Room-temperature tests			650°C tests		
	Burst pressure, 1000 psi	Calculated hoop stress, 1000 psi	Approx. radial expansion, %	Burst pressure, 1000 psi	Calculated hoop stress, 1000 psi	Approx. radial expansion, %
304 stainless (as drawn)						
Average	21.6	188.2	1.6	11.6	101.3	1.6
Range	21.0–21.95	183.2–191.1	1.5–1.7	11.3–11.8	99.7–102.4	1.3–1.8
304 stainless (annealed)						
Average	9.2	80	24.4	5.33	46.5	16.4
Range	8.95–9.45	78–82.4	23.0–25.1	5.3–5.4	46.2–47.1	15.8–17.6
V–15 Ti–7.5 Cr (as drawn)						
Average	19	168.1	1.2	14.3	125.8	3.0
Range	18.85–19.3	166.2–170.7	1.0–1.3	14.1–14.5	123.6–127	2.2–3.7
V–15 Ti–7.5 Cr (850°C anneal)						
Average	14.2	128.8	8.6	10.8	95	6.9
Range	13.85–14	122.1–126.9	7.3–10.4	10.6–11	93.4–96.6	5.6–8.6
V–15 Ti–7.5 Cr (1250°C anneal)						
Average				10.7	93.8	5.7
Range				10.6–10.75	92.9–94.8	4.8–6.3

*Nominal tube size 0.292-in. OD × 0.016-in. wall thickness.

stainless steel was about 10% stronger. In the annealed condition the V–Ti–Cr alloy was about 50% stronger than 304 stainless steel in the room-temperature tests. In the tube-burst tests at 650°C, the V–Ti–Cr alloy was about 25% stronger than 304 stainless steel in the as-drawn condition, and stronger by a factor of about 2 in the annealed condition.

Work on cyclic pressure tests of full-size pressure vessels has been summarized and presented in two parts by Southwest Research.[127] Part I contains a historical summary of the program and a detailed presentation of data from experimental stress analysis and fatigue tests. Part II contains discussions and results of investigations of crack initiation and propagation and terminal failure of the vessels. The vessel materials studied included A-201B, A-302B, T-1, and A-387D steels.

Fatigue tests were completed on 304 stainless steel at a temperature of 430°C with the strain amplitudes selected to produce fracture in 300 to 100,000 cycles.[50] The results from this investigation are plotted in Fig. III-19 as the relation between the

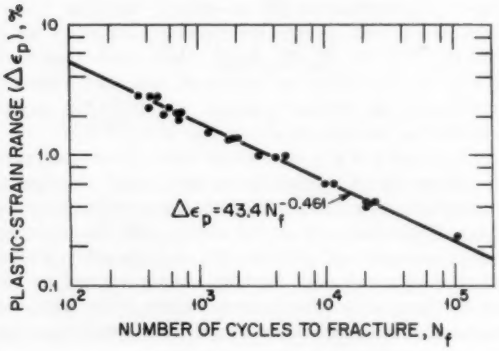

Material: Annealed 304 stainless steel, Heat No. 55697
Temperature: 430°C
Control mode: Triangular with zero mean strain
Nominal diametral strain rate: 1.8×10^{-3} sec^{-1}
Starting condition: Compression first
Specimen: Push–pull type, hourglass gauge section, longitudinal surface finish

Fig. III-19 Low-cycle fatigue-test results for 304 stainless steel[50] at 430°C.

logarithm of the plastic-strain range, $\Delta\epsilon p$, and the logarithm of the number of cycles to fracture, N_f. It is apparent that this relation is linear and that the test results are, therefore, in accord with the Coffin–Manson relation, $\Delta\epsilon p = cN_f^{-m}$, where c and m are material constants. The Coffin–Manson relation has been found to be valid for many metals and alloys at temperatures below the creep range.

Figure III-20 is a graphical representation of the cyclic relation between the strain range and stress

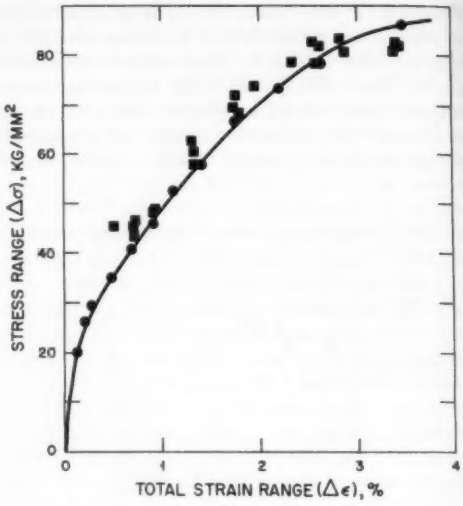

Fig. III-20 Cyclic stress–strain characteristics of 304 stainless steel[50] at 430°C.

range at 430°C. The data points shown as squares correspond to the values of $\Delta\epsilon$ and $\Delta\sigma$ obtained in various tests. A cyclic stress–strain diagram obtained with a single specimen is also shown in this figure. Each data point represented by a circle is the stress range recorded after approximately 100 cycles at the indicated strain range. The frequency of loading was 6.67 cycles/min. It is interesting to note that the diagram so obtained provides a reasonably accurate prediction for the stress range in the fatigue tests. The close correspondence is indicative of the relatively few cycles required to reach the steady state or saturation value of the stress range.

Nickel-Base Alloys

The creep-rupture properties of Hastelloy N at 982°C were reported by workers at Oak Ridge.[75] These data were obtained on specimens of a typical heat of air-melted Hastelloy N (Heat 5065) tested in air. The creep properties shown in Fig. III-21 indicate that the stresses to produce rupture and 5% strain in 1000 hr were reasonably well defined. However, the stresses for 1 and 2% strain in 1000 hr were not defined sufficiently. The minimum creep rate data were found to correlate very well. The ductility exhibited a minimum for test specimens having rupture lives over the approximate range of 50 to 200 hr. However, the minimum ductility observed still is slightly in excess of 20%. The reduction in area decreased rapidly with increasing rupture life to a value of about 15%. The increase in the elongation for long rupture lives was thought to be associated with the very extensive intergranular cracking that occurred.

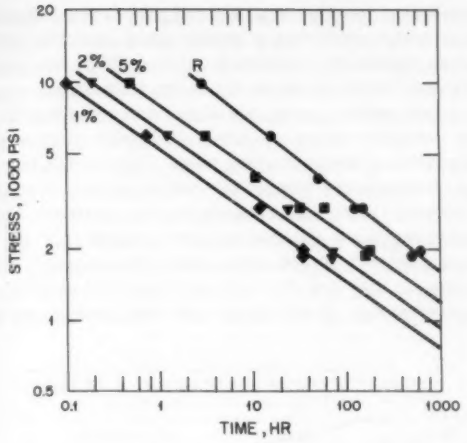

Fig. III-21 Creep-rupture properties[75] of Hastelloy N at 982°C. ●, rupture; ■, 5% strain; ▼, 2% strain; ◆, 1% strain.

Refractory Metals

An excellent state-of-the-art summary of the properties of chromium and chromium-base alloys has been issued by the Defense Metals Information Center.[128] This comprehensive review of the literature includes an interpretation of research data by the authors. An extensive bibliography is also given.

The Australians[129] have studied the effect of nitrogen contamination on the creep properties of Cr–2 wt.% Ta–0.1 wt.% Ti–0.5 wt.% Si and Cr–2 wt.% Ta–0.1 wt.% Ti–0.5 wt.% Si and Cr–2 wt.% Ta–0.05 wt.% B alloys. Tests were conducted in both air and argon environments. The alloys tested in air exhibited superior creep strength in comparison with those tested in argon. The difference in creep resistance was attributed to the internal precipitation of a complex Cr–Ta nitride. Differences in fracture behavior were observed, and alloys tested in air were considerably less ductile than those tested in argon.

An exploratory investigation was conducted at NASA–Lewis[130] to determine the high-temperature strength properties of as-extruded tungsten-base composites and dispersion-strengthened tungsten produced by novel powder-metallurgy techniques. Most of the materials studied exhibited 3000° F (1649° C) stress-rupture strengths that greatly exceeded those of unalloyed tungsten. Although somewhat limited in scope, rupture tests at 3500° F (1930° C) also indicated appreciable strength advantage relative to tungsten. This strengthening occurred despite the fact that a uniform distribution of fine dispersoids was generally not achieved.

At 3000° F the 100-hr stress-rupture strength of a W–5 vol.% HfO_2 composite was approximately twice that of unalloyed tungsten. At the same temperature and 8000 psi, the extrapolated rupture life was more than three orders of magnitude greater than that of unalloyed tungsten. This relative improvement in rupture life was still a factor of 10 at 2500° F (1371° C). These properties are comparable to those of some of the best tungsten alloys and composites presently available. Strengthening observed with this material is believed to result from a combination of fine dispersoids, fiber reinforcement, and solid-solution alloying of hafnium.

Tungsten–ZrO_2 exhibited 3000° F tensile strengths that were as much as 30% greater than those of the best W–HfO_2 material. The stress-rupture strengths of specimens from this composite were, however, considerably below those of W–HfO_2. An unidentified globular constituent in the elongated zirconia particles may account for the low rupture strengths.

A two-phase (one tungsten rich and one tantalum rich) W–0.47 wt.% Zr–5 wt.% Ta composite was produced by using a low-temperature high-pressure hot-pressing technique. The strength of this composite, while slightly below that of the other W–Zr–Ta materials, was almost twice that of unalloyed tungsten. This effect was believed due to the combination of the two-phase structure and the ease of extrusion, presumably associated with improved plasticity resulting from the presence of the tantalum-rich phase.

A report has been issued by Southern Research[131] describing an evaluation program that was performed to obtain preliminary design data for tungsten and TZM sheet produced in the Refractory Metal Sheet Rolling Program. Tungsten sheet 0.060 and 0.10 in. thick and TZM sheet 0.020, 0.040, and 0.060 in. thick were investigated. Both materials were examined in the optimum (warm worked and stress relieved) and recrystallized conditions. Mechanical properties evaluated included tensile, notched-tensile, compression, bearing, shear, creep, thermal-stability, and weld-joint efficiency. The recrystallization and bend-transition temperatures were also determined. Physical properties that were evaluated included density, thermal expansion, thermal conductivity, and specific heat.

Investigators at General Electric[50] have studied the creep behavior of W–Re–Mo alloys. Figure III-22 presents a summary of the results at 1600° C, indicating the effect of composition on rupture strain and the time required to give 5% strain. In general, there is a transition in the ductility (based on strain at rupture) and the creep resistance in the region of 23 to 25% rhenium. This is apparently due to the phase boundary existing in this region at 1600° C. Also, the ductility and creep resistance are decreased in the two-phase region by the addition of molybdenum for the same rhenium content (decreasing tungsten content). In the single-phase region for alloys with 20% rhenium, assuming that the material is reasonably fabricable, alloys containing 20 and 30% molybdenum with 18 and 17% rhenium, respectively, are promising

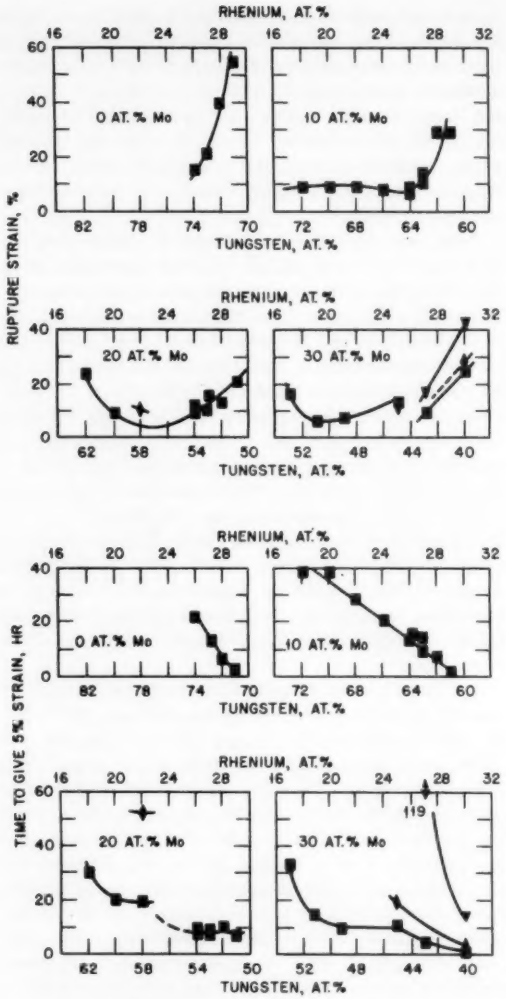

Fig. III-22 Creep-rupture results for W–Re–Mo alloys at 1600°C in hydrogen.[50] ▼, stressed at 2.11 kg/mm²; ◆, stressed at 3.37 kg/mm²; ■, stressed at 4.22 kg/mm².

alloys for performance at 1600°C since both the creep resistance and ductility are favorable.

An investigation of strain hardening in Nb–2 wt.% V and Nb–6 wt.% V was reported by workers at Knolls.[132] Variation in crosshead motion by a factor of 100 resulted in little variation in the notch strength and ductility (% reduction in area) of either alloy tested in the temperature range 315 to 649°C. The strain-rate sensitivity of these alloys appeared greater at ambient temperatures than at 315 to 649°C. This phenomenon was explained by the presence of a strain-aging reaction operative in this temperature range. The creep data from step-loading tests indicated that the Nb–V alloys had properties indicative of a metal exhibiting a strain-aging reaction. When creep tested at a constant stress, which was comparable to the yield stress in the temperature range favoring strain aging, the alloys deformed rapidly in the primary stage of creep, followed by slow deformation in the secondary stage. Alloys tested above the temperature range for strain aging, however, exhibited rapid deformation in the primary stage which continued until the specimen ruptured.

At Knolls[133] Nb–Si alloys were investigated. Hot-hardness data for Nb–0.05, 0.1, and 0.2 wt.% Si are shown in Fig. III-23 along with comparable data for

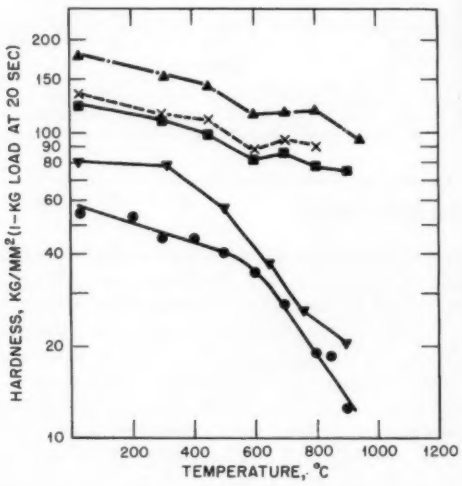

Fig. III-23 Hot hardness of Nb–Si alloys.[133] ■, Nb–0.05 wt.% Si; ×, Nb–0.10 wt.% Si; ▲, Nb–0.20 wt.% Si; ●, unalloyed wrought niobium; ▼, unalloyed powder-metallurgy niobium.

unalloyed niobium. These data indicated that the hot hardness of niobium was increased appreciably through the addition of small amounts of silicon.

In the temperature range 25 to 790°C, a Nb–0.22 wt.% Si alloy exhibited a yield stress 10,000 psi greater than that for Nb–0.18 wt.% Si alloy. The yield stress varied directly with temperature and decreased about 30% in this temperature range. At 790°C the yield stress of Nb–0.22 wt.% Si was about 45,000 psi compared with less than 10,000 psi for niobium.

Zirconium

The effect of vacuum (10^{-6} torr) on the creep rate and rupture life of zirconium at 1100 to 1300°C was reported by the Russians.[134] At 1200°C in a vacuum of about 10^{-5} torr, the creep rate was constant for more than 10 hr. The material was very ductile and

did not exhibit failure. Increasing the pressure to 10^{-4} torr caused the creep rate to decrease continuously with time. A drop in ductility and decreased rupture life were observed, with failure in less than 3 hr. Increasing the stress and temperature caused even further decreases in resistance to creep.

Zircaloy-4 sheet specimens were tensile tested from room temperature to 1800°C at General Electric.[50] The room-temperature tests were performed in air, whereas the tests at all other temperatures were performed in an argon atmosphere. The room-temperature results obtained with the load applied in the rolling direction are shown in Table III-13. The

Table III-13 ROOM-TEMPERATURE STRENGTH OF ZIRCALOY-4 SHEET[50]

Specimen	Yield strength (0.2% offset), kg/mm²	Ultimate tensile strength, kg/mm²	Young's modulus, kg/mm²
1	3380	5300	10,100
20	3420	5250	9,000
40	3330	5220	8,700

tests at elevated temperatures were performed at a loading rate of 0.13 cm/min based on the crosshead speed. Figure III-24 shows the ultimate tensile strength as a function of temperature. Maximum elongation of about 90% occurred in the region of 1100°C.

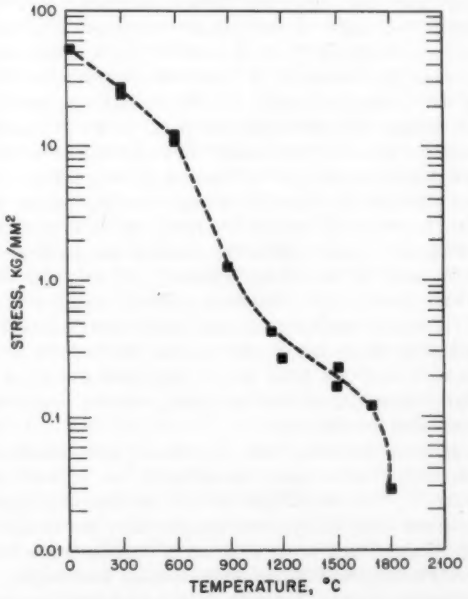

Fig. III-24 Ultimate tensile strength of 0.076-cm-thick Zircaloy-4 sheet in argon.[50]

An extensive evaluation of the properties of Zircaloy-4 tubing was reported by Bettis.[56] The results of mechanical-property determinations are summarized in Table III-14.

Table III-14 SUMMARY OF RESULTS OF MECHANICAL-PROPERTIES TESTS[56]

Tests	General results for three classes of materials: >70% cold worked, 15 to 20% cold worked, and recrystallization annealed
Short-term longitudinal tensile	Recrystallized is weakest but is still stronger than comparable plate material. This is probably a grain-size effect. The >70% cold worked is strongest, with the 15% cold-worked materials achieving ~40% of the strengthening increment due to cold work.
Longitudinal creep	Highly cold-worked materials retain some advantage at high stress levels, but all materials are similar at the low stress levels (18,000 psi and lower).
Short-term internal pressure	The highly cold-worked materials retain their strength advantage even though they are more susceptible to strength reduction by oriented hydrides. The fully annealed materials exhibit the best ductility under all hydride conditions. Yield strengths were unaffected by hydride and hydride orientation.
Internal pressure creep	At high stresses the >70% cold-worked materials exhibited the lowest creep rates, but the spread narrowed at 20,000 psi, the lowest stress used in these tests.
Ring	Results for ultimate strengths are similar to those in longitudinal tests with the 15% cold-worked materials attaining approximately 50% of the strengthening increment achieved by the >70% cold-worked materials. Aging up to 3000 hr at 850°F did not result in any degradation of strength or ductility.
Biaxial	Texture hardening does not depend on the final cold work. Both a 70% and a 15% cold-worked material exhibited texture hardening.
Creep collapse	Little difference exists among the three classes of material at the low stress levels; in fact, a 15% cold-worked material exhibited the lowest creep rate in a 16,000-psi test.
Irradiation	Limited in-pile data on the collapse of >70% cold-worked material indicates less resistance to collapse than would be anticipated from the out-of-pile results in the stress range where little difference was noted between materials out-of-pile.
	Short-time data (from ring and longitudinal tensile tests) indicate that highly cold-worked materials do not harden as much as annealed materials—the hardening due to cold work and that due to irradiation are not additive.

(J. A. De Mastry)

Nonfueled Refractories

Continuing work to prepare and fabricate refractory materials, especially the carbides, borides, and nitrides, for high-temperature applications has been conducted by researchers at the Albany Metallurgy Research Center.[135] Procedures are being developed

for preparing spin castings of various high-melting-point carbides for property studies at elevated temperatures. Several 2.54-cm-diameter CbC–C castings were evaluated for quality by radiography, metallography, and chemical and spectrographic analyses. Other carbide materials of interest include HfC–C, TaC–C, and ZrC–C. The hardness of HfC–C and CbC–C castings decreased with increasing carbon content, but, with increasing temperatures, the hardness of higher carbon alloys decreased at a lower rate than did lower carbon alloys. The variation in hardness of TaC–C and ZrC–C castings with increasing carbon content is not consistent. It was noted that stress relieving of the cast samples by annealing at 1800°C for 4 hr in vacuum prevented radial cracks from occurring during sectioning.

Russian investigators[136] have examined the manufacturing potential of fabricating thin plates of ZrC by pressing and sintering at high temperatures and by rolling and sintering. The most effective binder was a 3% rubber solution in trichloroethylene with metal zirconium (12 to 15% optimum); a sintering temperature of 2500 to 2600°C was necessary. The use of $NiCO_3$ and NiC_2O_4 as activating additives improved the pressing of the materials. On vacuum heating, the salts decompose into NiO and CO_2 and then nickel and CO by the reducing action of free carbon in the carbide. After pressing at 2 tons/cm^2 and sintering at 2400 to 2500°C, the material obtains a density of 6.3 g/cm^2, but consistent and uniform thicknesses were not obtainable. A rolling technique utilizing a −280-μ powder and a plasticizer (a rubber solution in benzene) produced plates of a more uniform thickness. Sintering in a vacuum at 2300°C resulted in a material with a density of 6.5 g/cm^3 (97% of theoretical).

A recent Italian publication[137] outlines the basic characteristics of several refractory materials. The principal methods of preparation and the most important uses are summarized. A review of the refractory compounds of the rare-earth metals has been compiled by Samsonov.[138] Physicochemical properties, crystal and electronic structure, methods of preparation, and technological applications are reviewed. Denker[139] discusses the bonding mechanisms in refractory materials and their relations to intrinsic mechanical, electrical, and chemical properties.

The elastic properties of ZrC have been studied by workers at Los Alamos Scientific Laboratory.[140] Hot-pressed ZrC had a measured Young's modulus of 3.866×10^{12} dynes/cm^2, a shear modulus of 1.623×10^{12} dynes/cm^2, a bulk modulus of 2.087×10^{12} dynes/cm^2, and Poisson's ratio of 0.191. The reported values have been adjusted to zero porosity.

Fesenko, Bolgav, and Gordienko[141] studied the stoichiometry of several carbides in the temperature range from 2770 to 3370°K. The character of the chemical bonding and its structure were examined, and the energies of formation, atomization, and dissociation were determined. In general, the compositions of the carbides of titanium, zirconium, and hafnium are close to stoichiometric, but under the same conditions, the compositions of niobium and tantalum carbides change considerably owing to the vaporization of carbon.

Adelsberg, Cadoff, and Tobin[142] have determined the metal carbide–carbon eutectic temperature for several materials composed of elements from Groups IV-B and V-B. The eutectic reaction temperatures, as determined by thermal analysis and isothermal-annealing metallographic examination, are reported in Table III-15.

Table III-15 CARBIDE–CARBON EUTECTIC TEMPERATURES[142]

Eutectic reaction	Temp.,* °C
TiC + C = liquid	2760 ± 50
ZrC + C = liquid	2890 ± 50
HfC + C = liquid†	3150 ± 50
VC + C = liquid	2670 ± 50
NbC + C = liquid	3220 ± 50
TaC + C = liquid	3450 ± 50

*Reproducibility ± 10°C.
†Hafnium contained 3% zirconium.

The structure and physical and mechanical properties of WC–TaC–Co alloys have been studied by Panov, Meerson, and Funke.[143] It was found that alloys containing 2 to 90 mole % TaC (with respect to total WC + TaC) have a three-phase structure (WC, TaC, and Co), whereas those containing over 90 mole % TaC have a two-phase structure (TaC and Co). Additions of 2 to 5 mole % TaC considerably increase the hardness of sintered carbides to 20°C and the bending strength at 800°C, whereas the impact toughness and bend strength at 20°C remain about the same or decrease very slightly. However, a further increase in TaC content greatly lowers the bend strength of all sintered-carbide specimens. An increase in cobalt content improves the bend strength at both 20°C and 800°C. It reaches a maximum at 800°C with 12 to 16 wt.% cobalt, and at 20°C with 20 wt.% cobalt. The following optimal composition of WC–TaC–Co sintered carbide was recommended for machining hard and tough metals and alloys: 2 to 5 mole % TaC (re total WC + TaC) and 6 to 12 wt.% cobalt, depending on the machining conditions and the material to be machined.

Carbides cemented with chromium- and vanadium-base alloys have been investigated by Hodson and Parikh.[144] The wettability of the carbides by liquid chromium-base alloys was measured by the sessile-drop method, and a correlation of wetting angle with the microstructure of sintered samples was made.

Investigators in Japan[145] have examined the influence of the binder-phase composition on the properties of WC–Co cemented carbides. The relation

between the properties of cemented carbides and the composition of the binder phase (cobalt phase) was studied in detail in and near the range where no eta phase and no free carbon phase appeared, using mainly WC–10 wt.% Co cemented carbides. It was found that the dissolved-tungsten content in the binder phase changes sharply from a minimum 2 to 3% (in the high-carbon two-phase alloy) to a maximum 9 to 10% (in the low-carbon two-phase alloy) because of a slight change in the carbon content of the alloy. As a result of this change, various properties of the alloy change remarkably. Transverse-rupture strength, hardness, specific gravity, electrical resistivity, saturation magnetization, and lattice parameter of the binder phase were studied in relation to the change. The effect of annealing the sintered alloy at rather low temperatures (about 800°C) was studied. The high-carbon alloy was approximately stable, but in the low-carbon alloys, a change in properties such as strength, electrical resistivity, and others was observed. The indicated reason for such property changes was the precipitation of tungsten contained in the cobalt phase, according to the reaction $\gamma(fcc) \rightarrow \gamma(fcc) + Co_3W$. For example, the binder phase is precipitation hardened by the precipitation of Co_3W, and it caused a decrease in the strength of the alloy. The precipitation takes place along the (0 0 1) crystallographic plane of γ(fcc).

The effect of carbon content in the cemented carbides was also investigated by researchers in Japan.[146,147] The researchers report[147] that the strength of the alloys of the composition WC–TiC–10 wt.% cobalt decreases with increasing TiC content, and a maximum strength was obtained in the high-carbon three-phase alloy system. Tungsten appears to dissolve in the binder phase but titanium does not.

Dawihl and Altmeyer[148] report that the ratio of fatigue strength to static bend strength of WC–Co alloys, at 6 to 15 wt.% cobalt and at room temperature, is 0.6 and is independent of the grain size. The notch sensitivity of a material containing 6 wt.% cobalt is relatively small, with a notch number of 1.6. It was also noted that the bending-fatigue strength of this material is decreased by a heat-treatment at 1000°C, owing to the reduction of compressive stresses in the WC phase, and is in accord with the permanent changes in length found in these alloys after such heat-treatment.

Several ceramic-metal alloys were examined by Russian investigators[149] for high-temperature applications. Several ternary alloys containing 40.8 to 60 wt.% TiC, 20 to 39.2 wt.% B_4C, and 20 wt.% SiC were compacted at 2100 to 2150°C under a pressure of 230 kg/cm^2, diffusion annealed at 1900°C for 12 hr in an argon atmosphere, cooled at the rate of 100°C/hr, and tested for oxidation resistance and thermal fatigue. Oxidation-resistance tests made on alloys oxidized in air at 900°C for 20 min, 1.5, 3.5, 10, and 15 hr showed that the most intensive oxidation, accompanied by oxide-film formation, occurs in the initial period of the exposure and practically ceases after 5-hr exposure. All tested alloys can be regarded as oxidation resistant since their weight gain in 15-hr tests was only 4 to 6 mg/cm^2, which is 3.5 times lower than that of TiC under identical conditions of oxidation. The thermal-fatigue resistance was evaluated from the number of quenches from 1200 and 2000°C sustained by alloy specimens before failure. In quenching from 1200°C, the alloys investigated sustained 40 thermal cycles without failure, which was double the number of thermal cycles sustained by TiC and 20 times as many as sustained by an alloy containing 85% SiC + 15% B_4C. Hence titanium-, boron-, and silicon carbide-based alloys can be recommended for operating at high temperature under conditions of frequent temperature changes.

Ferguson[150] investigated the fast-neutron lattice damage in silicon carbide by X-ray diffraction techniques. The irradiation behavior of Crusilite A (beta-silicon carbide) is characterized by an increase in the lattice parameter to a value which saturates at a fast-neutron exposure of 6×10^{20} neutrons/cm^2. The magnitude of this effect is about 0.3% at 700°C and is approximately inversely proportional to the square root of the irradiation temperature. These data correspond to the macroscopically observed length changes in the specimen and indicate that no defect clustering occurs on irradiation. On annealing, the unit cell contracts and reaches the unirradiated value at 1300°C. On annealing above 1300°C, further slight contractions for the unit cell were noted.

The irradiation and postirradiation annealing behavior of the phases in self-bonded silicon carbide was explicable in terms of a point-defect model. Although the macroscopic dimensional behavior of the self-bonded samples is clearly determined by the behavior of the major constituent (beta-silicon carbide), it seems that a complex stress pattern may result in the crystallites on irradiation. This is at a maximum at 1100°C. It is possible that other materials structurally related to alpha- and beta-silicon carbide, such as aluminum nitride, will behave similarly on irradiation.

The irradiation behavior of several other carbides was examined by Keilholtz, Moore, and Osborne.[151] The monocarbides of Ti, Zr, Ni, Ta, and W in the form of ½- by ½-in. cylinders made by (1) hot pressing, (2) slip casting and sintering, and (3) explosion pressing and sintering were selected for these studies. The gross damage results are summarized in Fig. III-25. Metallographic examination indicated that no grain-boundary separation was present in the materials after testing. The volume-expansion data for the tested materials is illustrated in Fig. III-26. The volume increases calculated from the lattice-parameter changes account for only 30 to 50% of the gross volume expansions. Fracturing of explosion-pressed specimens with ~1% nickel ad-

ditive generally occurred at lower neutron doses than did the corresponding hot-pressed and slip-cast carbide specimens with no additive. This was particularly true for explosion-pressed titanium and tungsten carbides, which were damaged at exposures above $\sim 2 \times 10^{21}$ neutrons/cm^2 (> 1 Mev). The volume expansion of explosion-pressed samples was approximately the same as that of the corresponding carbides fabricated by the other methods.

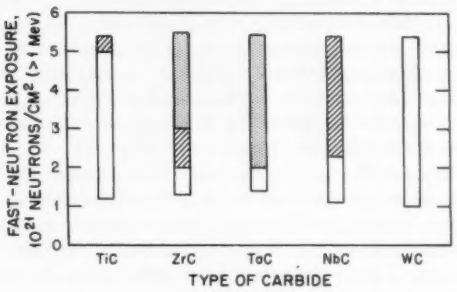

Fig. III-25 Fast-neutron damage to specimens of hot-pressed and slip-cast-sintered refractory metal monocarbides after irradiation at 300 to 700°C.[151] ▨, severe fracturing; ▨, minor fracturing; □, no damage or only very minor damage.

Gorbunov[152] has shown that it is possible to prepare, on an industrial scale, the borides of chromium, molybdenum, and zirconium from the oxides of these elements, boric acid, and soot. The effect of the charge composition, temperature of reaction, and rate of passage through the furnace on the composition of chromium, molybdenum, and zirconium borides was determined.

Sanders and Probst have fabricated several boride materials by induction zone melting and hot pressing.[153] The test samples were 0.25-in.-diameter by

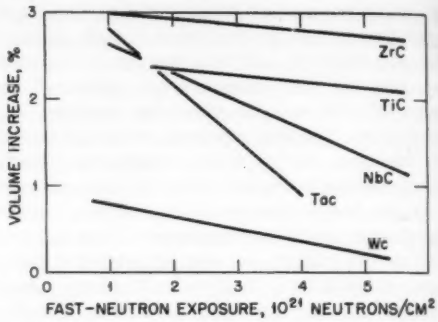

Fig. III-26 Volume increase of monocarbides of Ti, Zr, Ta, Nb, and W irradiated at low temperatures (300 to 700°C) as a function of fast-neutron exposure[151] (>1 Mev).

0.15-in.-thick disks. The materials tested and their hot hardness values at room temperature and 1625°C are listed in Table III-16.

The process of sintering ZrB_2 and MoS_2 was investigated by Kuzenkova and Kislyi utilizing microstructural, X-ray, and chemical analyses.[154] It was shown that, at a temperature above 1800°C, shrinkage was due to the appearance of a liquid phase, which disappeared during the sintering process. At temperatures up to 1800°C, an increase in the dimensions of the samples took place because of heterodiffusion processes with components having various partial diffusion coefficients and the evaporation of surplus silicon for an alloy with 15 wt.% $MoSi_2$.

Investigations by other Russian workers[155] on the high-temperature oxidation of the silicides of the rare-earth metals indicates that the scandium silicides were most stable in air at high temperature and the monosilicide was the most stable up to 1000°C. The least stable was YSi_2. The temperature dependence of the oxidation-rate constants for all the silicide phases investigated was established. The varia-

Table III-16 MATERIALS TESTED AND HARDNESS VALUES[153]

Borides and crystal structures	Fabrication technique	Measured density, g/cm^3	Theoretical density,* %	Grain size	Metallographic appearance	Hardness, kg/mm^2 Room temperature 50-g load	Room temperature Standard deviation	1625°C 2500-g load
Hafnium diboride, hexagonal	Induction zone-melted	10.87	97.1	~1/8 in.	Lamellar HfB second phase	2230	200	569
Zirconium diboride, hexagonal	Induction zone-melted	6.18	99.7	~1/8 in.	Lamellar ZrB second phase	2170	130	312
Niobium diboride, hexagonal	Induction zone-melted	6.87	95.3	~5/16 in.	Random unidentified second phase	2140	120	302
Lanthanum hexaboride, cubic	Induction zone-melted	4.72	99.4	0.025 in.	Single phase	2520	220	371
Holmium tetraboride, tetragonal	Hot pressed	6.42	94.7	11 μ	Random unidentified second phase	2220	220	155

*Based upon X-ray densities. No account taken of second phases present.

tion of the activation energy with temperature was observed for a series of compounds. Hypothetical conclusions on the mechanism of the oxidation process were made. The complexity of the oxidation process of these silicides was indicated by the variation of the apparent activation energy with a change in temperature. (W. C. Chard)

Ceramic Technology

Investigators at Marquette[156] measured the electrical conductivity of single crystal and sintered rutile through the temperature range 600 to 1400°C, at oxygen pressures from 0.005 to 1.0 atm. Above 1200°C, conductivity was proportional to $P_{O_2}^{-1/4}$. Conductivity below about 900°C was independent of oxygen pressure and was associated with the presence of impurity-controlled defects. In the intermediate temperature range, conductivity was interpreted on the basis of the preceding two mechanisms acting in parallel. Conductivity ranged from 5×10^{-5} $(ohm\text{-}cm)^{-1}$ at 600°C to 5×10^{-1} $(ohm\text{-}cm)^{-1}$ at 1400°C for the sintered specimens.

The Bureau of Mines[157] prepared an yttrium oxide powder by calcining yttrium carbonate for 3 hr at 610°C. After isostatically pressing at 25,000 psi, the powder was sintered to 98% of theoretical density in 5 hr at 1600°C. Linear firing shrinkage was 22%.

Eastman and Cutler[158] have investigated the effect of water vapor on the initial sintering of magnesia, made by thermal decomposition of magnesium oxalate, in the temperature range from 800 to 1100°C. Increasing the water–vapor partial pressure was found to increase the sintering rate. A model based on the solubility of the hydroxide ion in magnesia relates this increase to the increase in cation vacancy concentration. For water–vapor partial pressures up to 5 mm, the activation energy for sintering was 80 kcal/mole. Above 5 mm it was 48 kcal/mole. (H. D. Sheets)

References

1. F. W. Vahldiek, Epitaxial Oxidation of Zirconium at Various Temperatures, *J. Less-Common Metals*, 12: 9-28 (January 1967).
2. J. P. Pemsler, Studies on the Oxygen Gradients in Oxidizing Metals. V. The Oxidation of Oxygen-Saturated Zirconium, *J. Electrochem. Soc.*, 113(12): 1241-1244 (December 1966).
3. A. L. Lowe, Jr., and C. R. Johnson, Corrosion Behavior of Zircaloy-4—Evaluation of Surface Conditions, *Trans. Amer. Nucl. Soc.*, 9(2): 427-428 (November 1966).
4. T. J. Pashos, H. E. Williamson, and R. N. Duncan, Fuel Performance in Boiling Water Reactors, *Nucl. Appl.*, 2(6): 510-514 (December 1966).
5. B. Rubin and L. Lynam, Examination of Fuel and Cladding in PWR-1 Blanket Rods, *Nucl. Appl.*, 2(6): 499-504 (December 1966).
6. P. J. Harrop, N. J. M. Wilkins, and J. N. Wanklyn, The Effect of Neon Bombardment on the Corrosion of Zirconium, British Report AERE-R-5279, September 1966.
7. R. J. Davis, T. H. Mauney, and J. R. Hart, Corrosion of Zircaloy-2 by Hydrogen Peroxide at Elevated Temperature, *J. Electrochem. Soc.*, 113(11): 1222-1223 (November 1966).
8. P. Patriarca (Comp.), Oak Ridge National Laboratory, unpublished, December 1966.
9. P. Goldstein, A Research Study on Internal Corrosion of High Pressure Boilers, Report AD-637754, Combustion Engineering, Inc., 1966.
10. Société d'Etudes de Recherches et d'Applications, pour l'Industrie, Studies of Steel Corrosion in High-Temperature Water and Steam. Quarterly Report No. 16, July 1–September 30, 1966, USAEC–Euratom Report EURAEC-1744, Oct. 30, 1966.
11. L. F. Picone and W. D. Fletcher, The Post-Irradiation Examination of Saxton Fuel Cladding Corrosion Products, USAEC Report WCAP-3269-57, Westinghouse Electric Corp., Atomic Power Division, March 1966.
12. L. F. Picone, G. R. Taylor, A. J. Impink, and V. Rajagopal, Reactor Fouling Experiment, USAEC Report WCAP-3269-58, Westinghouse Electric Corp., Atomic Power Division, July 1966.
13. J. J. Koziol and S. S. Christopher, Correlations Between Sensitization and Stress Corrosion Cracking of 300 Series Stainless Steels, USAEC Report CEND-3256-264, Combustion Engineering, Inc., September 1966.
14. J. A. Bonnet, Jr., C. M. Bonet, and G. A. Vélez, Metallurgical Investigations and Repairs Made on BONUS Steam Dryer-Preheater and Nondestructive Tests of Other Reactor Components, USAEC Report PRWRA-102, Puerto Rico Water Resources Authority, Oct. 31, 1966.
15. J. Boulton, Some Aspects of Materials in Organic Cooled Reactors. A Summary of Canadian Experience, Canadian Report AECL-2640, May 1966.
16. M. J. Bennett, G. H. Chaffey, P. C. Blythe, and J. E. Antill, The Effect of Fission Fragment Irradiation Upon the Oxidation of a 20 Wt.% Cr, 25 Wt.% Ni, Nb Stabilized Stainless Steel by Oxygen at 650°C, *J. Nucl. Mater.*, 21(1): 1-13 (January 1967).
17. J. W. Wunderlich and N. E. Baker, Exposure of HTGR Candidate Core Plate and Thermal Insulation Materials to Impure Helium at 1650°F to 1850°F for 3000 Hours, USAEC Report GAMD-7377, General Atomic Division, General Dynamics Corp., Dec. 29, 1966.
18. P. D. Miller, W. E. Berry, W. N. Stiegelmeyer, and W. K. Boyd, Intergranular Modifications in Nickel from the Fluidized-Bed Fluoride-Volatility Process, USAEC Report BMI-X-417, Battelle Memorial Institute, Nov. 28, 1966.
19. W. C. Francis and R. A. Moen (Eds.), Annual Progress Report on Reactor Fuels and Materials Development for FY 1966, USAEC Report IDO-17218, Phillips Petroleum Company, November 1966.
20. J. R. Ogren, J. L. Blumenthal, and R. C. Ham, Radioisotope Propulsion Technology Program (POODLE). Vol. III. Oxidation and Diffusion in Noble Metal Claddings, Final Report, October 1, 1965–September 30, 1966, USAEC Report STL-517-0049(Vol. III), TRW Systems, October 1966.
21. P. M. S. Jones and W. Edmondson, Oxidation of Rare Earth Metals. Part 2. Praseodymium, British Report AWRE-0-72/66, October 1966.
22. J. S. Sheasby, G. R. Wallwork, and W. W. Smeltzer, Parabolic Oxidation Kinetics of Niobium, *J. Electrochem. Soc.*, 113: 1255-1257 (1966).
23. R. E. Pawel and J. J. Campbell, Effect of Anodic Films on the Gaseous Oxidation of Tantalum, *J. Electrochem. Soc.*, 113: 1204-1209 (November 1966).
24. R. E. Pawel and J. J. Campbell, Stress Measurements

During the Oxidation of Tantalum and Niobium, *Acta Met.*, 14: 1827-1833 (December 1966).
25. B. W. Marshall, Oxidation and Ablation Characteristics of Tantalum in Hyperthermal Environment, *Amer. Inst. Aeronaut. Astronaut.*, 4: 1899-1905 (November 1966).
26. R. F. Voitovich, Effect of Chromium on the Oxidation Kinetics of Niobium (in Russian), *Ukr. Khim. Zh.*, 32(5): 445-448 (1966).
27. V. A. Nieberlein, Oxidation Characteristics of Vapor-Plated Tungsten, *Corrosion*, 22: 291-293 (October 1966).
28. G. A. Etemad, Oxidation and Mechanical Performance of Tungsten at High Temperatures and High Pressures, *Amer. Inst. Aeronaut. Astronaut.*, 4: 1543-1548 (September 1966).
29. I. Uy. Lazareva, D. A. Prokoshkin, and E. V. Vasil'eva, Investigation of the Oxidation of Tungsten–Niobium Alloys (in Russian), *Izv. Akad. Nauk SSSR, Metal.*, 6: 161-167 (November–December 1965).
30. A. P. Gulyaev and V. T. Ababkov, Corrosion Resistance of Molybdenum Alloys in Sulfuric, Hydrochloric, and Phosphoric Acid at Elevated Temperatures Under Pressure (in Russian), *Zashch. Metallov*, 2: 444-449 (1966).
31. S. Priceman and L. Sama, Development of Fused Slurry Silicide Coatings for the Elevated-Temperature Oxidation Protection of Columbium and Tantalum Alloys, Report STR-66-5501.14, Sylcor Division, Sylvania Electric Products Inc., December 1966.
32. D. T. Dickson, R. T. Wimber, and A. R. Stetson, Very High Temperature Coatings for Tantalum Alloys, Report AFML-TR-66-317, Solar, a Division of International Harvester Co., October 1966.
33. G. F. Wakefield, Refractory Metal Coatings by Chemical Vapor Deposition, Report AFML-TR-66-397, Texas Instruments Co., December 1966.
34. P. F. Campbell, K. A. Gebler, and M. H. Ortner, Development of Oxidation Resistant Coatings for Use Above 3500°F, Report NASA-CR-65285, Vitro Laboratories, September 1965.
35. M. H. Ortner and S. J. Klach, Development of Protective Coatings for Tantalum T-222 Alloy, Report NASA-CR-54578, Vitro Laboratories, December 1966.
36. W. M. Phillips, Evaluation of Oxidation-Resistant Coatings for Inert-Atmosphere Applications, Report N-67-15683, California Institute of Technology, Jet Propulsion Laboratory, Jan. 15, 1967.
37. G. V. Zemskov and P. F. Shulenok, New Technique for Chemical-Thermal Treatment of Transition Metals in Molten Aluminum-Base Alloys (in Russian), *Metalloved. Term. Obrabotka Metal.*, 5: 52-55 (1966).
38. J. A. Leppard, Review of SCTI Bellows Failures, USAEC Report NAA-SR-Memo-11970, Atomics International, May 26, 1966.
39. D. W. Koch and P. J. Kovach, Materials Examination of a Model Sodium Heated Steam Generator. Final Report, USAEC Report BAW-1280-37, Babcock & Wilcox Co., June 30, 1966.
40. J. R. Weeks (Comp.), Brookhaven National Laboratory, unpublished, 1966.
41. Argonne National Laboratory, Reactor Development Program Progress Report, January 1967, USAEC Report ANL-7302, Feb. 24, 1967.
42. J. Sannier, L. Champeix, and R. Darras, Corrosion of Niobium by Circulating Molten Sodium Between 400 and 600°C (in French), French Report CEA-R-3028, October 1966.
43. A. Thiruvengadam and H. S. Preiser, Cavitation Damage in Liquid Metals, Report NASA-CR-72035, Hydronautics, Inc., Nov. 29, 1965.
44. W. O. Harms (Comp.), Oak Ridge National Laboratory, unpublished, January 1967.
45. Allison Division, General Motors Corp., Investigation of Bimetallic Liquid Metal Systems. Final Report, USAEC Report GMAD-3643-8, Sept. 30, 1966.
46. S. R. Hatcher, B. A. Finlay, and J. L. Smee, Heat Transfer, Impurities, and Fouling in Organic Coolants, A Summary of Canadian Experience, Canadian Report AECL-2642, May 1966.
47. A. F. Voigt (Ed.), Reactor Materials Development Quarterly for Division of Reactor Development, October–December 1966, USAEC Report IS-RD-8, Ames Laboratory.
48. W. M. Robertson, Propagation of a Crack Filled with Liquid Metal, *Trans. AIME*, 236: 1478-1482 (October 1966).
49. L. Baker, Jr., Metal–Water Reactions, *Nucl. Safety*, 8(1): 20-25 (Fall 1966).
50. General Electric Company, Nuclear Materials and Propulsion Operation, High-Temperature Materials Program Progress Report No. 63, USAEC Report GEMP-63, Dec. 30, 1966.
51. *Reactor Mater.*, 9(4): 237 (Winter 1966–1967).
52. General Electric Company, Nuclear Materials and Propulsion Operation, High-Temperature Materials Programs. Part A. Final Annual Report, USAEC Report GEMP-400A, Feb. 28, 1966.
53. L. Baker, Jr., and L. C. Just, Studies of Metal–Water Reactions at High Temperatures. III. Experimental and Theoretical Studies of the Zirconium–Water Reaction, USAEC Report ANL-6548, Argonne National Laboratory, May 1962.
54. A. W. Lemmon, Jr., Studies Relating to the Reaction Between Zirconium and Water at High Temperatures, USAEC Report BMI-1154, Battelle Memorial Institute, Jan. 3, 1957.
55. Argonne National Laboratory, Reactor Development Program Progress Report, December 1966, USAEC Report ANL-7286, Jan. 26, 1967.
56. C. R. Woods (Ed.), Properties of Zircaloy-4 Tubing, USAEC Report WAPD-TM-585, Westinghouse Electric Corp., Bettis Atomic Power Laboratory, December 1966.
57. A. L. Bement, Jr., Zirconium Cladding Alloys, USAEC Report BNWL-SA-672, Battelle–Northwest, May 3, 1966.
58. C. E. Ellis and A. Sawatzlay, The Effect of Neutron Irradiation on the Tensile Properties of the Zr–2.4 Wt.% Nb(Cb)–0.5 Wt.% Cu Alloy, *Trans. AIME*, 233: 2041-2051 (December 1965).
59. Atomic Energy of Canada Limited, unpublished, July–September 1966.
60. D. J. Seman and E. J. Pasierb, Annealing of Irradiated A-302B Steel, *Trans. Amer. Nucl. Soc.*, 9: 389-390 (October–November 1966).
61. R. E. Johnson and E. J. Pasierb, Fracture Toughness of Irradiated A-302B Steel as Influenced by Microstructures, *Trans. Amer. Nucl. Soc.*, 9: 390-392 (October–November 1966).
62. J. R. Hawthrone and L. E. Steele, Metallurgical Variables as Possible Factors in Controlling Irradiation Response of Structural Steels, paper presented at the 69th Meeting of American Society for Testing and Materials in Atlantic City, N. J., June 27–July 1, 1966.
63. R. A. Gray, Jr., and L. E. Steele, Microstructure: A Factor in Radiation Embrittlement Sensitivity of Structural Steels, *Trans. Amer. Nucl. Soc.*, 9: 392 (October–November 1966).
64. C. R. Brinkman and J. M. Beeston, Axial Fatigue of Pre- and Post-Irradiated A-302B and A-212B Steels, USAEC Report IN-1052, Idaho Nuclear Corp., January 1967.
65. P. Patriarca (Comp.), Oak Ridge National Laboratory, unpublished, March 1967.
66. W. R. Martin and J. R. Weir, Influence of Grain Size on the Irradiation Embrittlement of Stainless Steel at Elevated Temperatures, USAEC Report ORNL-TM-1043, Oak Ridge National Laboratory, March 1965.
67. H. Boehm and H. Hauck, Effect of Phase Transformation on the Occurrence of High Temperature Em-

brittlement After Neutron Irradiation, *J. Nucl. Mater.*, 21: 112-113 (1966).
68. S. Peterson (Comp. and Ed.), Metals and Ceramics Division Annual Progress Report for Period Ending June 30, 1966, USAEC Report ORNL-3970, Oak Ridge National Laboratory, October 1966.
69. Atomic Energy Research Establishment, May 1965–October 1965, unpublished, January 1966.
70. Reference omitted.
71. H. S. Rosenbaum, J. S. Armijo, and U. E. Wolff, Fission Fragment Damage to Type 304 Stainless Steel Fuel Cladding, USAEC Report GEAP-5002, General Electric Company, Atomic Power Equipment Department, January 1966.
72. Argonne National Laboratory, Reactor Development Program Progress Report, September 1966, USAEC Report ANL-7255, Oct. 26, 1966.
73. A. S. Froser, I. R. Birss, and C. Cawthorne, High Temperature Embrittlement of Stainless Steel Irradiated in Fast Flux, *Nature*, 211: 291-292 (July 16, 1966).
74. M. J. Makin (Ed.), Papers Presented at Consultants Symposium on the Nature of Small Defect Clusters, held at Harwell, England, July 4–6, 1966, British Report AERE-R-5269(Vols. I and II), September 1966.
    a. C. Cawthorne and E. J. Fulton, The Influence of Irradiation Temperature on the Defect Structures in Stainless Steel.
    b. B. L. Eyre and M. E. Downey, The Influence of Irradiation Temperature on the Damage Structure in Neutron Irradiated Molybdenum.
    c. G. P. Scheidler, M. J. Makin, F. J. Minter, and W. F. Schilling, The Effect of Irradiation Temperature on the Formation of Clusters in Neutron Irradiated Copper.
    d. M. J. Makin, F. J. Minter, and S. A. Manthrope, The Correlation Between the Critical Shear Stress of Neutron Irradiated Copper Single Crystals and Density of Defect Clusters.
    e. J. Diehl and D. Ast, Annealing of the Vacancy Agglomerates Responsible for the Enhancement of Critical Shear Stress on Neutron Irradiated Nickel.
    f. K. L. Merkle, Radiation Induced Point Defect Clusters in Copper and Gold.
    g. B. Ralph, M. A. Fortes, and K. M. Bowkett, Direct Observations of Small Defect Clusters in Irradiated Metals by Field Ion Microscopy.
75. Oak Ridge National Laboratory, Molten-Salt Reactor Program. Semiannual Progress Report for Period Ending August 31, 1966, USAEC Report ORNL-4037, January 1967.
76. F. W. Albaugh et al., Battelle–Northwest, unpublished, December 1966.
77. H. E. McCoy and D. O. Hobson, The Influence of Neutron Irradiation on Twinning in a Niobium–Vanadium Alloy (40% Vanadium), *Amer. Soc. Metals, Trans. Quart.*, 59: 568-570 (September 1966); also USAEC Report ORNL-P-2197.
78. P. Rao, Radiation Induced Defects in Molybdenum, USAEC Report UCRL-17078, University of California, Lawrence Radiation Laboratory, September 1966.
79. G. Burger et al., Effect of Oxygen Dopings on the Low Temperature Recovery of Tantalum After Nuclear Irradiation at 4.5°K, Report AI-Trans-214 [from *Phys. Lett.*, 20(5): 472-474 (Dec. 22, 1966)].
80. H. H. Kuhlmann and H. Schultz, Recovery Stage III in Decarbonized Tungsten After Neutron Irradiation at 4.5°K, USAEC Report AI-Trans-216 [from *Acta Met.*, 14: 798-800 (1966)].
81. R. P. Tucker, The Effect of Neutron Irradiation on Plastic Deformation in Niobium Single Crystals, USAEC Report ORNL-TM-1583, Oak Ridge National Laboratory, November 1966.
82. F. W. Albaugh et al., Battelle–Northwest, unpublished, March 1967.
83. E. N. Aqua, W. R. Smalley, and C. M. Owens, Electron Microscopy Study of Type 348 Stainless Steel Fuel Element Cladding, *Trans. Amer. Nucl. Soc.*, 9: 386-387 (October–November 1966).
84. J. P. Pemsler, E. C. W. Perryman, and W. W. Smeltzer, *Zirconium and Its Alloys*, Electrochemical Society, 1966.
85. M. J. Nasir and H. J. Bray, Growth of Single Crystals of Zircaloy-2, *J. Inst. Metals*, 94: 398-399 (1966).
86. G. D. Fearnehough and A. Cowan, The Effect of Hydrogen and Strain Rate on the Ductile-Brittle Behaviour of Zircaloy, British Report TRG-Report-1326, Sept. 1, 1966.
87. B. J. S. Wilkins and A. Sawatzky, Thermal Diffusion of Hydrogen in Finned Zircaloy-2 Pressure Tubes, Canadian Report AECL-2634, October 1966.
88. J. R. Kench, J. H. Foley, and S. A. Aldridge, The Effects of Dissolved Oxygen Upon the Mechanical Properties of Zirconium–2.5 Wt.% Niobium Alloy, Canadian Report AECL-2623, October 1966.
89. H. Pops, Influence of Molybdenum on the Structure and Properties of a Carbide-Bearing Austenitic Steel, *J. Iron Steel Inst. (London)*, 204: 1117-1121 (November 1966).
90. J. J. Irani and D. Dulieu, Precipitation in Austenitic Stainless Steels Containing Tantalum, *J. Iron Steel Inst. (London)*, 204: 1229-1238 (December 1966).
91. J. M. Silcock and N. T. Williams, Precipitation During Aging at 700°C of a Commercial Austenitic Steel Containing Titanium and Aluminum, *J. Iron Steel Inst. (London)*, 204: 1100-1107 (November 1966).
92. R. D. Nayborn, Hardening by Stacking Fault Precipitation in an 18Cr–12Ni–Nb Austenitic Steel, *J. Iron Steel Inst. (London)*, 204: 1200-1207 (December 1966).
93. P. D. Parsons, Addition of Yttrium to Stainless Steels, British TRG-Report-1345, 1967.
94. Virginia Polytechnic Institute, Some Physical Characteristics of AISI Type 304 Containing Nitrogen, USAEC–Euratom Report EURAEC-1732, September 1966.
95. J. J. Hegler, *Advances in the Technology of Stainless Steels and Related Alloys*, ASTM Special Technical Publication, No. 369, pp. 54-61, 1965.
96. B. R. Nijhawan, P. K. Gupte, S. S. Bhatmagar, B. K. Guha, and S. S. Dhanjal, Substitute Nickel-Free Austenitic Stainless Steels, *J. Iron Steel Inst. (London)*, 205: 292-304 (March 1967).
97. J. K. Mukherjee and B. R. Nijhawan, Some Precipitation Reactions in Chromium–Manganese–Nitrogen Stainless Steels on Aging and Cold Working, *J. Iron Steel Inst. (London)*, 205: 62-67 (January 1967).
98. A. Havalda, The Structural Changes in the System Ni–Cr–Ti–Al–W at Temperatures of 850°C (in French), *Metaux (Corros.-Ind.)*, 41: 225-234 (June 1966).
99. I. J. Duerden and W. Hume-Rothery, Equilibrium Diagram of the System Niobium–Nickel, *J. Less-Common Metals*, 11: 381-387 (December 1966).
100. P. B. Mee and R. A. Sinclair, Cold-Rolling and Annealing Behavior in Nickel–Thoria Sheet with Particular Reference to Preferred-Orientation Development, *J. Inst. Metals*, 94: 319-326 (September 1966).
101. V. A. Tracey and D. K. Worn, Some Observations on the Cold-Drawing and Annealing Behaviour of Nickel Containing a Dispersed Phase of Thoria, *Powder Met.*, No. 10: 34 (1962).
102. B. Harris, Solution Hardening in Niobium, *Phys. Status Solidi*, 18: 715-730 (Dec. 1, 1966).
103. M. L. Torti, Jr., Metallurgy, U. S. Patent No. 3,268,328, to National Research Corp., Aug. 2, 1966.
104. G. F. Zaboronok, V. B. Milova, M. D. Polyakova, and T. V. Simonishvili, Effect of Ultrasonic Vibration on the Structure of Electron-Beam-Melted Molybdenum (in Russian), *Tsvetn. Metal.*, No. 7: 83-85 (1966).
105. S. Feuerstein and L. Rice, Ultrahigh-Vacuum Effects on the Mechanical Behavior of Molybdenum, *Trans. AIME*, 236: 1675-1679 (December 1966).

106. G. K. Jun and M. Hoch, Thermal Conductivity of Molybdenum at Elevated Temperatures: Influence of Grain Size and Impurities, *Proceedings of the 4th Conference on Thermal Conductivity*, pp IV. A. 1-14, University of Cincinnati, 1964.
107. W. H. Chan, Molybdenum-Base Alloy, U. S. Patent No. 3,275,434, to General Electric Company, Sept. 27, 1966.
108. Ye. M. Savitsky and G. L. Tsarev, Investigations of Effect of Interstitial Impurities on the Structure and Properties of Tungsten Single Crystals, Report NASA-TT-F-10157 [from *Vestsi Akad. Navuk USSR, Ser. Fiz.-Tekh. Navuk*, No. 2: 84-91 (1965)].
109. H. Boehm and F. Mir, Appearance of a Yield Point in Vanadium Alloys, *J. Less-Common Metals*, 11: 408-416 (December 1966).
110. P. Guyot and R. Debeir, Hardening of SAP/Al_2O_3 Alloys at Low Temperatures, USAEC Report AEC-tr-6808 [from *Acta Met.*, 14: 42-55 (1966)].
111. W. F. Brizes, L. H. Cadoff, and J. M. Tobin, Carbon Diffusion in the Carbides of Niobium, *J. Nucl. Mater.*, 20: 57-67 (July 1966).
112. R. Resnick, R. Steinitz, and L. Seigle, Determination of Diffusivity of Carbon in Tantalum and Columbium Carbides by Layer Growth Measurements, *Trans. AIME*, 233: 1915-1918 (October 1965).
113. E. Fromm, E. Gebhardt, and U. Roy, Diffusion of Carbon in the Carbide Phase of Tantalum, *Z. Metallk.*, 57: 808-811 (November 1966).
114. A. V. Shovensin, G. V. Shcherbedinski, and A. N. Minkevich, On Some Peculiarities of Carbon Diffusion in Molybdenum Carbide, *Porosh. Met., Akad. Nauk Ukr. SSR*, No. 11: 46-51 (November 1966).
115. L. M. Gert, Determination of the Coefficient of Carbon Diffusion in Zirconium Carbide at High Temperature, *Zavodsk. Lab.*, 32: 970-973 (1966).
116. M. J. Fleetwood, Diffusion of Chromium into Nickel-Thoria Alloys, *J. Inst. Metals*, 94: 218-223 (June 1963).
117. P. V. Geld, E. Ya. Velmozhoyi, V. D. Lubinmov, and G. P. Shveikin, Self-Diffusion of Niobium in a Number of Its Molybdenum Alloys (in Russian), *Izv. Vyssh. Ucheb. Zaved., Tsvetn. Met.*, No. 2: 135-141 (1966).
118. G. M. Neumann, W. Hirschwald, and I. N. Stranski, Surface Diffusion of Tungsten (in German), *Z. Naturforsch.*, 21a: 807-811 (June 1966).
119. G. M. Neumann and W. Hirschwald, Self-Diffusion and Diffusion Mechanisms in Tungsten (in German), *Z. Naturforsch.*, 21a: 812-815 (June 1966).
120. R. F. Hehemann, Chemical Diffusion in the Columbium-Tungsten System, *Trans. AIME*, 236: 1040-1044 (July 1966).
121. R. I. Batista, G. S. Hanks, and D. J. Murphy, Diffusion Bonding of Tungsten to Tungsten, U. S. Patent No. 3,241,230, to USAEC, Mar. 22, 1966.
122. J. M. Criscione, J. Rexer, and R. G. Fenish, High-Temperature Protective Coatings for Refractory Metals. Progress Report No. 3, May 1-July 31, 1965, Report NASA-CR-68181 (N-66-12875), Union Carbide Corp., Carbon Products Division.
123. H. Beisswenger, M. Bober, and G. Schumacher, Thermodiffusion in System UO_2-CeO_2, *J. Nucl. Mater.*, 21: 38-52 (1967).
124. H. E. Roellig, Compatibility of Fissionable Materials with Construction Materials. Part I. Compatibility of Metallic Fissionable Materials with Cladding Materials, German Report ZFK-WF-13, March 1962.
125. E. J. Ripling and P. B. Crosley, Development of Test Procedures, Fracture Toughness of Reactor Pressure Vessel Steels, USAEC Report COO-1477-6, Materials Research Laboratory, Nov. 30, 1966.
126. Argonne National Laboratory, Reactor Development Program Progress Report, May 1966, USAEC Report ANL-7219, June 30, 1966.
127. A. G. Pickett and S. C. Gregory, Studies of the Fatigue Strength of Pressure Vessels. Part I. Cyclic Pressure Tests of Full-Size Pressure Vessels, USAEC Report SWRI-1228-1-29, Southwest Research Institute, September 1966.
128. D. J. Maykuth and A. Gilbert, Chromium and Chromium Alloys, Report DMIC-234, Battelle Memorial Institute, Defense Metals Information Center, Oct. 1, 1966.
129. G. R. Wilms and N. E. Ryan, Influence of Atmospheric Nitrogen on the Creep Properties of Chromium-Tantalum Alloys, *J. Less-Common Metals*, 12: 11-18 (1967).
130. T. P. Herbell, J. W. Weeton, and M. Quatinetz, Structure and Properties of Tungsten-Base Powder Metallurgy Composites, Report NASA-TN-D-3610, National Aeronautics and Space Administration, Lewis Research Center, September 1966.
131. Southern Research Institute, The Mechanical and Thermal Properties of Tungsten and TZM Sheet Produced in the Refractory Metal Sheet Rolling Program. Part I. Report AD-638631, Aug. 31, 1966.
132. C. D. Calhoun and F. W. Wiesinger, Tensile and Creep Properties of Niobium-Vanadium Alloys as Influenced by Strain Rate, USAEC Report KAPL-3145, Knolls Atomic Power Laboratory, June 1, 1966.
133. C. D. Calhoun, Preliminary Study of Niobium-Silicon Alloys, USAEC Report KAPL-M-6574, Knolls Atomic Power Laboratory, January 1966.
134. E. A. Abramyan, L. I. Ivanov, N. S. Kudryavtsev, and V. A. Yanushkevich, Effect of Vacuum on the Creep of Beta Zirconium at High Temperature, *Fiz.-Khim. Mekh. Mater.*, 2: 422-425 (1966).
135. Bureau of Mines, Albany Metallurgy Research Center, Metallurgical Progress Report No. 33 for Quarter Ending December 1966, USAEC Report USBM-RC-1273.
136. B. G. Ignat'ev, L. B. Nezhevenko, A. V. Kovalev, N. I. Poltoratskie, G. S. Fomin, and M. V. Yakutovich, Manufacture of Thin Plates From Refractory Carbides, *At. Energ. (USSR)*, 20: 489-494 (June 1966); translated as JPRS-38834.
137. E. Lubatti, S. Pappalardo, and V. Mirarchi, Metallic Oxides, Carbides, Nitrides, Borides, and Silicides in the Technology of High and Very High Temperature: Present State and Future Development, *Termotecnica (Milan)*, 20: 540-551 (September 1966).
138. G. V. Samsonov, *Refractory Compounds of Rare-Earth Metals with Non-Metals*, translated from the Russian, Consultants Bureau, New York, 1965.
139. S. P. Denker, Bonding, Stability, and Formation of Cubic Refractory Monocarbides, Mononitrides, and Monooxides, USAEC Report CU-3553-5, Columbia University, Nov. 21, 1966.
140. H. L. Brown and C. P. Kempter, Elastic Properties of Zirconium Carbide, USAEC Report LA-DC-8206, Los Alamos Scientific Laboratory, 1966.
141. V. V. Fesenko, H. S. Bolgav, and S. P. Gardienko, Study of the Speed of Vaporization of the Vapor Pressure of the Compaction Discontinuity and of Certain Thermodynamics Properties of Refractory Compounds at Temperatures up to 3000°C, *Rev. Hautes Temp. Refract.*, 3: 261-271 (July-September 1966).
142. L. M. Adelsberg, L. H. Cadoff, and J. M. Tobin, Group IV-B and V-B Metal Carbide-Carbon Eutectic Temperatures, *J. Amer. Ceram. Soc.*, 49: 573-574 (Oct. 21, 1966).
143. V. S. Panov, G. H. Meerson, and V. F. Funke, Structure and Physical and Mechanical Properties of WC-TaC-Co Hard Alloys, *Izv. Akad. Nauk SSSR, Metal.*, No. 2: 120-124 (March-April 1966).
144. R. L. Hodson and N. M. Parikh, Cemented Carbides with High-Melting Binders, *Int. J. Powder Met.*, 2: 55-63 (October 1966).
145. H. Suzuki and H. Kubota, The Influence of Binder Phase Composition on the Properties of WC-Co Cemented Carbides, *Planseeber. Pulvermet.*, 14: 96-109 (August 1966).
146. H. Kubota, R. Ishida, and A. Hara, On Influence of

Carbon Content on the Cobalt Phase Contained in WC Base Cemented Carbides, *Sumitomo Elec. Tech. Rev.*, 6: 87-93 (July 1965).

147. H. Suzuki, K. Hayashi, and I. Kauakatsu, Properties of WC–TiC–10% Co Alloys in Connection with the Carbon Content of Carbides, *Nippon Kinzoku Gakkaishi*, 30: 689-693 (1966).
148. W. Dawihl and G. Altmeyer, On the Influence of Notches and Heat Treatment on the Fatigue Strength of Tungsten Carbide–Cobalt Alloys, *Z. Metallk.*, 57: 688-690 (September 1966).
149. V. S. Dergunova, G. K. Komissarov, M. P. Ermakova, L. I. Kuznetsov, and A. A. Goldenberg, Metal-Ceramic Alloy for Work at Elevated Temperatures, *Vestn. Mashinostr.*, 6: 63-65 (1966).
150. I. F. Ferguson, Fast-Neutron Lattice Damage in Silicon Carbide: An X-Ray Diffraction Investigation, British TRG-Report-1232, Mar. 28, 1966.
151. Oak Ridge National Laboratory, Reactor Chemistry Division Annual Progress Report for Period Ending December 31, 1966, USAEC Report ORNL-4076, March 1967.
152. A. E. Gorbunov, Carbothermal Method of Preparation of Chromium, Molybdenum, and Zirconium Borides, *Porosh. Met., Akad. Nauk Ukr. SSR*, No. 11: 52-56 (November 1966).
153. W. A. Sanders and H. B. Probst, Hardness of Five Borides at 1625°C, Report NASA-TM-X-56851 (N-66-29370), National Aeronautics and Space Administration, Lewis Research Center, Sept. 1, 1965.
154. M. Kuzenkova and P. S. Kislyi, Investigation of the Sintering of Alloys of Zirconium Diboride with Molybdenum Disilicide, *Porosh. Met., Akad. Nauk Ukr. SSR*, No. 9: 11-16 (September 1966).
155. T. S. Verkhoglyadova and L. A. Dvorina, High Temperature Oxidation of Silicides of Rare Earth Metals, *Zh. Fiz. Khim.*, 40: 2250-2254 (September 1966).
156. W. M. Hirthe, Research on Defect Controlled Electrical Properties of Rutile, Report ARL-66-0071, Marquette University, April 1966.
157. L. R. Furlong and L. P. Domingues, Sintering of Yttrium Oxide, *Amer. Ceram. Soc. Bull.*, 45(12): 1051-1054 (December 1966).
158. P. F. Eastman and I. B. Cutler, Effect of Water Vapor on Initial Sintering of Magnesia, *J. Amer. Ceram. Soc.*, 49(10): 526-530 (October 1966).

Section IV

Reactor Materials

Special Fabrication Techniques

Melting and Fabrication of Cast Materials

Combustion Engineering[1] is conducting a program to develop a commercial melting process for producing high-purity vanadium and to assess the mechanical properties and weldability of a vanadium alloy produced from high-purity feed material. In this program, several button melts were made to determine the effects of aluminum, silicon, and yttrium as gettering agents in vanadium. The buttons were produced by nonconsumable-electrode arc melting and electron-beam melting and were evaluated for hardness and interstitial impurity level. Preliminary results indicated that:

1. Of the three gettering elements, yttrium was the most effective for scavenging oxygen from vanadium.

2. All three gettering agents were ineffective in reducing the nitrogen content of vanadium.

3. Silicon was the least satisfactory gettering agent for all interstitials and was not effectively removed by electron-beam melting.

4. Electron-beam melting removes interstitial carbon that combines with oxygen to form CO or CO_2. Yttrium, however, was found to hinder this reaction.

Alloys of aluminum with 18 and 24 wt.% uranium in the shape of ingots 70 to 100 mm in diameter were produced by continuous casting in Germany.[2] A specially constructed feeding system was useful in overcoming the gravitational segregation that occurs in the course of casting. After heat-treatment at 600°C, the ingots could be rolled into strip or extruded successfully.

Electron-beam zone melting today is one of the most important methods for the ultrahigh-purity preparation and single-crystal growth of metals with a high melting point. A German report[3] describes the status of electron-beam melting of tungsten and molybdenum. In particular, the melting behavior of various raw materials, their influence on the attainable purity, recrystallization, and the distribution of impurities, as well as the separation effects and the purity of zone-melted crystals as a function of the melting conditions are discussed in this report.

The characteristics of an electron-beam zone refiner that is currently being used in the Soviet Union has been described by the Russians.[4] The basic units of the electric part of this apparatus were a type FRS ferroresonance stabilizer, a high-voltage transformer, a type RNO-250-2 regulating autotransformer, and two type TRI-6/15 thyratrons fed by heating transformers. A high voltage was applied to the sample, which formed the anode. The emission current could be uniformly regulated from 0 to 300 ma. As a result of the evolution of gases and the vaporization of impurities, the emission current varied within wide limits and made the melting process difficult, sometimes even leading to an electrical discharge and to fracture of the sample. The mechanical part of the apparatus made possible the movement of the emitter at the required rate, as well as rotation of the sample. A type D-104 motor (33 rpm) was used to displace the cathode. A reducer permitted varying the rate from 0.04 to 1.2 rpm, which corresponded to a change in the rate of movement of the cathode from 10 to 300 mm/hr. The emitter was made of tungsten filament and surrounded the sample. The optimum diameter of the annulus was 25 to 30 mm. Zone-melting experiments were carried out on a number of metals: Fe, Ni, Cu, Mo, W, V, Nb, and Ti, as well as on Fe–Ni, Fe–Ni–Cr, and other alloys. It was impossible to use this apparatus for melting metals that had a high vapor pressure because of discharges between the anode and the cathode.

The effect of certain parameters of zone recrystallization (speed of travel of the liquid zone and number of passes) on the degree of refining of molybdenum was also studied by the Russians.[5] The metal purity was determined by measuring the ratio of the electrical resistance at room temperature to that at the temperature of liquid helium. The zone refining was done with an electron-beam gun. It was noted that the refining of molybdenum is due mainly to the vaporization of volatile impurities, and also to the mechanism of zone refining itself. The character of the distribution of impurities over the length of the specimen indicated that molybdenum contains many impurities with a distribution coefficient $K < 1$, such as carbon. A change in the speed of travel of the liquid zone from 1 to 5 mm/min did not appreciably affect the distribution of impurities along the specimen.

The effect of subsonic and ultrasonic vibrations on the crystallization of molybdenum, electron-beam melted in a 5×10^{-4} mm Hg vacuum, was also investigated by the Russians.[6] Subsonic vibrations at a frequency of 1000 cpm reduced the grain size from a range of 3 to 5 mm to a range of 2 to 3 mm. Ultrasonic vibrations with a frequency of 2 to 18 kc substantially reduced the grain size in the transverse direction but had very little effect on the grain size in the longitudinal direction, leaving the columnar structure unchanged. The Brinell hardness of molybdenum melted with ultrasound amounted to 153 to 156 kg/mm^2, i.e., it was of the same order as that of molybdenum melted without ultrasound. Preforged ingots were rolled into sheets 1 mm thick. The respective tensile strength and elongation of cold-rolled sheets melted with ultrasound were 75.0 kg/mm^2 and 4.8% compared with 62.1 kg/mm^2 and 2.8% for conventionally electron-beam-melted metal. Vacuum annealing at 600 to 1400°C for 1 hr greatly affected the strength and ductility of conventionally melted metal, but only slightly affected these properties of metal melted with the application of ultrasound.

A process has been developed at Ames[7] for the preparation of high-purity ductile niobium metal by the reduction of Nb_2O_5 with aluminum powder in a bomb-type process. Aluminum, oxygen, nitrogen, and iron impurities can be removed in subsequent treatments by volatilization. Purified niobium sponge obtained by heating to 2000 or 2200°C can be converted to massive ductile metal by nonconsumable-electrode arc melting. A two-step melting process in which the vacuum-arc-cast ingot is remelted in an electron-beam furnace yields high-purity ductile niobium.

General Atomic[8] has examined the properties of tungsten prepared by the hydrogen reduction of WF_6 for application as a thermionic emitter. Areas investigated include the quality of material available and the resistance of this material to grain growth. Properties determined during the evaluation program were microstructure, both before and after extensive thermal treatments; ductile-to-brittle transition temperature; impurity content; and hardness. Experimentation has shown that the resistance of vapor-deposited tungsten to grain growth is primarily structure sensitive; and, in all cases where grain growth is observed, it starts at regions of marked grain misorientation, primarily a layer of small, equiaxed, randomly oriented grains which extends into deposited material up to 0.003 in. from the substrate surface. If the layer is removed prior to thermal treatment, resistance to grain growth is markedly improved.

Pilot-plant cell operations for the production of reactor-grade uranium-metal castings from UO_2 are described in a Maryland University report.[9] In these operations, uranium oxide and fluoride are fed down an axial hole in the anode columns in the cell. The powders contact molten BaF_2–LiF–UF_4 electrolyte in the anode region. The UF_4 dissolves readily, and the UO_2 dissolves perhaps less readily and certainly less extensively (2 to 4% maximum). Carbon monoxide and CF_4 gases are evolved at the anodes, and metal is deposited on the cathodic crucible. The metal is withdrawn periodically by way of a vacuum life tube and is cast into suitably prepared molds.

For elimination of the hydriding problem in Zircaloy tubes for organic-moderated reactors, it was suggested that aluminum be clad on the inside of Zircaloy-4 or other zirconium alloys to act as a barrier against hydrogen. Nuclear Metals[10] is investigating fabrication methods by which this may be accomplished. Because bonding was required to withstand thermal cycling, the bond was determined primarily by ultrasonic testing before and after various thermal treatments. Methods involving low deformation showed little promise of success and therefore were not investigated extensively. Ball-sizing, i.e., extrusion of an aluminum sleeve by pulling an oversize plug through it so that the sleeve elongated and came in contact with the surrounding Zircaloy, gave results that were usually good at 950°F (510°C). However, the quality of the bond decreased as the processing temperature was lowered. Lubrication was not satisfactory at the higher temperature, but better inside surfaces were obtained as the processing temperature was decreased. It appeared that a zinc electroplate on the mating surface of the aluminum permitted bonding to occur by ball-sizing at about 650°F (343°C). There was evidence that zinc on the inner surface facilitated lubrication at this temperature.

Coextrusion was investigated in a small auxiliary effort. The two metals could be coextruded, but wavy surfaces were obtained. When SAP alloy was substituted for 2S aluminum, good surfaces resulted. The coextruded samples were used in diffusion experiments which showed that interdiffusion between aluminum and Zircaloy was greater than between the SAP alloy and Zircaloy.

The Zircaloy structurals envisioned for new Bettis[11] cores are long tubular cans having various cross sections that must be fabricated to restrictive tolerances. These structurals, manufactured as weldments from Zircaloy-4 strip, range in length from 9 to 20 ft and have cross sections from 3 in. up to 19 in. in actual diameter or diameter of circumscribing circle. In cross sections the shapes are quite varied and include the following: circular, angular (i.e., chevron and keystone), fluted, and corrugated. Because of the restrictive tolerances required for each of the cans, it is not feasible to attempt to achieve the final dimensions in the as-welded condition. Each can therefore requires a sizing operation, subsequent to welding, during which the desired nominal dimensions and reduced tolerances are achieved.

As part of the Large Seed-Blanket Reactor (LSBR) fabrication development program at Bettis, feasibility studies are being performed in the sizing of circular and angular shapes by three processes: thermal sizing, explosive sizing, and cold hydraulic sizing. Experiments concerning these processes reveal that thermal sizing is the most suitable process of the three in achieving the required tight diametral and boundary surface tolerances. With cylindrical tubes up to 11½ in. in diameter by 103 in. long and wall thicknesses of 0.062 in., tolerances that can be met consistently around any desired nominal diameter are ±0.020 and +0.025 in. for the diametral tolerance and boundary diameter, respectively. As a result of the strain-rate sensitivity of Zircaloy and limitations placed on the amount of elongation permitted which precluded removal of ovality, experiments in explosive sizing were discontinued. Cold hydraulic sizing experiments were discontinued because of the dimensional instability of the sized component under subsequent thermal cycling.

The British[12] have been attempting to grow single crystals of Zircaloy-2. Three methods of growing large single crystals were tried: cycling the specimen between 840 and 1200°C; prolonged annealing in the alpha phase at 840°C; and heating at 1200°C for 30 min, followed by quenching to room temperature, and then annealing at 840°C for 12 days. The results indicated that any successful attempt to grow large grains of Zircaloy-2 must include elimination of the beta phase by quenching or annealing in the alpha-phase range.

On the basis of the results of screening tests involving a number of alloys, the V–15 wt.% Ti–7.5 wt.% Cr alloy has emerged from studies at Argonne[13] as a promising cladding candidate for sodium-cooled fast reactors. "Scale-up" or pilot-plant production technology was developed at Argonne. Consolidation involved consumable-electrode arc melting of compacted electrodes, followed by arc remelting. The double-melted ingots were broken down by extrusion and reextruded into rod, sheet-bar, and tube blanks. Rod and sheet products were easily cold rolled to finished sizes. Extruded tube blanks were processed by swaging, tube reducing, and drawing. After some early processing problems were solved, high yields were realized in the production of reactor-grade tubing.

Papers on the fabrication of refractory-metal tubing are included in the Proceedings of the Third Technical Conference of the Metallurgical Society of the AIME held in Los Angeles, Calif., Dec. 9 and 10, 1963 (Ref. 14). In one of these papers, Oak Ridge[14a] described the feasibility of manufacturing refractory-metal-alloy tube shells both by high-temperature extrusion and flow-turning techniques. Unlike with most conventional tube-shell extrusion methods, a floating-mandrel technique was used to extrude uncanned tube shells of molybdenum and tungsten alloys. This technique was selected since the volatile oxides of these refractory metals minimized contamination by air during hot working. Satisfactory tube shells of molybdenum and molybdenum-base alloys were extruded by this technique, using a reduction ratio of 8.8 to 1 and a temperature range of 1590 to 2065°C. Flow turning, a low-temperature process, was explored as a tube-shell production technique for refractory metals, such as niobium and tantalum, which are easily contaminated by air at elevated temperatures. Procedures were developed for flow turning hollow cylinders of the Nb–1 wt.% Zr alloy prepared from both wrought bar stock and cast ingots.

The production of heavy-walled vacuum-arc-cast molybdenum tubes by extrusion was described by Universal Cyclops.[14b] A double extrusion practice was developed that consisted of back extrusion to achieve the inside diameter, followed by forward extrusion to produce the outside diameter. Such extruded rings were suitable for subsequent ring-rolling and mandrel-forging applications.

The Russians[15] have prepared molybdenum and rhenium foils (1 to 7 μ thick) for nuclear studies by the thermal dissociation of pentachlorides. Thermal dissociation was achieved in a vacuum chamber at 850 to 900°C using a copper backing. The foils that were obtained were reported to be free of copper impurities. (S. G. Nelson)

Powder-Metallurgy Materials

Investigators at Argonne[16] have produced tungsten and W–25 wt.% Re tube blanks by double extrusion. The starting material, generally a pressed-and-sintered product, was in the form of a sleeve 3.17 cm in outside diameter by 2.54 cm in inside diameter by about 10 cm long. Both initial and reextrusion processes involved the filled-billet technique. The resultant tube blanks, 0.64 cm in outside diameter by 0.51 cm in inside diameter by 75 cm long, were structurally sound and suitable for secondary fabrication operations.

In a continuation of earlier work,[17] General Electric has developed tube-processing procedures for W–30 wt.% Mo and W–25 at.% Re–30 at.% Mo alloys. Initial studies involved the fabrication of 0.421-cm-OD by 0.345-cm-ID tubes. In the most recent work, larger (0.096 to 1.29 cm in outside diameter), thinner-walled tubes were the objective. A preconditioning procedure was introduced to produce high product yields.

Techniques developed by the 3M Company[18] have been utilized to fabricate small-diameter tubing from W–26 at.% Re and W–30 at.% Mo–30 at.% Re powder-metallurgy billets. The tubes were used as

starting material for subsequent drawing operations. Tubes in the size range 0.120 to 0.130 in. in outside diameter and 0.080 in. in inside diameter to 0.100 in. in outside diameter and 0.080 in. in inside diameter, with lengths of at least 12 in., were prepared with densities in excess of 95% of theoretical and with total impurity content of less than 300 ppm. Tubing having good mechanical properties was successfully processed by plug and mandrel drawing.

Investigators at Lewis[19] have fabricated thin-wall tungsten tubing by hot extrusion over a floating mandrel. Successful extrusion of ½-in.-diameter tubing over 0.4-in.-diameter mandrels was accomplished in the temperature range 3000 to 4000°F (1649 to 2205°C). Tubing ⅜ in. in diameter was extruded successfully over 0.3-in.-diameter mandrels at 4000°F. Variables studied included extrusion temperature, initial density of the powder-metallurgy billet, and composition of the canning material.

Nuclear Metals[14c] has devised a process for the production of seamless tungsten tubing. The process consists of the extrusion of sintered-powder sleeves at elevated temperatures to sizes close to the final dimensions. The tubing is finished by warm drawing. Tubing 0.100 to 1.5 in. in diameter has been fabricated. A preliminary evaluation of the properties of the extruded tubes was conducted.

The Hoskins Manufacturing Company[14d] found that specialized techniques for the preparation of the initial tubing blank, use of a "filled-billet" concept as a consolidation medium, development of a chemical drilling method for mandrel removal, and special adaptations of conventional tube-reduction methods enabled production of a variety of seamless tube sizes of W–26 wt.% Re alloy. High-temperature extrusion of powder-metallurgy billets is described as a means of preparing breakdown tubes for subsequent swaging and drawing operations.

Kinney et al.[14e] have described the relations between permeability, void volume, and particle size in porous sintered tungsten. For original particle sizes ranging from 1 to 60 μ, and for densities of sintered material ranging from 60 to 85% of theoretical, the permeability varied as the fourth power of the fractional void volume and as the three-halves power of the nominal particle size in the original powder. From these data it was possible to prepare sintered tungsten to a specified permeability and to anticipate items such as the pressure drop required to produce a specified rate of flow for a fluid through the sintered material.

The fabrication of porous refractory ionizer material from prealloyed, spherical powders of narrow size range was investigated at Hughes.[20] Alloy powders used were pure Ir, Ir–50 W, W–5 Re, and W–25 Re (presumably wt.%). Pellets from mixtures of elemental powders were also prepared in high-density form. Fabrication techniques studied included warm pressing, joining methods, and surface treatment to keep pores open.

The French[21] have considered the theoretical and practical aspects of sintering techniques employed with numerous metals and alloys to provide porous materials with high corrosion resistance, particularly for nuclear and industrial purposes. Such materials and their processing were described and illustrated. Reliability testing was considered, as well as some characteristics of stainless-steel and bronze products. Special properties of sintered porous elements for specific uses were reviewed.

(C. A. MacMillan)

Pressure Bonding

Joining of dissimilar-metal combinations by a hot-press bonding technique has been described by the Canadians.[22] This method involves pressing a tapered tube into a grooved end of another thick-walled tube or plug which is restrained in a die. For this operation the heavier component and restraining die are generally preheated, and, where there is a large difference in hardness of the two components, both members are preheated. Force is rapidly applied to the system and maintained until the full depth of the taper has penetrated the groove. Of the 10 materials combinations investigated, it was found that strong joints were readily obtained between Zircaloy-2 and 1S aluminum, Zircaloy-2 and 416 stainless steel, and mild steel and aluminum. Other systems showed promise but will require additional study. This technique had been used previously for producing diffusionless transition pieces for experimental fuel rods and irradiation-facility components for the NRX and NRU reactors, respectively.

A method for high-temperature isostatic pressing is the subject of a U. S. patent.[23] In this technique, articles are formed from powders contained in a flexible membrane. Pressure is transmitted to the powder mass through solid particulate matter, and the flexible membrane is of such a material that it decomposes below the sintering temperature of the powder mass.

Necker[24] has reviewed the hot-gas isostatic-pressing process from the standpoint of equipment and applications. The equipment described consisted of a water-cooled pressure vessel with the associated fluid pumping system, pressure-recording and -control equipment, and an electric-resistance furnace with its power supply, temperature sensors, and associated controls. This system is designed to provide pressures up to 15,000 psi and temperatures up to 3500°F (1930°C), which are sufficient to accomplish most jobs. Applications of the process included hot pressing of complex shapes from powders, cladding-to-core bonding, forming complex shapes from wrought materials, and fabrication of complex assemblies from premachined components.

Hot isostatic pressing has been used as a method to fabricate fiber-reinforced composites from coated filaments.[25] Graphite filaments initially coated with nickel by electroless plating were densified by pressing for 1 hr at 10,000 psi and at temperatures ranging from 700 to 1000°C. It was noted that composites containing from 25 to 60 vol.% nickel were successfully densified at the higher temperature. Similarly, cobalt composites containing up to 57 vol.% Thornel yarn were bonded into fully dense structures under the same conditions. Boron fibers coated with titanium powder were hot isostatically pressed for 1 hr at 1350°F (732°C) and 10,000 psi, producing platelets. Examination of the boron-reinforced structures revealed no chemical interaction between the matrix and reinforcement phases. With all of the composite systems studied, it was observed that hot isostatic pressing produced good filament-to-matrix bonding and resulted in a minimum of filament damage. (S. W. Porembka)

Plating

Nonelectrolytic Chemical Plating

A large percentage of the work reported in this area during the period relates to various aspects of the chemical vapor deposition of tungsten and its alloys as coatings or for the fabrication of shapes, principally tubing. Research at the Bureau of Mines has been reported on the preparation of binary alloys of molybdenum and tungsten by hydrogen reduction of their hexafluorides.[26] Reaction efficiency in the temperature range of 650 to 750°C was greater than 75%, and dense homogeneous alloys were obtained. Uniform alloy composition was obtained with hydrogen ratios less than three times stoichiometric. The alloys were extremely brittle, and tensile-strength measurements could not be made.

The progress of studies on the chemical vapor deposition of tungsten and tungsten-base alloys was reported by Oak Ridge workers.[27] Tungsten is deposited from the WF_6-H_2 system. A statistical program requiring 81 deposition experiments is under way which will attempt to correlate deposition rate and nucleation and growth mechanisms with experimental parameters. The range of experimental conditions to be covered is as follows:

Temperature, °C	450 to 820
Pressure, torrs	5 to 20
Total flow rate, cm^3/min	750 to 6010
WF_6 flow rate, cm^3/min	50 to 380

The tungsten is deposited inside 0.81-in.-diameter copper mandrels, and the deposit thickness is measured by an X-ray attenuation technique. Deposition of W – Re has been accomplished from a mixture of WF_6-ReF_6. A moving hot zone was used in conjunction with a water-cooled gas injector.

Additional Oak Ridge work on the deposition of W–Re alloys was described in a subsequent report.[28] Uniformity of composition through the thickness of a tubular deposit was studied by electron-probe measurements. Maximum variations of ±1.3 wt.% rhenium were found in a deposit of average composition W–22 wt.% Re. A study of the phases produced in the alloy deposits is being conducted.

Lawrence Radiation efforts on the SNAP reactor program include chemical vapor deposition of W–Re alloys.[29] Processes for coating refractory-metal composites, welding refractory-metal alloys, and preparation of tubing were examined. Rotating molybdenum mandrels ½ in. in diameter by 1½ in. long were employed. The mixed fluoride gases were fed by mechanically metering small slugs of liquid fluorides to a flash vaporizer. In some experiments the deposit was burnished during plating with a water-cooled rubbing device in an attempt to decrease grain size and increase strength. This technique had previously been successful with pure tungsten, but the alloy deposits tended to grow unevenly when rubbed. The effects of variation of pressure from 3 to 100 torrs, temperature from 500 to 1000°C, gas velocity from 367 to 2200 cm^3/min, and the ratios of hydrogen to total fluoride from 7 to 40 have been studied.

A patent[30] has been issued for a process for carbide deposition on tantalum. The process consists in heating the tantalum part in contact with lampblack (< 1-μ average particle size) in a hydrogen atmosphere. Treatment at temperatures in the range 800 to 1160°C gives a thin (1 to 3.5 μ) coherent coating of tantalum carbide, and the base metal retains its ductile characteristics. The patent notes that lampblack was the only source of carbon tried which was effective. Also, the lampblack packing could be used effectively only one time.

The Proceedings of the December 1963 Third Technical Conference sponsored by the Refractory Metals Committee, Institute of Metals Division, of the Metallurgical Society[14] contains a number of papers on the coating of refractory metals. These papers cover broadly the state of the art as of the time of the conference. Heestand and Leitten[14f] reported on the production of refractory-metal tubing by vapor forming from the WF_6-H_2 system. Disckind[14g] gave details of the joining of tungsten sheet by chemical vapor deposition using the same reaction. The scale-up of pack-cementation-coating processes for TZM molybdenum was discussed by Dioguardo and others.[14h] Aves and Ecord[14i] reported advances in coating-deposition techniques for refractory-metal structures. Procedures for arc-plasma coating of refractory metals were described by Jones and others.[14j] Battelle–Columbus workers reviewed results obtained by pack-cementation application of

silicide coatings to tantalum and tantalum-base alloys.[14k] A program to study the coating of refractory-metal foil was described by Moore and Stetson.[14m] Experience in scale-up of coating systems from the laboratory to application in structures was discussed by Rummler and others.[14n] (E. H. Hall)

Electroplating

During research on the electrodeposition of tungsten alloys, the use of radioisotope ^{185}W showed that the reduction of WO_2 at cathode surfaces was promoted by the addition of hydrazine sulfate and was decreased by additions of tartrate or citrate ions, which have been used heretofore for complexing ions of metals codeposited with tungsten.[31]

A nonaqueous electropolishing bath developed[32] for uranium reduced roughness 33% in 10 min and nearly 60% in 46 min. The solution contained 600 g/liter sodium hypophosphate in 1.2 ethanediol and was operated at a temperature of 90 to 110°C. The water content was reduced to <0.1 vol.% by bubbling with a continuous stream of dry argon for 12 hr. Uranium was electropolished at a constant voltage (13 volts). The current density was initially 120 amp/sq ft but fell to 40 amp/sq ft as polishing progressed. The procedure might be useful for pretreating uranium prior to cladding or plating. (W. H. Safranek)

Welding and Brazing

Brazing

Two recent patents cover new alloys for brazing the refractory metals. An alloy consisting of 30 to 50 wt.% V–30 to 50 wt.% Ti–20 to 30 wt.% Ta for general refractory-metal brazing is identified.[33] The second patent is directed to the use of 40 to 87 wt.% Mo–5 to 40 wt.% Ru–8 to 55 wt.% Re alloys for brazing molybdenum and tungsten.[34]

Steel

A 3-year program covering the study of welding procedures and filler materials for high-strength, low-alloy steels at Thompson Ramo Wooldridge has been completed.[35] During the earlier work the martensitic steels, HP-9-4-20, HP-9-4-25, AMS 6435, VascoJet X2, and D-6ac, were investigated.[36,37] The latter part of the study was devoted to the expansion of the welding technology for HP-9-4-25 in thicknesses of 0.50, 0.25, and 0.09 in. by the TIG, MIG, electron-beam, and plasma-arc processes. Pressure vessels were also fabricated from HP-9-4-25 and tested in the as-welded condition. The inability to overcome poor fracture toughness discouraged a continuing effort on D6ac.

Automatic TIG welding of HP-9-4-25 using commercial filler wire and no preheat or postheat treatments gave welds with yield strengths in excess of 180 ksi. Fracture toughness was comparable to that of the unwelded plate for each thickness, when low heat inputs were used to make the welds. It was necessary to use chill bars to prevent heat-affected-zone tempering with certain thicknesses and joint designs. Root passes in the thicker plates required low welding speeds to prevent cracking. Welds made in 0.090-in. sheet at 4 to 15 in./min with low heat inputs were tougher than those made at 20 to 25 in./min.

Satisfactory MIG welds were made in 0.50-in. HP-9-4-25 plate using filler wires containing small aluminum and titanium additions. A gas mixture of argon +2% oxygen stabilized the MIG arc and produced a uniform spray transfer. Globular transfer obtained when using argon shielding or aluminum- and titanium-free filler wire produced excessive porosity. The MIG welds, however, had low yield strengths and exhibited very low weld-metal ductility. The low ductility was attributed to microcracking that was not found by conventional inspection techniques. The cracks became visible in the plastically deformed regions of tensile specimens and caused premature tensile failures.

Electron-beam-welded HP-9-4-25 0.50-in. plate exhibited strength, ductility, and fracture toughness comparable to that of the unwelded plate. A plasma-arc weld in a 0.375-in. plate contained excessive root voids and possessed a wide heat-affected zone.

The United States Steel metallurgists have been investigating the mechanical properties and transformation characteristics of several steels in the 180- to 210-ksi yield-strength range.[38] The group included the HP-9-4-25 steel. As-welded and welded-and-aged simulated heat-affected zones were used.

The mechanical-property tests of weld heat-affected-zone microstructures in the HP-9-4-25 steel indicated that, in the peak-temperature region 1300 to 2400°F (704 to 1316°C), the strength was excessively high and Charpy V-notch toughness was quite low. Postweld aging at 950 to 1000°F (510 or 538°C) for 5 hr lowered the strength to a level similar to that of the unwelded plate, but the toughness remained low. Two 10 Ni–Cr–Mo–Co steels exhibited satisfactory heat-affected-zone strength and good toughness. The toughness of the steel containing 2% chromium was better than that of the steel containing 1% chromium.

In general, the results of the study showed that the HP 9-4-25, the 9 Ni–0.3 Al, and the 7 Ni–3 Cr–Mo–Co steels all exhibit deficiencies in weld-heat-affected-zone mechanical properties, whereas the two 10 Ni–Cr–Mo–Co steels, particularly the steel containing 2% chromium, show promising weld-heat-affected-zone mechanical properties.

A literature survey on the 3.5 and 9 nickel steels has been published by the Canadians.[39] General cov-

erage of the applicable welding processes, procedures, costs, and weldment properties are included.

(R. M. Evans)

Nondestructive Testing

Ultrasonic Techniques

The incipient boiling detector developed by personnel at Aeroprojects[40] has undergone successful experiments in liquid potassium using the facilities of MSA Research Corp. Tests were conducted at equilibrium temperatures ranging from 400 to 1200°F (204 to 649°C). The unit is based upon the fact that conditions productive of equilibrium boiling can be detected by monitoring the ultrasonic power required to produce cavitation in the liquid phase.

Several ultrasonic techniques have been used for determining bond quality. Some of these are capable of locating areas of complete unbond and some can provide data relative to the cohesive strength of the adhesive. Schmitz and Frank[41] have reported on work with an acoustic emission technique for testing bond strength. When a material is subjected to a tensile stress, it emits sonic energy, and the amplitude of the sound energy increases rapidly as the yield stress is approached. Inclusions and discontinuities in the adhesive cause stress risers and contribute to the failure of a bond. If a tensile stress is applied to the bond line, small inclusions and discontinuities are subjected to very high stresses long before the whole bond line reaches the point of failure, and sonic and ultrasonic energy is generated at these points of high stress.

The acoustic emission testing of bond strength is very simple. A transducer capable of detecting ultrasonic energy is mounted to the surface of the specimen in the vicinity of the bond. For a large structure, several transducers can be used. The output of the transducers is amplified and selectively filtered so that only vibrations in a particular frequency band are passed on to the data-translation system. The point of initiation of the change in amplitude of acoustic emission as the stress approaches the yield stress of the bond can be used to predict the yield point very accurately without noticeable damage to the structure.

The acoustic emission method is well suited to whole structures tests. The test is fast and economical. Instrumentation is inexpensive; however, several sensors would be required to pinpoint areas of weakness. The technique is useful on both metal and honeycomb cores, and its effectiveness is nearly independent of face sheet or core thickness. Phenolic honeycomb cores, which usually fail before the bond, may introduce too much noise and mask the emission from the adhesive.

Ultrasonic energy may be generated by the forces of magnetic repulsion associated with the generation of eddy currents. Several investigators have studied the possibility of generating ultrasonic energy in this manner for nondestructive testing as a means of avoiding the need of liquid coupling media. A prototype system called "eddysonic" which is based on this principle has been developed and is in use at North American and NASA.[42]

(D. Ensminger)

Techniques Other Than Ultrasonics

Diagrams representing the distribution in the magnetic field surrounding an eddy-current test coil are presented in an Oak Ridge[28] report. The vector potential and phase of the fields of a circular coil adjacent to a conducting plane are shown for the cases with and without a ferrite cup-shaped core. Vector-potential values within the conducting plane are said to define induced eddy-current values. It was found that the ferrite cup serves to concentrate the field to provide greater sensitivity to defects. Other work in progress at Oak Ridge has involved a phase-sensitive eddy-current instrument for which circuit diagrams are being prepared for the Division of Technical Information for external distribution. Optimum probe coils for 50 and 500 kHz have been designed. With the 500-kHz coil on stainless steel, the instrument will measure conductivity within ±0.5% despite a lift-off variation from 0 to 30 mils.

Investigation of a new thermal-wave transducer method for measuring thermal properties and detecting flaws is being continued at Battelle–Northwest.[43] A small transducer on the order of 1 cu in. in size was applied to the specimen surface being inspected. The transducer could be coupled to the sample by a gas or other heat-transfer medium so that direct contact was not necessary. The area of the exciter–detector region of one transducer discussed was about 0.094 sq in. A thermoelectric heat pump was used in conjunction with the exciter–detector region to provide a sinusoidal temperature wave in the specimen of about ±1°C amplitude around ambient. The thermal waves were generated by exciting the transducer with an electronic system which also recorded the response of the transducer, and hence the response of the sample surface. Temperature waves at frequencies up to about 1 count/sec were possible with the transducer. A block diagram of the system was given, and some data on measurement of coating thicknesses were presented in the form of an "impedance" plot. The thermal input impedance of the transducer relates to a characteristic thermal surface impedance of the sample. Materials included Teflon and paper on stainless steel, and stainless steel on quartz or glass. Although much work remains to be done in refining and applying these techniques, the initial measurements look promising for the use of this system as a nondestructive testing tool.

(A. F. Leatherman)

References

1. S. Worcester and S. S. Christopher, Vanadium Purification. Quarterly Progress Report No. 1, July 1–September 30, 1966, USAEC Report CEND-3742-288, Combustion Engineering, Inc., November 1966.
2. W. Duerrschnabel and E. Lange, On the Continuous Casting of Aluminum–Uranium Alloys, *Z. Metallk.*, 57: 451-454 (June 1966)
3. J. Barthel and R. Petri, Electron-Beam Zone Melting of Tungsten and Molybdenum, USAEC Report ORNL-tr-1402 (translated from German report), 1966.
4. Yu. M. Korobochkin, V. D. Pantov, and V. I. Shiryaev, Some Characteristics of Electron-Beam Zone Refining of Metals, *Izv. Akad. Nauk SSSR, Metal.*, No. 1: 73-79 (January–February 1966).
5. G. P. Lovtun, A. D. Kryglykh, and I. G. D'yakov, Zone Refining of Molybdenum, *Izv. Akad. Nauk SSSR, Metal.*, No. 1: 71-72 (January–February 1966).
6. G. F. Zaboronok, V. B. Milova, M. D. Polyakova, and T. V. Simonishvili, Effect of Ultrasonic Vibration on the Structure of Electron-Beam-Melted Molybdenum, *Tsvetn. Metal.*, No. 7: 83-85 (1966).
7. F. A. Schmidt and T. G. Ellis, Columbium Metal by the Aluminothermic Reduction Process of Cb_2O_5, *J. Metals*, 18: 1303-1308 (December 1966).
8. A. F. Weinberg, J. R. Lindgren, and R. G. Mills, Vapor Deposited Tungsten for Application as a Thermionic Emitter Material, Report NASA-CR-67182 (GA-6473), General Atomic Division, General Dynamics Corp., June 28, 1965.
9. J. W. Stevenson, Electrolytic Uranium Project: Cell Operation, USAEC Report MCW-1514, Maryland University, Oct. 31, 1966.
10. A. M. White, Fundamental and Applied Research and Development in Metallurgy, Development of a Fabrication Process for Zircaloy-Aluminum Composite Pressure Tubing, USAEC Report NMI-2200.11, Nuclear Metals, Inc., July 15, 1966.
11. J. H. Suldan and R. J. Krahn, Sizing of Zircaloy Structurals, USAEC Report WAPD-TM-620, Westinghouse Electric Corporation, Bettis Atomic Power Laboratory, February 1967.
12. M. J. Nasir and H. J. Bray, Growth of Single Crystals of Zircaloy-2, *J. Inst. Metals*, 94: 398-399 (November 1966).
13. W. C. Kramer, W. R. Burt, Jr., F. J. Karasek, J. E. Flinn, and R. M. Mayfield, Vanadium Alloy Screening Studies and Fabrication of V–15 Wt.% Ti–7.5 Wt.% Cr Tubing for Nuclear Fuel Cladding, USAEC Report ANL-7206, Argonne National Laboratory, August 1966.
14. R. I. Jaffe (Ed.), Proceedings of the Third Technical Conference, Los Angeles, California, December 9–10, 1963, *Met. Soc. Conf.*, 30(1966):
    a. R. E. McDonald and C. F. Leitten, Jr., Production of Refractory-Metal Tube Shells by Extrusion and Flow-Turning Techniques, pp. 85-89.
    b. R. H. Hicks, Production of Double-Extruded Heavy-Wall Tubing, pp. 137-149.
    c. P. Lowenstein, J. G. Hunt, and R. G. Jenkins, Fabrication and Properties of Seamless Tungsten Tubing, pp. 151-167.
    d. B. F. Hall, Jr., and N. F. Spooner, Consolidation and Application of Tungsten–26 Wt.% Rhenium Alloy Seamless Tubing, pp. 99-111.
    e. G. F. Kinney, E. E. Conabee, and L. J. Cronin, Permeability of Sintered Tungsten, pp. 295-306.
    f. R. L. Heestand and C. F. Leitten, Jr., Parameters for the Production of Refractory-Metal Tubing by the Vapor-Deposition Process, pp. 113-123.
    g. M. J. Disckind, Joining Tungsten by Chemical Vapor Deposition, pp. 379-392.
    h. P. R. Dioguardo, G. J. Dormer, E. G. Pike, and B. S. Payne, Jr., Scale-Up of Pack Cementation Coatings, pp. 651-661.
    i. W. L. Aves, Jr., and G. M. Ecord, Advances in Coating Deposition Techniques for Refractory-Metal Structures, pp. 663-669.
    j. F. L. Jones, S. R. Elkins, Jr., B. Wilkins, Jr., and E. S. Barland, Arc Plasma Coatings for Refractory Metals, pp. 707-717.
    k. J. B. Hallowell, D. J. Maykuth, and H. R. Ogden, Silicide Coatings for Tantalum and Tantalum-Base Alloys, pp. 737-753.
    m. V. S. Moore and A. R. Stetson, Progress in the Coating of Refractory-Metal Foil, pp. 795-812.
    n. D. R. Rummler, W. B. Lisagor, and G. R. Wichorek, Coated Refractory Metals for High-Temperature Structural Components, pp. 813-826.
15. A. P. Klyucharev, V. N. Karev, A. D. Nikolaichuk, T. S. Nazarova, V. N. Medyanik, and A. N. Rozen, Preparation of Molybdenum and Rhenium Foils for Nuclear Studies, *Prib. Tekh. Eksp.*, No. 4: 198-199 (July–August 1966).
16. W. R. Burt, Jr., D. C. Brilleart, and R. M. Mayfield, Development of Techniques for Fabrication of Small-Diameter, Thin-Wall Tungsten and Tungsten-Alloy Tubing, USAEC Report ANL-7151, Argonne National Laboratory, July 1966.
17. General Electric Company, Nuclear Materials and Propulsion Operation, High-Temperature Materials Program Progress Report No. 63, USAEC Report GEMP-63, Dec. 30, 1966.
18. H. G. Sowman, A. Milner, and D. D. Rowenhorst, Fabrication of Tungsten Alloy Tubing, USAEC Report COO-1518-4, Minnesota Mining and Manufacturing Co., Dec. 23, 1966.
19. C. P. Blankenship and C. A. Gyorgak, Extrusion of ½- and ⅜-In.-Diameter, Thin-Wall Tungsten Tubing Using the Floating-Mandrel Technique, Report NASA-TN-D-3772, National Aeronautics and Space Administration, Lewis Research Center, December 1966.
20. R. R. Turk and W. E. McKee, Alloy Ionizer Fabrication, Report N66-30489, Hughes Research Laboratories, May 1966.
21. R. Meyer, P. Potet, and J. Pillot, Sintered, Porous Metallic Elements: Their Properties and Applications, *Chim. Ind. (Paris)*, 96: 317-332 (August 1966).
22. R. D. Watson, Techniques for Hot-Press-Bonding Dissimilar Metal Combinations, Canadian Report AECL-2583, May 1966.
23. A. H. Ballard and R. Hendricks, Jr., High Temperature Isostatic Pressing, U. S. Patent 3,279,917, to USAEC, Oct. 18, 1966.
24. W. C. Necker, The Hot Isostatic Pressing Process—A New Tool for Complex Operations, *Research/Development*, 18(2): 40-45 (February 1967).
25. S. W. Porembka, D. E. Niez, J. N. Fleck, and C. W. Kistler, Jr., Control of Composite Microstructures Through the Use of Coated Filaments, Paper No. 67-175 presented at AIAA 5th Aerospace Science Meeting, New York, N.Y., January 23–26, 1967.
26. J. G. Donaldson and H. Kenworthy, Vapor Deposition of Molybdenum–Tungsten Alloys, USAEC Report BM-RI-6853, Bureau of Mines, 1966.
27. W. O. Harms, Oak Ridge National Laboratory, unpublished, January 1967.
28. P. Patriarca, Oak Ridge National Laboratory, unpublished, March 1967.
29. University of California Lawrence Radiation Laboratory, Advanced Space Nuclear Power Program, Progress Report No. 3, April–June 1966, USAEC Report UCRL-50004-66-2, Nov. 15, 1966.
30. J. McGuire, Carbide Deposition on Tantalum, U. S. Patent 3,266,948, to USAEC, Aug. 16, 1966.
31. K. Tashhiyuki, Studies on Electrodeposition of Tungsten Alloys. V. The Initial Stage of Electrodeposition of Tungsten Alloys by Using Radioisotope ^{185}W, *J. Metal Finishing Soc. Japan.*, 17: 255-257 (July 1966).
32. E. L. Childs and F. E. Evans, Nonaqueous Electropolishing Bath for Uranium, USAEC Report RFP-816, Rocky Flats Division, Dow Chemical Co., Dec. 21, 1966.

33. R. G. Gilliland, Brazing Alloys for Refractory Metals, U. S. Patent 3,293,741, to USAEC, Dec. 27, 1966.
34. J. C. Marshall, and H. G. Smith, Brazing Alloys for Tungsten and Molybdenum, U. S. Patent 3,292,255, to USAEC, Dec. 20, 1966.
35. J. V. Peck and J. M. Gerken, Development of Welding Procedures and Filler Materials for Joining High-Strength Low-Alloys Steels, Report AFML-TDR-64-255(Pt. III), Thompson Ramo Wooldridge Inc., October 1966.
36. J. M. Faulkner, G. L. Hanna, and J. V. Peck, Development of Welding Procedures and Filler Materials for Joining High-Strength Low-Alloy Steels, Report ML-TDR-64-255, Thompson Ramo Wooldridge Inc., August 1964.
37. J. M. Faulkner, G. L. Hanna, and J. V. Peck, Development of Welding Procedures and Filler Materials for Joining High-Strength Low-Alloy Steels, Report AFML-TDR-64-255(Pt. II), Thompson Ramo Wooldridge Inc., September 1965.
38. P. J. Konkol and A. G. Lee, Jr., Welding Characteristics of Carbon-Containing Experimental HY-180/210 Steels, Technical Report, United States Steel Corp., Jan. 1, 1967.
39. M. B. Watson, Literature Review of the Welding of 3½ Percent and 9 Percent Nickel Steels, Canadian Report AECL-2630, September 1966.
40. Aeroprojects Inc., Applications of Ultrasonic Energy: Ultrasonic Instrumentation for Nuclear Applications, USAEC Report NYO-3622-6, December 1966.
41. G. Schmitz and L. Frank, Nondestructive Testing for Evaluation of Strength of Bonded Material, Report N66-11761, General American Research Division, General American Transportation Corp., September 1965.
42. Anon., Eddy-Sonics Testing, *Ind. Res.*, 36 (February 1967).
43. F. W. Albaugh, S. H. Bush, J. J. Cadwell, D. R. deHalas, and D. C. Worlton, Battelle–Northwest, unpublished, March 1967.

LEGAL NOTICE

This journal was prepared under the sponsorship of the U. S. Atomic Energy Commission. Neither the United States, nor the Commission, nor any person acting on behalf of the Commission:

A. Makes any warranty or representation, expressed or implied, with respect to the accuracy, completeness, or usefulness of the information contained in this journal, or that the use of any information, apparatus, method, or process disclosed in this journal may not infringe privately owned rights; or

B. Assumes any liabilities with respect to the use of, or for damages resulting from the use of any information, apparatus, method, or process disclosed in this journal.
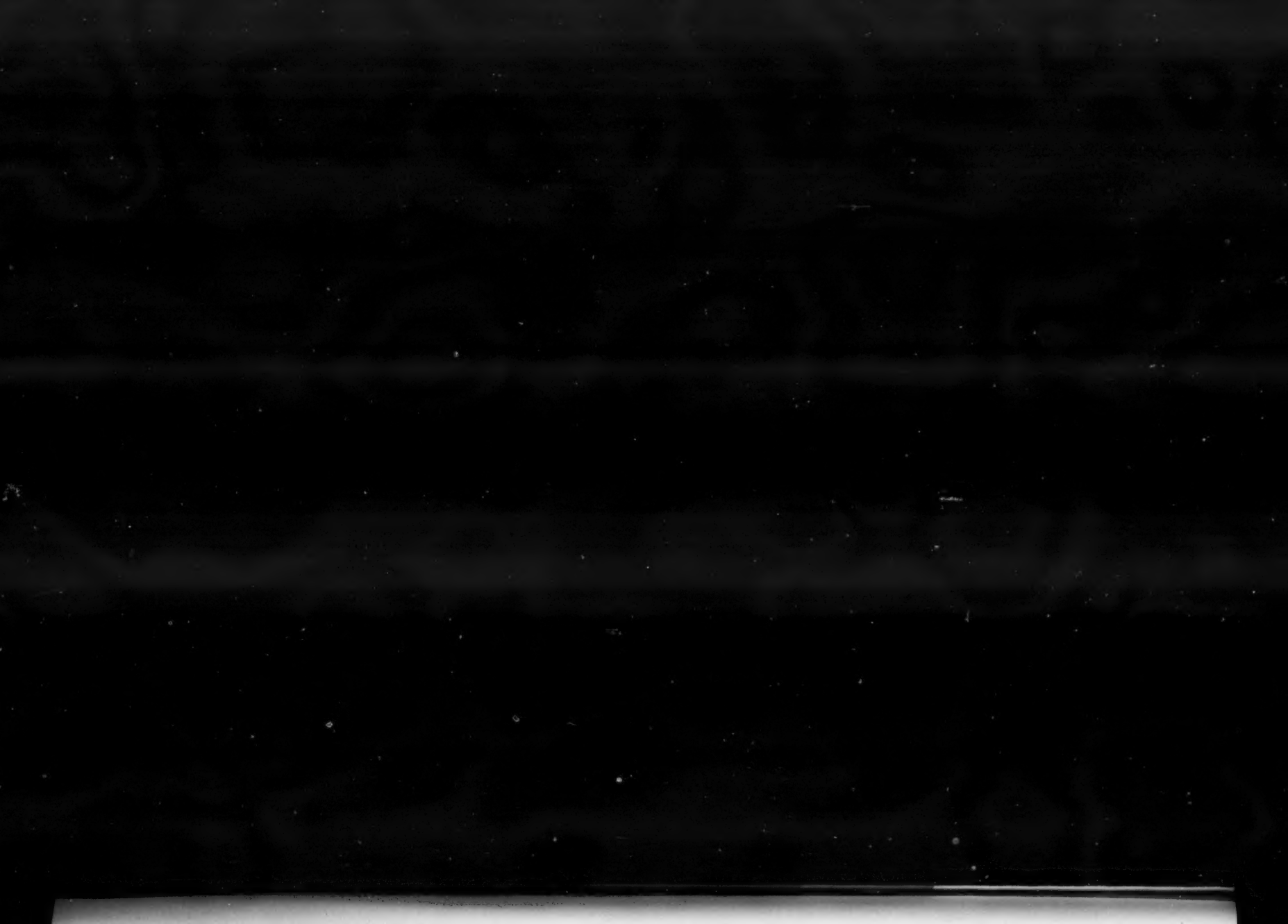
As used in the above, "person acting on behalf of the Commission" includes any employee or contractor of the Commission, or employee of such contractor, to the extent that such employee or contractor of the Commission, or employee of such contractor prepares, disseminates, or provides access to, any information pursuant to his employment or contract with the Commission, or his employment with such contractor.